Serie R
No 324

ISSN 0909-587X
ISBN 87-7740-165-4

Afdelingen for Bærende Konstruktioner
Department of Structural Engineering
Danmarks Tekniske Universitet • Technical University of Denmark

Ultra High-Strength Steel Fibre Reinforced Concrete

Part II

Structural Applications of Compresit

Claus Vestergaard Nielsen

Serie R No 324 1995

Ultra High-Strength Steel Fibre Reinforced Concrete

Part II

Structural Applications of Compresit
With Emphasis on Long Span Bridge Design

July 1995

Carl Bro Civil & Transportation a|s
Consulting Engineers and Planners

Claus Vestergaard Nielsen
Ph.D. Thesis – EF 457

ABK Afdelingen for Bærende Konstruktioner
Department of Structural Engineering
Danmarks Tekniske Universitet • Technical University of Denmark

ATV
Danish Academy of Technical Sciences
Industrial Research Fellowship

Ultra High-Strength Steel Fibre Reinforced Concrete. Part II. Structural Applications of Compresit

Tryk:
Afdelingen for Bærende Konstruktioner
Danmarks Tekniske Universitet
Lyngby
ISBN 87-7740-165-4
ISSN 0909-587X
Bogbinder:
H. Meyer, Bygning 101, DTU

Preface

The present report is the *second part* of the thesis required to obtain the Ph.D. degree. The study is carried out as required by the Danish Academy of Technical Sciences (ATV) throughout the period October 1st 1992 to March 31st 1995.

The first part of the thesis is titled:

> **Ultra High-Strength Steel Fibre Reinforced Concrete, Part I: Basic Strength Properties of Compresit Matrix**

and it is named *Part I* for reference purposes throughout the present report. Both reports are written so that they can be read separately without any lack of information. However, the present second part contains a conclusion for the complete thesis.

The project is divided between the Department of Structural Engineering, Technical University of Denmark, under the supervision of Professor, Dr.techn. Mogens Peter Nielsen, and the consulting engineers and planners Carl Bro Civil and Transportation a|s under the supervision of Managing Director, Professor Bjarne Chr. Jensen. The third party of the project is Aalborg Portland A/S, which is represented by Managing Director Palle Nepper-Christensen from the Cement- and Concrete Laboratory in Aalborg.

I wish to thank the staff at the university, the company and the third party for their help and especially my colleague M.Sc. John Forbes Olesen for fruitful discussions. Also the assistance from M.Sc. Jesper H. Schaarup is acknowledged. Furthermore the Cement- and Concrete Laboratory has provided invaluable help by casting all test specimens.

This print of the report includes minor corrections to my original thesis.

Copenhagen
July 1995

Claus Vestergaard Nielsen

Abstract

The present report contains structural considerations of the steel fibre reinforced matrix compresit. Compresit matrix is an ultra high-strength, steel fibre reinforced cementitious matrix. The properties of the matrix are investigated in Part I of the thesis. The structural applications focus on bridge design, i.e. especially the behaviour of slender beams.

First the report treats the triaxial failure criterion for compresit matrix, which has been experimentally observed. This investigation is based on the theory of plasticity and a modification of the normal Coulomb friction criterion is proposed. It appears that the presence of steel fibres does not influence the triaxial strength behaviour significantly.

The main part of the investigation concerns the behaviour of slender beams made of high-strength concrete, fibre reinforced concrete or compresit. First the bending behaviour is analyzed in both the ultimate and the serviceability limit state. Then the beam shear strength is considered with basis in the theoretical plastic solution to the problem. Especially the effect of steel fibre reinforcement on the beam shear strength is treated. Finally an example of compresit bridge design is given together with a comparison with an existing concrete solution. The conclusions are, that relatively small fibre contents are significant for the shear strength. The plastic effectiveness factor is significantly raised by the fibres. Furthermore the investigation shows, that compresit seems competitive in bridge structures.

Resumé

Denne rapport indeholder konstruktionsmæssige overvejelser for compresit matrix. Compresit matricen er betegnelsen for et cementbaseret produkt, som er armeret med stålfibre og udviser ekstrem høj trykstyrke. Matricens egenskaber er behandlet i Del I af den foreliggende afhandling. Konstruktionstyperne sigter primært mod brodesign, dvs. den mekaniske opførsel af lange slanke bjælker

Først er den treaksede brudbetingelse for compresit matrix behandlet vha. egne forsøgsresultater. Denne undersøgelse er baseret på plasticitetsteorien og giver en modifikation af den normale Coulomb brudbetingelse. Fibrene synes ikke at influere den treaksede trykstyrke i nogen særlig høj grad.

Hovedparten af afhandlingen omhandler slanke bjælker af højstyrkebeton, fiberarmeret beton eller compresit. Først er bøjningsopførslen undersøgt i både brud- og anvendelsestilstand. Dernæst er bjælkers forskydningsstyrke behandlet udfra en plastisk løsning, især mht. fibrenes effekt. Til slut gives et konkret broeksempel med compresit design. Konklusionen er at selv små fiberindhold øger forskydningsstyrken markant, hvilket ses på effektivitetsfaktoren. Ydermere vises broeksemplet, at compresit er et konkurencedygtigt materiale.

Table of contents

Appendices

Notation

Throughout this report SI units are used and in the following a list of the most important symbols are given. Furthermore most of the symbols are described in the text, when they first occur.

Abbreviations

Compresit	Compact reinforced composite.
FRC	Fibre reinforced concrete.
HSC	High-strength concrete.
NSC	Normal-strength concrete.
SLS	Serviceability limit state.
ULS	Ultimate limit state.

Roman letters

a	Shear span.
a_w	Distance between stirrups.
A_c	Cross-sectional concrete area.
A_s	Longitudinal reinforcement area.
A_{sw}	Shear reinforcement area.
b	Beam width.
b_{min}	Minimum column width.
b_w	Width of beam web.
c, c_1, c_2	In Section 2.3: Cohesions in the Coulomb failure criterion. In Chapter 3: Parameters in rectangular stress block expressions.
C_j	Compressive internal force in the jth vertical truss.
d	Effective beam depth.
d_a	Maximum aggregate size.
d_b	Steel bar diameter.
d_c	Depth to compression reinforcement.
d_f	Fibre diameter.
e	Distance from prestress force to center of gravity.
E_c, E_s	Moduli of elasticity for concrete and steel respectively.
f_c	Uniaxial compressive strength.
f_{cd}	Uniaxial compressive strength to be used in ULS design.
f_t	Direct tensile strength.

f_y	Yield strength.
f_{yd}	Yield strength to be used in ULS design.
f_{yw}	Yield strength of shear reinforcement (stirrups).
f_{ywd}	Yield strength of shear reinforcement to be used in ULS design.
F_j	Tensile internal force in the jth inclined truss.
G_F	Fracture energy per unit crack area.
h	Beam depth.
h_f	Flange depth.
h_l	Internal moment arm lever.
i	Radius of inertia.
I	Moment of inertia for transformed uncracked cross-section.
I_{cr}	Moment of inertia for transformed cracked cross-section.
I_{FRC}	Moment of inertia for transformed fibre reinforced cross-section.
k, k_1, k_2	Parameters dependent on the angle of friction, $k \geq 1$.
k_{up}, k_{low}	Core radii.
K_j	Compressive internal force in upper flange of truss beam.
l	Section length of truss beam.
l_s	Buckling length of column.
L	Beam span.
L_f	Fibre length.
m	Normalized bending moment.
M, M_{cr}	Bending moment and moment at first cracking.
M_p, M_q	Bending moments from dead and live loads respectively.
n	In Chapter 3: Normalized normal force. In Chapter 5: Number of sections in truss beam.
n_b	Number of steel bars per reinforcement layer.
N	Compressive normal force.
p	Dead load per unit length.
P	Prestress force.
q	Live load per unit length.
q_d	Total design load per unit length in the ULS.
q_s	Design load per unit length in the SLS.
r_c, r_t	Maximum allowable SLS stresses in compression and tension respectively.
t	Thickness of discontinuity line.
T_j	Tensile internal force of lower flange in truss beam.
u	Displacement in discontinuity line.
V	Shear force on beam cross-section.
V_c	Volume of compresit matrix in vertical trusses.
V_f	Fibre content by volume.
V_s	Volume of prestressing steel in truss beam.
w_{up}, w_{low}	Normalized moments of resistance.
W	Energy density.
W_l	Energy density per unit length of discontinuity line.
W_{up}, W_{low}	Moments of resistance for upper and lower beam side respectively.

x	Coordinate axis along the beam through the geometrical center of gravity.
y	Coordinate axis of cross-section downward-directed from the x-axis.
y_0	Depth of compression zone.
X, Y	Uniaxial compressive strains and stresses respectively normalized with respect to their peak values.
X_{cu}	Normalized strain corresponding to ε_{cu}.

Greek letters

α	In Chapter 2: Displacement angle of discontinuity line. In Chapter 3 and 5: Elasticity ratio between E_s and E_c.
β	In Section 3.1.2: Parameter in analytical compressive stress - strain relationship for concrete, $\beta \geq 1$. In Chapter 5: Angle of inclined truss with respect to horisontal.
γ_c, γ_s	Partial coefficients for concrete and steel respectively.
δ	In Section 2.4: Width of displacement field. In Chapter 3 and 5: Downward-directed beam deflection.
δ_∞	Long-term deflection.
δ_{inl}	Initial upward-directed deflection of bridge girder.
δ_C	Mid-span deflection contribution from vertical trusses.
δ_F	Mid-span deflection contribution from inclined trusses.
δ_K	Mid-span deflection contribution from upper flange.
δ_T	Mid-span deflection contribution from lower flange.
ε	Longitudinal strain.
ε_c	Compressive strain at peak load.
ε_{cr}	Tensile concrete strain at first cracking.
ε_{cu}	Ultimate compressive strain.
ε_{ij}	Second order strain tensor (i,j = 1,2,3).
ε_{pre}	Steel strain corresponding to prestressing.
ε_s	Tensile steel strain.
ε_{sc}	Compressive steel strain.
ε_{sy}	Tensile steel strain corresponding to yielding.
η	Depth to geometrical center of gravity of uncracked cross-section.
θ	Crack angle in diagonal compression field theory.
φ	Angle of friction.
ϕ	Reinforcement ratio.
ϕ_w	Shear reinforcement ratio.
Φ	Reinforcement degree.
Φ_{bal}	Reinforcement degree corresponding to balanced cross-section.
Φ_w	Shear reinforcement degree.
κ	Beam curvature.

λ, λ^*	Parameters of energy dissipation expressions.
μ, μ^*	Parameters of energy dissipation expressions.
ν	Effectiveness factor on the uniaxial compressive strength, $\nu \leq 1$.
σ	Normal stress.
σ_1, σ_2, σ_3	Principal stresses.
σ_3^*	Minor principal stress corresponding to the transition point in the bi-linear failure criterion.
σ_c	Diagonal compressive stress in beam web.
σ_{cr}	Critical compressive stress for centrally loaded column.
σ_{ij}	Second order stress tensor (i,j = 1,2,3).
σ_{pre}	Steel stresses corresponding to P.
σ_s	Tensile steel stress.
τ	Nominal shear stress on cross-section.
Ψ	Long-term creep coefficient.

1. Introduction

There are many opinions of what characterizes a high-quality/high-performance concrete. The most popular quality indicator is the *compressive strength*, probably because it is well-understood and well-determined amongst concrete researchers and users. However, high-quality concrete is also characterized by its *price*, *durability*, *workability*, etc. For the contractor, the workability and the early-age properties are important, while the owner focuses more on price and durability.

The general opinion is that a lower water to cement ratio gives higher strength and durability because of its more dense structure, while the workability gets poorer. The goal is to find a combination that satisfies the demands during casting/curing together with the *structural demands* for strength and durability. However, new techniques and chemical additives make it possible to increase the concrete density and still keep the mix workable in practice.

At a recent conference in Singapore[1] it was accepted that a definition of high-performance concrete does not necessarily include any demand for high strength. The definition is from the authors point of view: *concrete that fulfils demands beyond the normal range*, i.e. a very broad definition. High-performance behaviour is often identical with good durability, which is often directly connected with high strength.

Concrete quality	Normal permeability	High permeability
No fibre reinforcement	Experience Low price Workability	Strength Durability
Fibre reinforced concrete (FRC)	Ductility Durability	Strength Durability Ductility

Table 1.1 Quality indicators of various concrete types.

In table 1.1 concrete matrix is divided into 4 groups: normal and high *permeability*, which causes normal and high-strength (abbreviated *NSC* and *HSC*) and reinforced with fibres, or without fibres (*fibre reinforced concrete* is abbreviated *FRC*). Both here and in the following chapters, the term fibres mean steel fibres mixed randomly with respect to both position and direction.

[1] ACI International Conference on High-Performance Concrete, Singapore, November 1994. See the author's contribution in Appendix 1.

For NSC the major advantage is the huge *experience* from the last century. Both the design tools and the material properties are well-documented from numerous tests and observations. It is inevitable that whenever the concrete density is increased or fibres are added, the workability of the mix gets poorer. However, the decreased permeability makes it more difficult for the aggressive materials, such as chloride ions to penetrate the concrete cover and reach the steel reinforcement. Thus, the risk of steel corrosion is reduced. Similarly, the presence of fibres reduces the crack widths and therefore also increases the durability.

It is a fact that HSC is very *brittle* and often suffers from almost explosive failure modes. The material gets sensitive towards micro-cracks/flaws and inhomogeneities within the material. The fibres counteract this crack sensitive behaviour and provide the concrete with extra *ductility*. As explained in the following section, *compresit*[2] *matrix* is based on a brittle high-strength matrix, which is provided with ductility from plenty of steel fibres, i.e. compresit matrix is included in the lower-right box of table 1.1.

1.1 Compresit as a structural material

The composition of the compresit matrix is described in Part I of this thesis[3], and it is not repeated here. Compresit matrix consists of a dense *Densit*[4]*-binder* with a high amount of *micro silica* and quartz sand with maximum aggregate size of 4 mm. Furthermore randomly mixed steel fibres[5] are added. The most common *fibre content* is 6 % by volume of *straight* fibres with dimensions $d_f \times L_f = 0.4 \times 12$ mm. In Part I the material properties of the matrix are treated experimentally with varying fibre content and geometry. The uniaxial compressive cylinder strength is measured to exceed 140 MPa, cf. Part I.

The Densit-binder provides the matrix with an extremely *dense* pore structure, where the water to binder ratio is below 0.2. Furthermore the specially patented packing of the binder together with *dispersing agents* make it possible to add high amounts of steel fibres by means of normal mixing techniques. The *casting* of compresit matrix demands vibrations in order to make the matrix flow. The aspects concerning casting and curing are being investigated elsewhere[6].

[2]Compact Reinforced Composite.

[3]Basic Strength Properties of Compresit Matrix.

[4]Registered trademark of Densit A/S, Aalborg, Denmark.

[5]Dramix fibres from N.V. Bekaert S.A. Building Products, Belgium.

[6]Through the Brite EuRam project Ministruct running from 1993 through 1995.

The term *compact reinforced* in the compresit name describes the conventional reinforcement with steel bars, that is an essential part of a compresit structure, while the term *composite* denotes the dense fibre reinforced matrix. The relatively small aggregates, together with the short fibres make it possible to reduce the steel bar spacing and thus obtain a compact system of reinforcement. Furthermore the dense nature of the matrix makes it almost impenetrable from the environment and thus provides the reinforcement with protection against corrosion. The principles and ideas behind the compresit material are described by its inventor H.H. Bache in *Bache (1981)* and *Bache (1987)*.

Another useful material property, which is due to the dense binder, is its high *interfacial bond strength* to both fibres, aggregates and reinforcement bars. The combination of good bond and the confinement provided by the fibres make it possible to reduce the necessary *anchorage length* considerably, compared to both NSC and HSC. A reduction to about one third of the normal anchorage length is expected, see e.g. Heshe (1988) and Heshe & Nielsen (1992). These bond properties are currently being further investigated. The significance of these findings for the structural application of compresit is obvious: more simple reinforcement arrangements and smaller anchorage zones. Furthermore the confinement effect of the fibres is valuable in case of concentrated forces, where splitting cracks parallel to the load cause a problem, e.g. around the supports and in the anchorage zones of prestress tendons.

A disadvantage of fibre reinforced materials such as compresit is its relatively high *material price*. The Dramix steel fibres cost approximately DKK 8 per kg. Thus, one per cent by volume of these fibres cost approximately DKK 700 per m^3 compresit matrix. Therefore a fibre content, equal to 3 %, is likely to double the material price compared to plain compresit matrix without fibres. As a consequence of this material price, a better *optimization* of the material consumption in structural elements is needed.

1.2 Scope of present investigation

The use of high-strength concrete in structures such as bridges has primarily been connected with its good durability properties. However, it is the intention with the present report to analyse some of the advantages that are obtained from the increased strength of these new concretes. The present analysis consider only *hardened concrete* and does not include any investigation of the early-age stages of compresit matrix.

The emphasis of the analysis is beams with *long spans*, e.g. the girder of a bridge crossing a motorway. It is believed that this particular task is interesting to investigate for the following reasons:

- The compresit girder may be *precast* and then transported to the site, where it is assembled. Thus, it can act as scaffolding for the bridge deck mould. This procedure causes the minimum disturbance for the crossing traffic.

- The concept of longer spans may reduce the number of mid-supports (columns).

From an architectural point of view, the above reasons will also give more freedom in designing the appearance of the bridge.

The ultra high-strength of compresit matrix ($f_c > 140$ MPa) is utilized in the *ultimate limit state* (ULS). The strong matrix makes the need for high-quality steel reinforcement such as prestressing tendons more urgent. In the *serviceability limit state* (SLS) the stiffness of the material is essential, e.g. to minimize the beam deflections. Part I of the thesis shows that the modulus of elasticity does not increase with the same rate as the strength. Therefore, especially in case of long spans, the SLS demands get more restrictive than the ULS demands and the analysis shows that it is necessary to consider actions such as prestressing.

The fibres make the SLS demands to avoid concrete cracking less important in a design situation. The cracks are smaller and better distributed within the structure because of the fibre reinforcement. It is noted that the present analysis does not include any prediction of the crack widths in a compresit structure, but only treats the topic qualitatively.

The analysis includes comparisons of the compresit concept with both normal-strength concretes and conventional high-strength concretes. The difference between NSC and HSC is not unique, but in this thesis the compressive cylinder strength $f_c = 50$ MPa is chosen as the transition from NSC to HSC. This value corresponds to the upper limit for the validity of the Danish concrete code DS 411 (1984). The term HSC covers compressive strengths ranging from 50 MPa to approximately 100 MPa. It is noted that the Norwegian concrete code allows compressive strengths up to 95 MPa, while CEB (1990) allows f_c up to 80 MPa, i.e. both of these codes consider HSC.

The contents of the present report cover various design aspects of compresit beams with long spans. The report is divided into 4 different subjects:

- The theory of plasticity including a multiaxial compressive failure criterion is considered in Chapter 2.

- The conditions in both ULS and SLS for long beams subjected to bending is considered in Chapter 3.

- The shear strength of beams is considered in Chapter 4.

- A numerical example of a footbridge made of prestressed compresit is given in Chapter 5.

The *theory of plasticity* is based on the triaxial test results reported in Chapter 4 of Part I of the present thesis. A failure criterion, based on the well-known Coulomb criterion, is presented and discussed. Appendix 1 contains a paper by the author, which was presented at ACI 1994 International Conference on High-Performance Concrete in November 1994. This paper also treats the triaxial compression strength results from compresit tests.

The *bending* analysis in Chapter 3 concerns both the ULS and the SLS with prestressed beams. As mentioned above, prestressing is often needed in order to fulfil the SLS demands and to utilize the high compressive strength. The stress distribution in the compressive zone of a compresit beam in bending is analyzed.

The *shear* analysis in Chapter 4 investigates the effect of steel fibres on the shear strength of beams. The emphasis of the investigation is on HSC beams. The theoretical plastic solution to the shear strength of beams is applied to several experimental investigations.

Finally Chapter 5 contains an analysis of a *footbridge* crossing a motorway. A compresit solution is compared with the actual prestressed concrete girder, and the costs are compared for the two solutions. Appendix 2 contains the calculations that are connected with this analysis.

Chapter 6 contains the *conclusions* on the complete project. Thus, both Part I and II of the thesis are concluded. Furthermore each chapter contains concluding remarks, where the results are summarized.

The *references* are listed at the end of each chapter, and Chapter 7 includes all references in chronological order. The reference notation consists of the author's surnames followed by the publication year in brackets.

Following the chronological reference list are 2 *appendices*. The first appendix is the paper presented at the Singapore conference as mentioned above. The second contains numerical calculations for Chapter 5.

1.3 References

Bache, H.H. (1981), *Densified Cement/Ultra-Fine Particle-Based Materials*, Paper presented at The Second International Conference on Superplasticizers in Concrete, June 10-12, Ottawa, Canada, Also CBL Report No. 40, Aalborg Portland A/S, 35 pp.

Bache, H.H. (1987), *Compact Reinforced Composite, Basic Principles*, CBL Report No. 41, Aalborg Portland A/S, 87 pp.

CEB (1990), *CEB - FIP Model Code*, CEB Bulletin D'information No. 213/214, Thomas Telford, London, 437 pp.

DS 411 (1984), *Danish Code of Practice for the Structural Use of Concrete*, 3rd Ed., Dansk Ingeniørforening, 98 pp.

Heshe, G. (1988), 'Experimental Research on Compact Reinforced Composite (CRC)', *Bygningsstatiske Meddelelser*, Vol. 59, No. 1, Danish Society for Structural Science and Engineering, 79 pp.

Heshe, G. & C.V. Nielsen (1992), *EU 264 - COMPRESIT, Subtask 1.7 - Anchorage of Reinforcement Bars*, NOVI's Udviklingsfond, Aalborg, 29 pp.

2. Theory of plasticity

A mild steel bar in direct tension produces an almost rigid-plastic stress - strain curve. The term *rigid-plastic* covers the behaviour, where no deformations occur until the stresses reach a *yield point* followed by arbitrarily large deformations under constant yield stress. After a linear-elastic behaviour the steel bar yields under constant or slightly increasing stresses until rupture. The plastic strains are much higher, than the elastic strains and therefore it is reasonably to consider steel rigid-plastic when the ultimate limit state is considered.

The application of plastic theory to the field of reinforced concrete structures has been going on at the Department of Structural Engineering, Technical University of Denmark throughout most of the present century. A thorough description of the historical details is provided in *Nielsen (1984), pp. vii-xii.* Clearly the plastic behaviour of concrete structures is mainly attributed to the reinforcement bars, but attempts to model the strength of plain concrete by means of the theory of plasticity together with a *Coulomb failure criterion* have been successful in case of e.g. beams in shear. Furthermore the methods are now included into the new codes such as Eurocode 2.

The theory of plasticity only applies to *ultimate limit analysis* because no deformations are included until failure. Thus the method concerns the load capacity of structures, whereas serviceability limit states are rather treated through the theory of elasticity.

The present chapter first describes the general theory of plasticity in Section 2.1. Then the failure criterion (or the yield surface) for plain concrete is treated in Section 2.2 with emphasis on the Coulomb criterion, which is often applied to NSC. The considerations concerning the failure criterion of HSC and in particular compresit matrix are given in Section 2.3 and finally Section 2.4 contains energy dissipation formulas.

2.1 The normality condition

The present description of the fundamentals of the theory of plasticity is brief, whereas a detailed presentation is found in Nielsen (1984), pp. 1-14. The complete formulation of the theory of rigid-plastic materials is mainly due to D.C. Drucker and W. Prager at Brown University in the 1950ies.

$$f(\sigma_{ij}) \begin{cases} < 0\,, & \text{Deformations impossible} \\ = 0\,, & \text{Deformations possible} \\ > 0\,, & \text{Impossible situation} \end{cases} \quad i, j = 1,2,3 \qquad (2.1)$$

It is assumed, that there exists a state of stress, defined by the second order tensor σ_{ij}, for which the *yield condition* has the form stated in eq. (2.1). The *yield surface* which is defined

by $f(\sigma_{ij}) = 0$ is assumed to be differentiable and convex in a σ_{ij}-coordinate system with the stress free point $\sigma_{ij} = 0$ inside the safe region. The safe region is defined by $f(\sigma_{ij}) < 0$. The *normality condition* is due to *von Mises* in 1928 and states, that the resistance of a material against a given deformation results in maximum work. We consider a point on the yield surface $f(\sigma_{ij}) = 0$ and impose a small variation $d\sigma_{ij}$ of σ_{ij} along the yield surface. This change does not result in any change of the work $W = \sigma_{ij}\varepsilon_{ij}$ because this corresponds to a maximum value. The two conditions to determine ε_{ij} corresponding to σ_{ij} yield

$$\left.\begin{aligned} dW &= d\sigma_{ij}\varepsilon_{ij} = 0 \\ df &= \frac{\partial f}{\partial \sigma_{kl}} d\sigma_{ij} = 0 \end{aligned}\right\} \Rightarrow \quad \varepsilon_{ij} = \lambda \frac{\partial f}{\partial \sigma_{ij}} \tag{2.2}$$

where λ is an arbitrary positive constant. This relation forms the normality condition, which means, that the strain vector in the σ_{ij}-coordinate system forms an *outward-directed normal* to the yield surface. Thus eq. (2.2) is the constitutive equations for a rigid-plastic material following the von Mises flow rule. It is emphasized that only the magnitude of the strain components relative to each other is known, i.e. the length of the strain vector is unknown. In case of constitutive models, where eq. (2.2) is not fulfilled, the flow rule is termed non-associated.

2.1.1 Extremum principles

The *ultimate capacity* of the structure is termed the yield load or the failure load. The existence of eq. (2.2) makes it possible to state the extremum principles to be used in plastic limit analysis.

The lower bound theorem. It is possible to find a *safe* state of stress, satisfying the *equilibrium conditions* both within the structure and on its surfaces. The corresponding load, that produces this state is *smaller* than, or equal to the ultimate load of the structure.

The upper bound theorem. It is possible to find a *kinematically possible* strain field, which satisfies the *normality condition*. The corresponding load is *greater* than, or equal to the ultimate load of the structure.

The uniqueness theorem. There exists one load, which satisfies both the lower and the upper bound theorem and this load is the correct ultimate load of the structure. It is possible that there exists several upper and lower bound solutions to the same problem. Thus, only the ultimate capacity is uniquely determined, neither the stress field or the strain field is.

The normal approach to solve a structural *ultimate limit state* problem by means of the extremum principles is to consider a *geometrically possible failure mechanism* with rigid bodies moving relatively to each other. Then by imposing the *work equation* to the

mechanism an upper bound yield load is obtained. Thus, there exist displacement *discontinuities* within the structure.

In order to verify the upper bound yield load it is necessary to construct a stress field within the body and along its surfaces, which fulfil the equilibrium conditions and at the same time lies within the yield surface. This stress field is often constructed by dividing the body into regions with *homogeneous* states of stress, i.e stress discontinuities exist. If the lower bound yield load equals the upper bound load the solution is exact.

2.2 Modified Coulomb failure criterion for NSC

The present presentation only concerns the socalled *friction hypothesis*, which states that the shear resistance of a material consists of two components, viz. cohesion, which is constant, and friction, which increases with the normal pressure on the failure plane. In a Mohr stress diagram this hypothesis forms a straight line. It is noted that *compressive normal stresses* are considered to be positive in the following.

In Chapter 4 of Part I of the thesis[1] the fundamentals of the multiaxial failure criteria for concrete are described. The *modified Coulomb* failure criterion, which is useful for the limit state analysis of concrete, is given by the relations

$$\left.\begin{aligned} |\tau| &= c + \sigma\tan\varphi \\ \sigma_1 &= k\sigma_3 + f_c\,, \qquad k = \frac{1+\sin\varphi}{1-\sin\varphi} \end{aligned}\right\} \tag{2.3}$$

where $\sigma_1 \geq \sigma_2 \geq \sigma_3$ are the principal stresses. Furthermore this *sliding criterion* is extended with the *tension cut-off* criterion to model separation failure instead of a sliding failure, e.g. under direct tension. The analytical representation of the tension cut-off criterion is $\sigma_3 = -f_t$. In figure 2.1 an illustration is given of the modified Coulomb failure criterion in both a Mohr stress diagram and a principal stress diagram.

An important characteristic of the friction hypothesis is, that the intermediate principal stress σ_2 is not represented in the criterion. For instance this means, that the biaxial compressive strength of a Coulomb material equals the uniaxial compressive strength f_c. However, biaxial compression tests on concrete show, that the biaxial strength is up to 30 % higher than f_c. Thus, the friction criterion seems to give a safe prediction. Another important reason to apply the modified Coulomb criterion is its simplicity.

[1] Basic Strength Properties of Compresit Matrix.

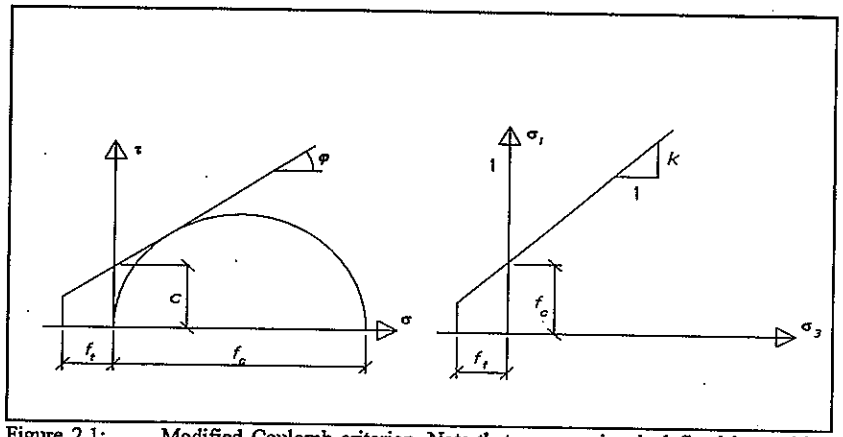

Figure 2.1: Modified Coulomb criterion. Note that compression is defined by positive normal stresses.

Triaxial tests on NSC show, that the angle of friction φ is approximately 37°, which yields the slope $k = 4$ in the σ_1 - σ_3 relationship, see figure 2.1. This is investigated in numerous experiments all over the world, see e.g. Section 4.1.3 of Part I, Dahl (1992) and Nielsen (1984).

2.3 Bi-linear failure criterion for compresit and HSC

The triaxial compression tests on compresit matrix are described in Section 4.2 of Part I. Furthermore Appendix 1 contains a conference paper by the author on these tests.

One of the well-known differences between NSC and HSC is, that the mortar strength is increased significantly, which causes the cracks to ignore the presence of aggregate rather than to follow the mortar - aggregate interfaces. Thus the interfaces between mortar and aggregate, which is traditionally the weak link for NSC, seem to be strong enough to make the failure zones pass through the stones in HSC. This results in *smoother crack surfaces* for HSC and therefore it is expected, that the coefficient of friction (tanφ in eq. (2.3)) decreases.

Dahl (1992) has tested concrete cylinders with uniaxial strengths ranging from $f_c = 10$ MPa to 110 MPa. The cylinders are subjected to a constant hydraulic sidepressure, while the axial load is increased until failure. The results on HSC clearly show a reduced φ from approximately 37° for NSC to 30° for HSC, i.e. the slope k in eq. (2.3) is reduced from 4 to 3, see

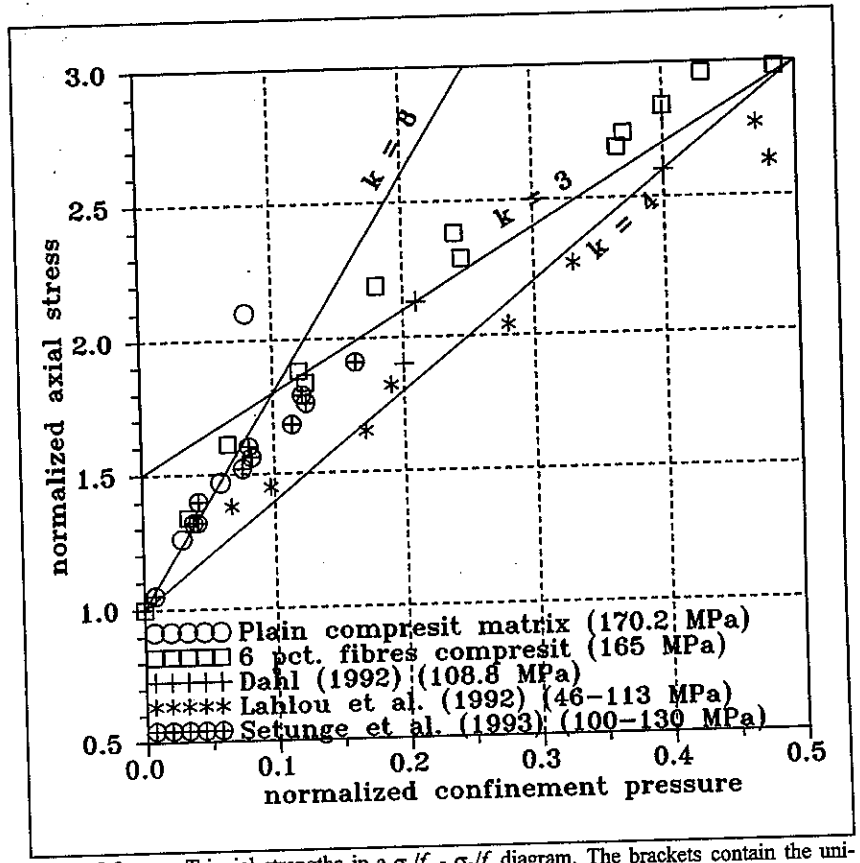

Figure 2.2: Triaxial strengths in a σ_1/f_c - σ_3/f_c diagram. The brackets contain the uniaxial strengths. The compresit tests are described in Section 4.2 of Part I.

figure 1 of Appendix 1.

For small values of the sidepressure (below 10 % of f_c) compressive triaxial tests on HSC cylinders seem to predict a higher angle of friction (about 51°) before the angle decreases to a value of about 30°. In figure 2.2 these test results are shown in a σ_1/f_c - σ_3/f_c diagram together with straight lines having slopes k = 3, 4 and 8. The diagram also includes experimental results from both compresit matrix and other HSC mixes. The line with slope $k = 4$ corresponds to the NSC criterion and it seems to predict a safe failure criterion also for the HSC results. The line with $k = 3$ passes through $\sigma_1 = 1.5f_c$ for $\sigma_3 = 0$. This line fits the HSC data points for relatively high values of the sidepressure. However, if these test

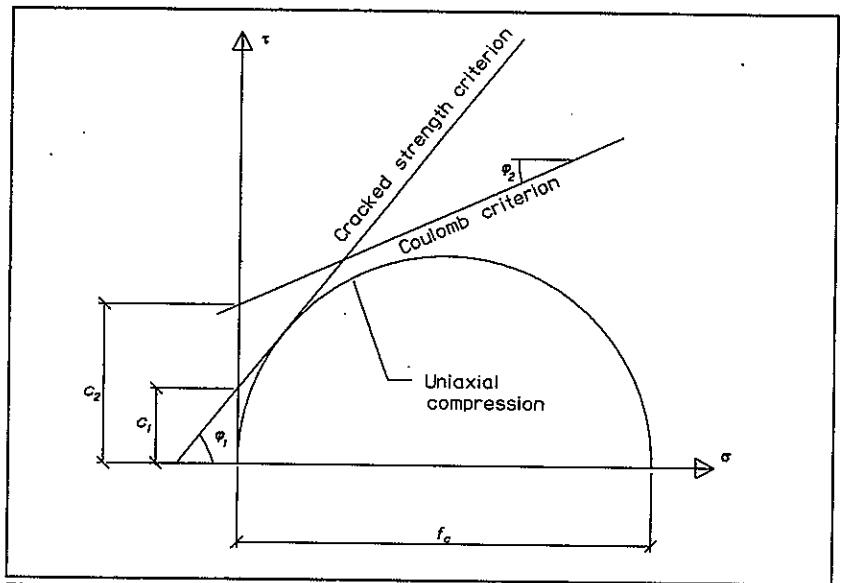

Figure 2.3: Proposed bi-linear failure criterion for HSC and compresit in Mohr diagram.

data are extrapolated towards the uniaxial case, we predict a uniaxial strength 50 % higher than the actual strength. Therefore a *bi-linear failure criterion* is proposed.

The bi-linear model, outlined in figure 2.3, consists of 2 straight lines with different slopes k_1 and k_2:

$$\sigma_1 = \begin{cases} k_1\sigma_3 + f_c\,, & \sigma_3 \le \sigma_3^* \\ k_2\sigma_3 + f_c + \sigma_3^*(k_1-k_2)\,, & \sigma_3 > \sigma_3^* \end{cases} \qquad (2.4)$$

where σ_3^* denotes the minor principal stress (the sidepressure) at which the *transition* between the two lines happens. The two straight lines of figure 2.3 are denoted by subscript 1 and 2. The steepest line is characterized by φ_1 and k_1 and it is termed the *cracked strength criterion*, while the normal *Coulomb line* is characterized by φ_2 and k_2. From the experimental observations in figure 2.2 it seems, that $\sigma_3^* \approx 0.1 f_c$, $\varphi_1 \approx 51°$ and $\varphi_2 \approx 30°$ in order to fit the test data.

The tensile regions of the triaxial failure criterion are not investigated experimentally in the present thesis, but it is expected, that the normal tension cut-off is applicable. In Appendix 1 these aspects are further discussed.

2.3.1 Physical interpretation of the bi-linear failure criterion

In the following an explanation is given to the question, why it seems reasonably to consider a bi-linear criterion instead of the normal approach to describe failure of concrete, see also Appendix 1. The description is a *qualitative* treatment of the phenomena corresponding to the various parts of the failure criterion in figure 2.3.

In *Horii & Nemat-Nasser (1986)* the compression failure of brittle materials (e.g. rock) is treated by means of linear-elastic fracture mechanics. The theory is not included here, but the findings of a *brittle - ductile* transition as the confinement pressure increases are undoubtedly similar to what is observed in triaxial compression of HSC. Horii & Nemat-Nasser investigate a plane micro-crack (flaw) within the material, which is subjected to biaxial compression, see figure 2.4.

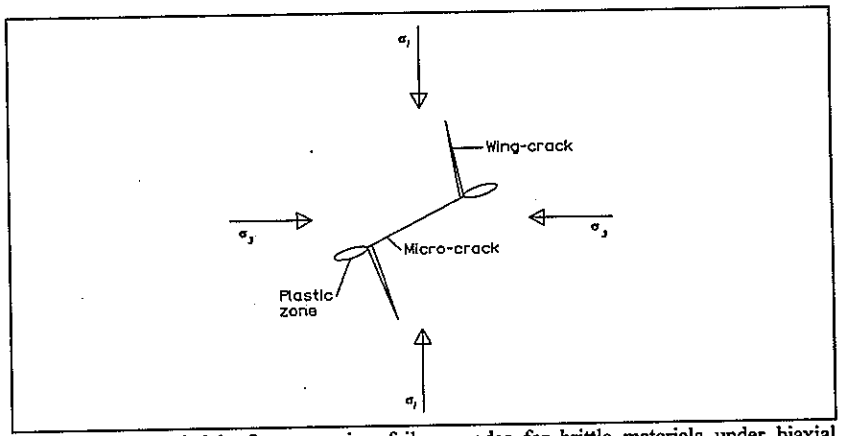

Figure 2.4: Model of compression failure modes for brittle materials under biaxial stresses.

The sliding displacements along the micro-crack cause *wing-cracks* to originate from the crack tips. The growth of these wing-cracks is approximately parallel to the most loaded direction and they tend to stabilize, if the confinement pressure σ_3 is suffiently high. Furthermore a socalled *plastic zone* develops in extension of the initial micro-crack. During proportional biaxial loading the wing-crack and the plastic zone emanate from the micro-crack tips. If the stress ratio σ_3/σ_1 is sufficiently high, then the wing-cracks stabilize at a

given length, or even close again. Instead the plastic zone develops, i.e. a more ductile sliding failure instead of the brittle splitting failure, cf. Section 3.1.2 of Part I.

The initial failure line with subscript 1 in figure 2.3 is interpreted as the *brittle failure mode*. The term cracked strength criterion is chosen, because this criterion is expected to depend on the actual state of damage within the material, e.g. the number and the sizes of initial flaws. Thus, it is mainly the tensile characteristics, that govern the cracked strength criterion. The obvious parameters, that influence the presence of initial micro-cracks, are the loading prior to testing and the curing and mixing conditions. Therefore it is questionably, whether the cracked strength criterion is a *material property*.

However, a survey of test results from NSC subjected to combined compression and tension suggests, that the cracked strength criterion fits the data satisfactorily. In this case the tension cut-off criterion only has a little influence, see figure 5 of Appendix 1. Like it is generally accepted the large experimental scatter on direct tensile tests makes any clear conclusions difficulty.

The second line, that is termed the *Coulomb line* in figure 2.3, is similar to the Coulomb criterion normally applied to concrete. Like it is mentioned previously an observed difference between HSC and NSC is, that the crack zones of HSC do not necessarily follow the interfaces between mortar and aggregates, but develop through the stones. Thus, the angle of friction is decreased like it is observed in several triaxial experiments. The interception of the σ_1/f_c-axis at $\sigma_3 = 1.5f_c$ in figure 2.2 is an apparent uniaxial strength increase. This increase is an indication of the fact, that in case of a perfect material without flaws, the uniaxial strength would be about 50 % higher, than what is actually observed.

The reason why the cracked strength criterion is only experimentally visible for certain test series on HSC (and compresit) is probably the following. For NSC it is hard to detect any bi-linear behaviour because the transition stress σ_3^* of eq. (2.4) is close to zero. It is well-known, that the uniaxial tensile strength of concrete does not increase at the same rate as the uniaxial compressive strength, when we pass from NSC to HSC. This means that the Coulomb line moves outwards along the τ-axis at a higher rate than the cracked strength line, when f_c is increased, cf. figure 2.3. Furthermore the presence of experimental scatter does not encourage testing of the behaviour at rather small confinement pressures.

It is expected, that the *fibre reinforcement* of compresit matrix decreases the brittle behaviour under compression like in the uniaxial case, but the tests do not support this. The uniaxial compressive behaviour of a plain compresit matrix without fibres and a fibre reinforced ditto is very different: the plain cylinder shows almost explosive failure, while the fibre reinforced cylinder keeps its coherence after failure. In Chapter 3 of Part I this behaviour is investigated, where it is found, that the energy dissipation is increased significantly by the presence of fibres. However, in triaxial compression the fibres do not seem to avoid the initial cracked strength failure criterion. Thus, there is still a transition from brittle strength behaviour towards a more ductile Coulomb behaviour even though 6 % steel fibres are applied.

2.4 Energy dissipation in lines of discontinuity

In order to utilize the failure criterion in *upper bound solutions*, where the work equation is applied, we must be able to express the internal energy dissipation. The presentation only considers the cases of plane stresses and plane strains, which are the most important. The solutions for the modified Coulomb criterion are originally due to Jensen (1977), see also Jensen (1975).

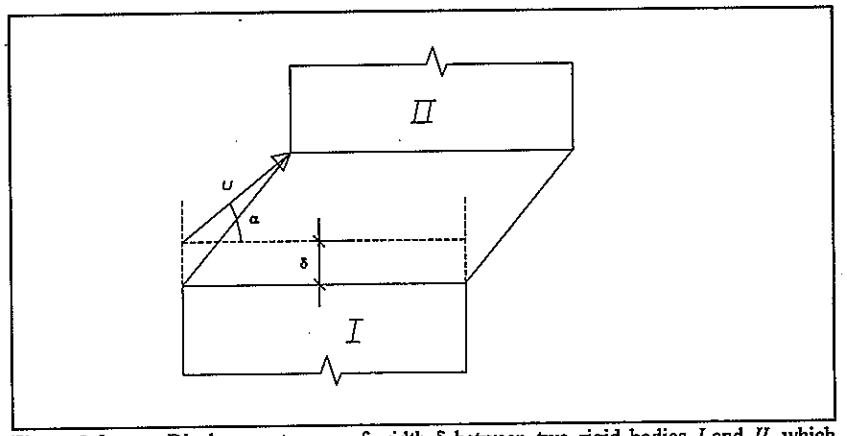

Figure 2.5: Displacement zone of width δ between two rigid bodies *I* and *II*, which move relatively to each other corresponding to the *u*-vector.

Like it is mentioned in Section 2.1.1 a geometrically possible failure mechanism is constructed from rigid bodies, that move relatively to each other, i.e. there exist geometrical discontinuities. In figure 2.5 such a displacement discontinuity between two rigid bodies, denoted *I* and *II*, is outlined.
It is assumed that *II* moves relatively to *I* according to a displacement vector with length *u* and inclination α, see figure 2.5. Furthermore the deformations are assumed to be *homogeneous* within a displacement zone of width δ. In the following the strains are defined *positive as compression* similar to the normal stresses. By means of the transformation rules for plane strains the principal strains in the displacement zone are written as

$$\left.\begin{matrix}\epsilon_1\\ \epsilon_2\end{matrix}\right\} = \frac{u}{2\delta}(\pm 1 - \sin\alpha)\,, \qquad -90^\circ \le \alpha \le 90^\circ \tag{2.5}$$

The energy dissipation occurs solely along the displacement zones and the dissipation per unit volume reads $W = \varepsilon_1\sigma_1 + \varepsilon_2\sigma_2 + \varepsilon_3\sigma_3$. In case of plane stresses or strains one of the 3 terms is always zero, which is utilized in the following. In figure 2.6 the trace of the yield

surface is depicted in the σ_1 - σ_2 plane for both plane stress and plane strain conditions. It is important to note, that the condition $\sigma_1 \geq \sigma_2 \geq \sigma_3$ does not necessarily apply to this diagram.

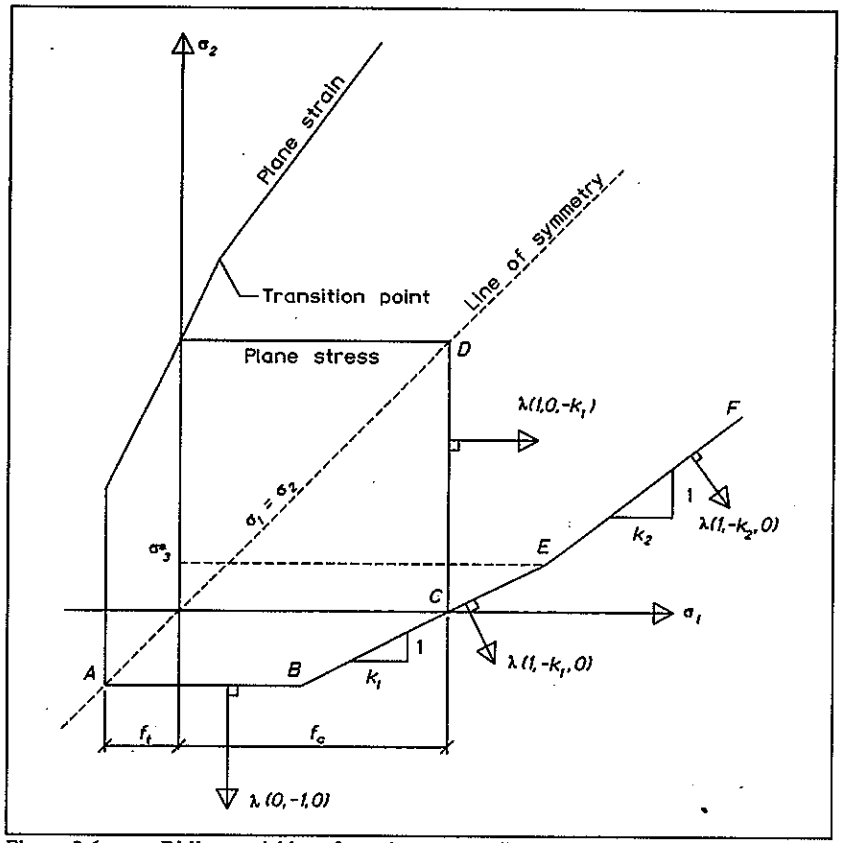

Figure 2.6: Bi-linear yield surfaces in σ_1 - σ_2 diagram for both plane stresses and plane strains.

The line corresponding to the letters *A* - *B* - *C* - *D* corresponds to *plane stresses*, while the line *A* -*B* - *E* - *F* represents *plane strain* conditions. The strain vectors are given along these lines according to the normality condition, cf. eq. (2.2). The strain vectors at the points *B*, *C* and *E* are constructed as linear combinations of those corresponding to the adjacent lines. Point *E* is the transition point between the cracked strength criterion and the Coulomb criterion. In table 2.1 a survey of the conditions in figure 2.6 is given.

Region	Failure criterion	Displacement angle	Conditions
A - *B*	Tension cut-off	$\alpha = 90°$	Plane stress Plane strain
B	-	$\varphi_1 \leq \alpha \leq 90°$	Plane stress Plane strain
B - *C*	Cracked strength	$\alpha = \varphi_1$	Plane stress Plane strain
C	-	$-90° \leq \alpha \leq \varphi_1$	Plane stress
C - *D*	Compression	$\alpha = -90°$	Plane stress
C - *E*	Cracked strength	$\alpha = \varphi_1$	Plane strain
E	-	$\varphi_2 \leq \alpha \leq \varphi_1$	Plane strain
E - *F*	Coulomb	$\alpha = \varphi_2$	Plane strain

Table 2.1: Conditions for the regions in figure 2.6.

In case of plane stresses the major principal stress never exceeds the uniaxial compressive strength because the intermediate principal stress does not influence the triaxial strength. In case of plane strains we follow the Coulomb line, when the compressive stresses increase, and the normality condition gives a *lower limit* for the displacement angle α equal to φ_2.

The energy dissipation in case of plane stress or strain yields

$$W = \epsilon_1\sigma_1 + \epsilon_2\sigma_2 = \frac{u}{2\delta}((1-\sin\alpha)\sigma_1 - (1+\sin\alpha)\sigma_2) \tag{2.6}$$

where eq. (2.5) is inserted. In order to calculate the energy dissipation per unit length of the displacement zone we apply $W_l = W\delta t$, where t is the thickness of the displacement zone perpendicular to the plane of figure 2.5. Thus, the width δ of the displacement zone vanishes and the displacement zone is reduced to a *line of discontinuity*, where the energy dissipation is concentrated according to the dissipation W_l.

Along the lines *B* - *E* and *E* - *F* in figure 2.6 the energy dissipation is independent of the actual stress values. For instance by inserting eqs. (2.3) into eq. (2.6) along *B* - *E* we obtain

$$\begin{aligned} W_l = W\delta t &= \frac{u}{2\delta}((1 - \sin\varphi_1)(k_1\sigma_2 + f_c) - (1 + \sin\varphi_1)\sigma_2)\delta t \\ &= \frac{ut}{2}(1 - \sin\varphi_1)f_c \end{aligned} \tag{2.7}$$

Thus, it is sufficiently to calculate the energy dissipation according to the points B, C and E in order to express W_l as a function of α, which is done in the following.

Plane stress conditions. In point B we have $\sigma_1 = f_c - k_1 f_t$ and $\sigma_2 = -f_t$ and by inserting these values into eq. (2.6) the dissipation energy reads

$$W_l = \frac{ut}{2}(\lambda - \mu\sin\alpha)f_c \,, \quad \varphi_1 \le \alpha \le 90° \tag{2.8}$$

where the parameters λ and μ are defined as

$$\lambda = 1 - \frac{f_t}{f_c}(k_1-1) \,, \qquad \mu = 1 - \frac{f_t}{f_c}(k_1+1) \tag{2.9}$$

In point C we have $\sigma_1 = f_c$ and $\sigma_2 = 0$, which give

$$W_l = \frac{ut}{2}(1 - \sin\alpha)f_c \,, \quad -90° \le \alpha \le \varphi_1 \tag{2.10}$$

In the special case of zero tension cut-off ($f_t = 0$), i.e. the socalled *square yield locus*, we have $\lambda = \mu = 1$. In this case eqs. (2.8) and (2.10) are identical, i.e. eq. (2.10) applies for the whole range of the displacment angle α.

Plane strain conditions. The solution for point B is identical to eqs. (2.8) and (2.9). For the transition point E we have $\sigma_1 = f_c + k_1\sigma_3^*$ and $\sigma_2 = \sigma_3^*$ and the dissipation energy reads

$$W_l = \frac{ut}{2}(\lambda^* - \mu^*\sin\alpha)f_c \,, \quad \varphi_2 \le \alpha \le \varphi_1 \tag{2.11}$$

where the parameters λ^* and μ^* are defined as

$$\lambda^* = 1 + \frac{\sigma_3^*}{f_c}(k_1-1) \,, \qquad \mu^* = 1 + \frac{\sigma_3^*}{f_c}(k_1+1) \tag{2.12}$$

A simple control of the expressions shows, that W_l from eq. (2.8) is identical to W_l from eq. (2.11) at $\alpha = \varphi_1$, viz. $W_l = utf_c(1-\sin\varphi_1)/2$.

In figure 2.7 the linear variation of the 4 parameters in eqs. (2.9) and (2.12) is given. These parameters have the following physical meaning. The *center* and the *radius* of the Mohr circle, normalized with respect to the compressive strength f_c, that tangent both the cracked strength line and the line corresponding to tension cut-off, are given by $\lambda/2$ and $\mu/2$ respectively. Likewise the circle, that tangent the cracked strength line and the Coulomb line

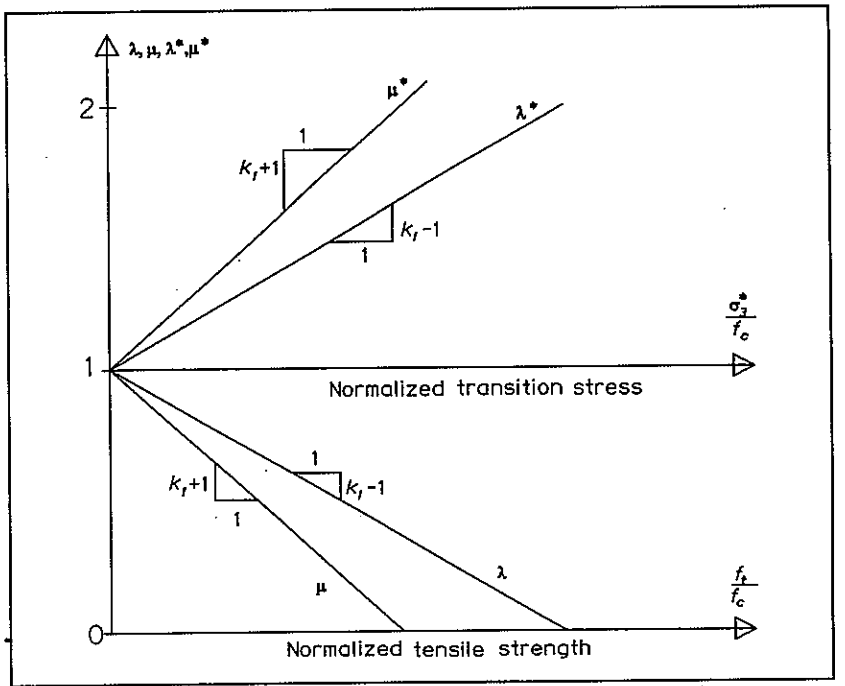

Figure 2.7: Variation of the parameters defined in eqs. (2.9) and (2.12).

has center and radius equal to $\lambda^*/2$ and $\mu^*/2$ respectively.

2.4.1 Practical use of the bi-linear failure criterion

This section includes both a parameter study of the dissipation energies given in eqs. (2.8) - (2.12) and a practical evaluation of the bi-linear criterion compared to the normal approach.

The modified Coulomb criterion exists as a special case of the bi-linear criterion. If the two angles of friction in the bi-linear failure criterion are identical ($\varphi_1 = \varphi_2 = \varphi \Leftrightarrow k_1 = k_2 = k$), then the dissipation energy formulas correspond exactly to those of the modified Coulomb criterion, see e.g. Nielsen (1984) and Jensen (1977).

It is recalled, that the normal value of φ in the *modified Coulomb criterion* is experimentally determined approximately 37° for NSC, while tests on both compresit matrix and HSC indicate, that $\varphi_1 \approx 51°$ and $\varphi_2 \approx 30°$ with the transition point given as $\sigma_3^* \approx 0.1f_c$ seem to be a fair suggestion. In figure 2.8 and 2.9 these values are inserted in the energy dissipation

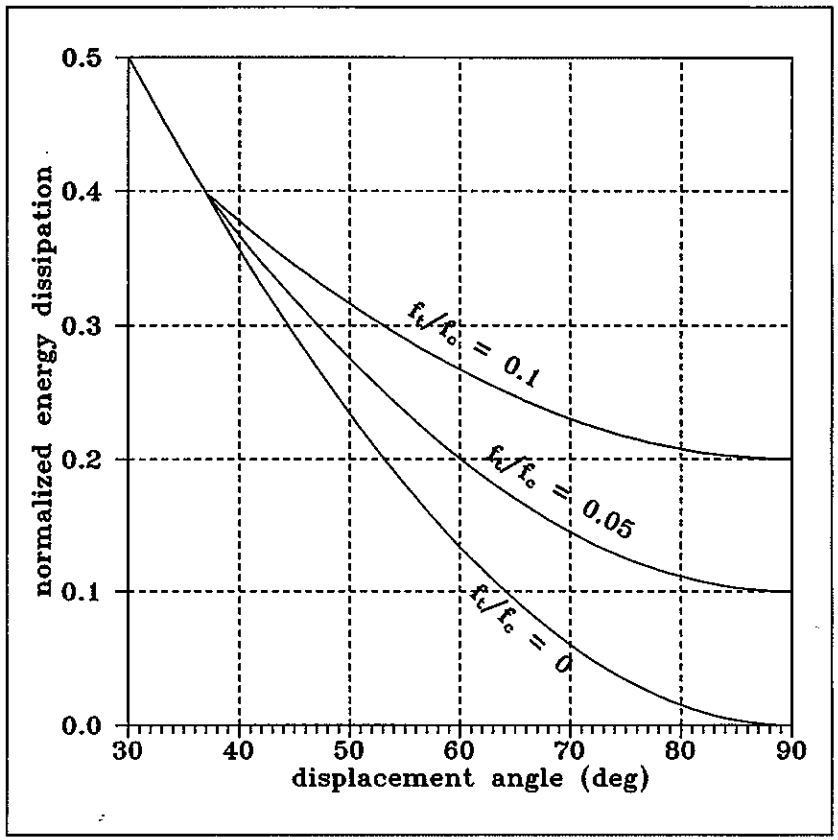

Figure 2.8: Normalized energy dissipation $2W_i/(utf_c)$ from eq. (2.8) with $\varphi_1 \approx 37°$, i.e. corresponding to the modified Coulomb criterion.

formulas to compare the normal approach and the bi-linear proposal for *plane strain* conditions.

For the modified Coulomb criterion the energy dissipation is controlled by the *tensile strength*, when the displacement angle α exceeds $\varphi \approx 37°$. This also applies to the bi-linear criterion for the range $\varphi_1 \approx 51° \leq \alpha \leq 90°$, see figure 2.9. However, when the displacement angle α is less than $\varphi_1 \approx 51°$ the energy dissipation is controlled solely by the *transition stress* σ_3^*. Figure 2.9 shows great sensitivity with respect to σ_3^*. Therefore it is expected, that upper bound solutions, where small values of α are essential to the correct solution, may show significant difference between the two criteria. It is noted, that in case of plane

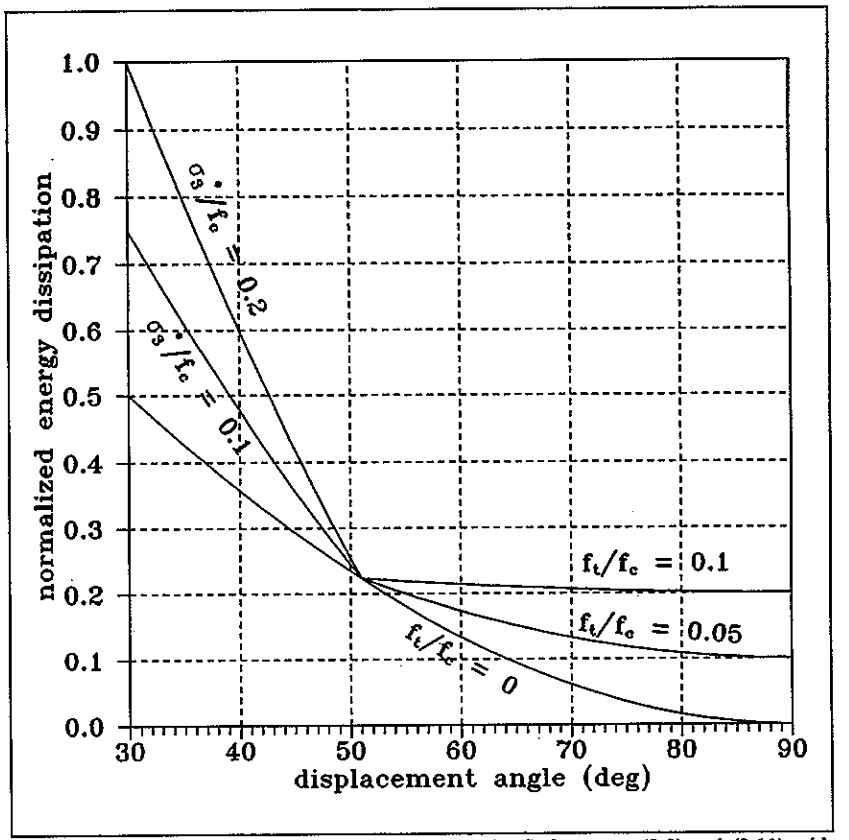

Figure 2.9: Normalized energy dissipation $2W_i/(utf_c)$ from eqs. (2.8) and (2.11) with $\varphi_1 \approx 51°$ and $\varphi_2 \approx 30°$.

stress conditions the difference between the two criteria is modest because the transition stress does not influence this particular case.

In figure 2.10 the modified Coulomb criterion and the bi-linear criterion is compared in a Mohr stress diagram normalized with respect to f_c. For tensile minor principal stresses the modified Coulomb criterion gives higher capacities than the bi-linear criterion, whereas this is reversed for compressive minor principal stresses. Because of the difference in angle of friction this is again reversed for high compressive stresses. However, the differences are modest and they obviously change with the actual value of the transition stress σ_3^*. Taking into account, that the cracked strength criterion is subject to great experimental scatter it

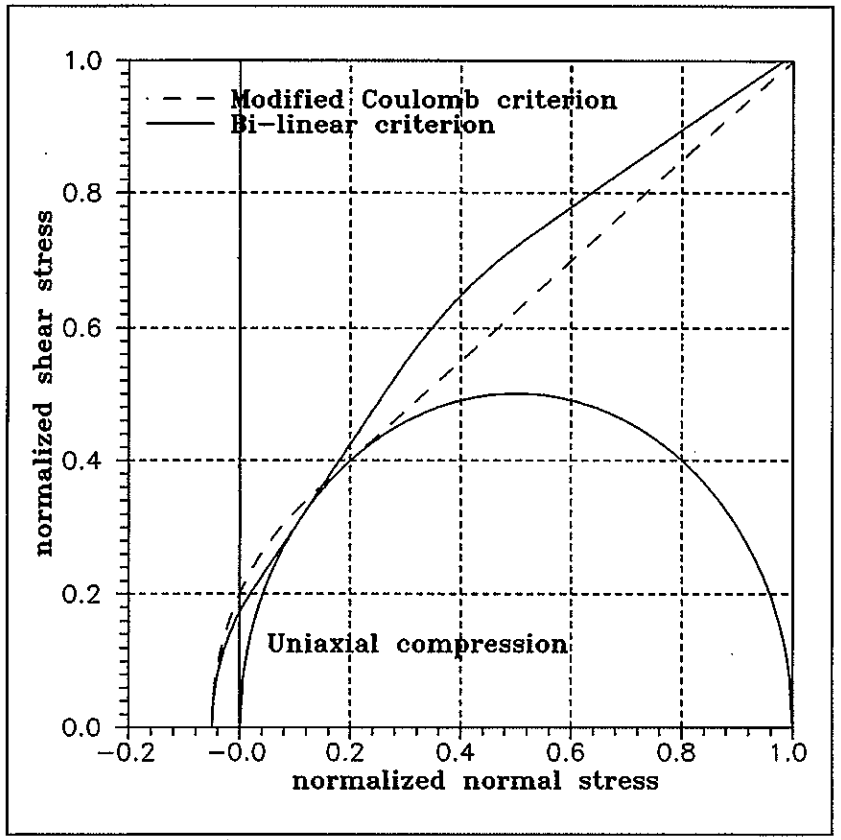

Figure 2.10: Mohr diagram normalized with respect to f_c, including both the modified Coulomb criterion and the bi-linear criterion. Note that $f_t/f_c = 0.05$.

seems reasonable to keep utilizing a Coulomb criterion together with a single-valued φ for practical purposes.

In the following example a simple plastic upper bound solution is given for uniaxial compression of a concrete prism under plane strain conditions. The example is based on Jensen (1975) and it points out some of the differences between the normal approach and the bi-linear model.

Example 2.1: Load capacity of a concrete prism. In figure 2.11 the problem is outlined with a prism loaded by the stress p over the width b. The upper part moves u along the straight discontinuity line, which is inclined β with horisontal.

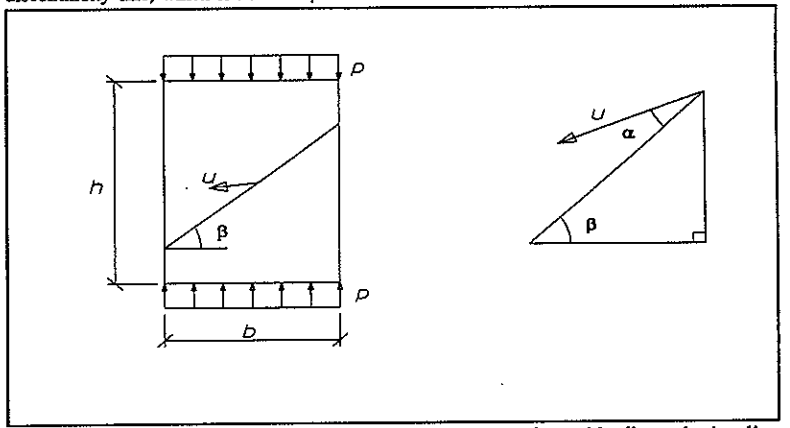

Figure 2.11: Concrete prism loaded under plane strains with discontinuity line inclined the angle β with horisontal.

The vertical displacement is $u\sin(\beta-\alpha)$ and the external work per unit thickness reads

$$W_{ex} = pbu\sin(\beta-\alpha) \tag{2.13}$$

The discontinuity line has the length $b/\cos\beta$ and the internal dissipation energy is

$$W_{in} = \frac{f_c bu}{2\cos\beta}\begin{cases}\lambda - \mu\sin\alpha\,, & \varphi_1 \le \alpha \le 90^\circ \\ \lambda^* - \mu^*\sin\alpha\,, & \varphi_2 \le \alpha \le \varphi_1\end{cases} \tag{2.14}$$

per unit thickness, where eqs. (2.8), (2.9), (2.11) and (2.12) are applied. The geometrical restrictions on the angle β are $\alpha \le \beta \le \arctan(h/b)$. By imposing the *work equation* $W_{ex} = W_{in}$ we obtain

$$\frac{p}{f_c} = \frac{1}{2\cos\beta\,\sin(\beta-\alpha)}\begin{cases}\lambda - \mu\sin\alpha\,, & \varphi_1 \le \alpha \le 90^\circ \\ \lambda^* - \mu^*\sin\alpha\,, & \varphi_2 \le \alpha \le \varphi_1\end{cases} \tag{2.15}$$

from which we seek the smallest load capacity by altering the angles within their ranges.

A differentiation of the denominator of eq. (2.15) with respect to β yields a maximum value of (1-sinα) for $\beta = 45^\circ + \alpha/2$. After inserting these values into eq. (2.15) and differentiating with respect to α we get

$$\frac{d}{d\alpha}\left(\frac{p}{f_c}(\beta = 45° + \alpha/2)\right) = \frac{\cos\alpha}{(1-\sin\alpha)^2}\begin{cases}\lambda - \mu, & \varphi_1 \le \alpha \le 90° \\ \lambda^* - \mu^*, & \varphi_2 \le \alpha \le \varphi_1\end{cases} \quad (2.16)$$

The parameters outlined in figure 2.7 give $\lambda-\mu = 2f_t/f_c$ (≥ 0) and $\lambda^*-\mu^* = -2\sigma_3^*/f_c$ (≤ 0) and together with the fact, that $\cos\alpha \ge 0$, we have opposite signs on $d(p/f_c)/d\alpha$, corresponding to the 2 α-ranges in eq. (2.16).

For $\varphi_1 \le \alpha \le 90°$ the capacity increases with α and for $\varphi_2 \le \alpha \le \varphi_1$ it decreases. Thus the lowest capacity corresponds to $\alpha = \varphi_1$ and $\beta = 45° + \varphi_1/2$ and the correct upper bound solution is $p/f_c = 1$ as it should be.

If instead the modified Coulomb criterion is applied the final solution gets identical, but only the first range of eqs. (2.14) - (2.16) exists.

For upper bound solutions similar to the above example, where the displacement angle is not restricted by external limits the optimal α is expected to equal the initial angle of friction φ_1 and the presence of φ_2 has no influence. However if the displacements are forced to occur under angles below φ_1, e.g. like it is the case of punching shear failure and pull-out of an embedded reinforcement bar, then both lines of the bi-linear criterion is involved. It is recalled that under plane strains, the lower limit $\alpha = \varphi_2$, gives a theoretical limit for the application of the theory of plasticity in order to fulfil the normality condition.

2.5 Concluding remarks

It is experimentally validated, that HSC under multiaxial compression behaves differently from what is normally used for NSC. The behaviour is due to the increased toughness of HSC, which is known to cause *brittle* splitting failure instead of the usual *sliding* failure. However as the confinement stresses increase a transition from the brittle failure mode towards a more ductile mode is observed.

A simple way to model these observations is to consider a *bi-linear* failure criterion, where a relatively high angle of friction is replaced by a smaller value as the confinement pressure increases, cf. figure 2.2. Triaxial experiments on compresit matrix with 6 % fibres together with other experiments on HSC indicate, that an initial angle of friction $\varphi_1 \approx 51°$ is followed by $\varphi_2 \approx 30°$. The transition between these two angles is found to correspond to a confinement stress of approximately 10 % of f_c. However, especially the transition stress value needs further experimental investigation.

An interesting outcome of the triaxial results is, that the presence of steel fibres does not seem to effect the triaxial strength behaviour compared to HSC without fibres. Thus, no influence of fibres on the triaxial strength.

In table 2.2 the *energy dissipation* formulas for lines of discontinuity are summarized for the case of a bi-linear failure criterion. The modified Coulomb failure criterion for NSC corresponds with the special case $\varphi_1 = \varphi_2 = \varphi \approx 37°$.

Range	W_t	Note
$-90° \le \alpha \le \varphi_1$	$0.5(1 - \sin\alpha)utf_c$	Plane stress conditions.
$\varphi_1 \le \alpha \le 90°$	$0.5(\lambda - \mu\sin\alpha)utf_c$	Plane stress and plane strain conditions. λ and μ defined in eq. (2.9).
$\varphi_2 \le \alpha \le \varphi_1$	$0.5(\lambda^* - \mu^*\sin\alpha)utf_c$	Plane strain conditions. λ^* and μ^* defined in eq. (2.12).

Table 2.2: Energy dissipation per unit length discontinuity line under bi-linear failure criterion. The parameters α, t and u are defined in figure 2.5.

The practical use of the bi-linear failure criterion is not expected to replace the existing modified Coulomb expression, which is well-documented throughout the past 20 years. Instead it is assumed to be a supplement to the well-known expressions. In each case it must be assessed, whether a change of the angle of friction, or even an extension to the bi-linear case is profitable for the calculations. Especially in case of HSC these possibilities have to be included in the considerations.

2.6 References

Dahl, K.K.B (1992), *A Failure Criterion for Normal and High-Strength Concrete*, Serie R, No. 286, Department of Structural Engineering, Technical University of Denmark, Lyngby. x + 115 pp.

Horii, H. & S. Nemat-Nasser (1986), 'Brittle Failure in Compression: Splitting, Faulting and Brittle-Ductile Transition', *Philosophical Transactions of the Royal Society of London. Series A, Physical Sciences and Engineering*, Vol. 319, pp. 337-374.

Jensen, B.C. (1975), 'Lines of Discontinuity for Displacements in the Theory of Plasticity of Plain and Reinforced Concrete', *Magazine of Concrete Research*, Vol. 27, No. 92, pp. 143-150.

Jensen, B.C. (1977), *Some Applications of Plastic Analysis to Plain and Reinforced Concrete*, Report No. 123, Institute of Building Design, Technical University of Denmark, Lyngby, 119 pp.

Lahlou, K., P.-C. Aïtcin & O. Chaallal (1992), 'Behaviour of High-Strength Concrete Under Confined Stresses', *Cement & Concrete Composites*, Vol. 14, pp. 185-193.

Nielsen, M.P. (1984), *Limit Analysis and Concrete Plasticity*, Prentice-Hall Inc., Englewood Cliffs, New Jersey, xii + 420 pp.

Setunge, S., M.M. Attard & P.LeP. Darvall (1993), 'Ultimate Strength of Confined Very High-Strength Concretes', *ACI Structural Journal*, Vol. 90, pp. 632-641.

3. Bending of slender beams

This chapter concerns the behaviour of beams subjected to bending. The beams are *simply supported* and loaded perpendicular to the beam axis with a constant load per unit length.

In Section 3.1 some basic considerations, concerning both serviceability limit state (SLS) and the ultimate limit state (ULS), are given with emphasis on FRC and HSC. In Section 3.2 the *ultimate moment* capacity for a *T-beam* with tensile reinforcement bars in its lower side is investigated. The *serviceability limit state* in Section 3.2 concerns both deflection demands together with stress limits in order to prevent concrete cracking and crushing.

Finally the special applications of *compresit beams* are considered in Section 3.4 with comparison to both HSC and NSC beams. Emphasis is put on relatively slender beams because this is expected to be one of the future tasks for application of high-quality concrete into structural elements.

3.1 Background

For reinforced concrete beams it is well-known, that a very plastic behaviour is observed. A *moment - curvature* relationship of a reinforced concrete beam shows almost linear-elastic behaviour until the mild steel bars start to yield under constant tensile stress. Thereafter the moment - curvature curve gets almost horizontal and the curvature is mutiplied under constant moment. Thus, it seems reasonably to model a concrete cross-section by means of a *plastic hinge*, where the rotational capacity is many times greater than the maximum elastic curvature.

The basic assumption is the *Bernoulli assumption*, which states, that plane cross-sections remain plane and perpendicular to the beam axis during deformations. This assumption is found to be valid in both the ULS and the SLS even though the concrete starts to crack.

Another important assumption to simplify the calculations is, that the *tensile strength* of the concrete is neglected in determining the moment capacity. Thus, in the ULS the stresses on a cross-section are assumed to consist of a compressive stress block over the compression zone together with the tensile stresses in the reinforcement bars. It is assumed, that the cracks in the tension zone of a beam open significantly during yielding and therefore it does not seem plausible to include the tensile stresses due to e.g. aggregate interlock across these bending cracks, when the moment capacity in ULS is analyzed. In case of FRC beams, where fibres are known to cross the cracks, there might be a contribution from the tensile stresses, but they are most significant, when the SLS is considered, like it is shown in the following sections.

3.1.1 Moment - curvature relationship

As a result of the Bernoulli assumption the cross-sectional deformation state is completely determined by knowing the extension of the beam axis together with the slope of the strain distribution over the cross-section. The latter corresponds to the *beam curvature* κ and it is related to the bending moment M through

$$M = E_c I \kappa \tag{3.1}$$

where $E_c I$ denotes the *bending stiffness*. The M - κ relationship of a reinforced concrete cross-section has the following characteristics:

- Linear-elastic until the occurrence of *first cracking*.
- After first cracking the bending stiffness decreases towards the *cracked stiffness*, where only the reinforcement and the compression zone contribute.
- At the socalled *balanced moment* the reinforcement starts to yield and the bending stiffness is reduced to almost zero.
- After *yielding* and eventually *strain-hardening* the beam fails by either concrete crushing, or by rupture of the steel bars.

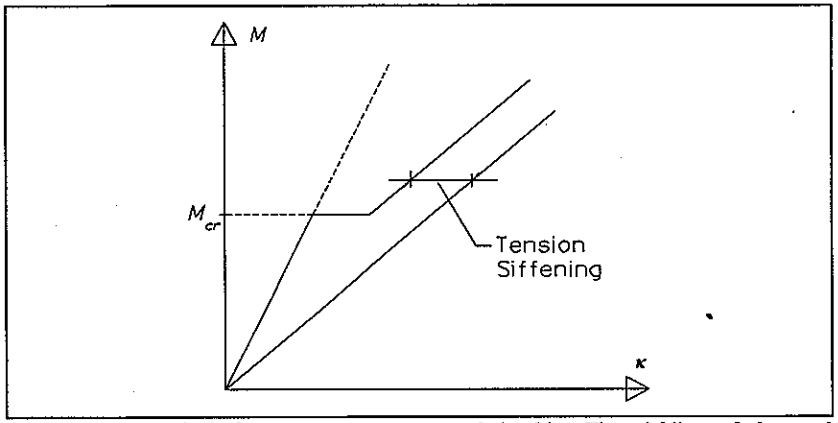

Figure 3.1: Principal moment - curvature relationship. The yielding of the steel reinforcement is not included.

The normal approach is to consider uncracked behaviour, characterized by the initial modulus of elasticity E_c, until the *cracking moment* M_{cr}, which is defined by the tensile bending strength of the material, is reached. Then the M - κ curve follows a *transition curve*

towards the cracked curve. The transition curve never equals the cracked behaviour because the intact concrete in between the cracks has a stiffening effect. In figure 3.1 we have a simple M - κ model, which involves a sudden increase in κ at first cracking, followed by a straight line parallel with the cracked curve, see Favre & Charif (1994). The distance between the cracked and the actual M - κ curve along the κ-axis is termed the *tension stiffening*.

Favre & Charif also include a description of a more complex model, where the tension stiffening is reduced with increasing bending moment according to a hyperbolic law. This type of model forms the basis for most code rules and may include both shrinkage and creep.

Deformational behaviour of FRC beams. There exist several investigations of the flexural deformations and strengths of FRC beams. One of the earliest, including both fibres and conventional reinforcement, is *Henager & Doherty (1976)*, but also *Swamy & Al-Ta'an (1981)* and *Alsayed (1993)* report load - deflection curves of FRC beams. These investigations typically concern fibre contents of $V_f = 0.5$ - 2 % of relatively long steel fibres with aspect ratios ranging from 50 to 100. The general conclusion is, that the ultimate flexural strength is only slightly influenced by the fibres, while the deformational characteristics are improved significantly.

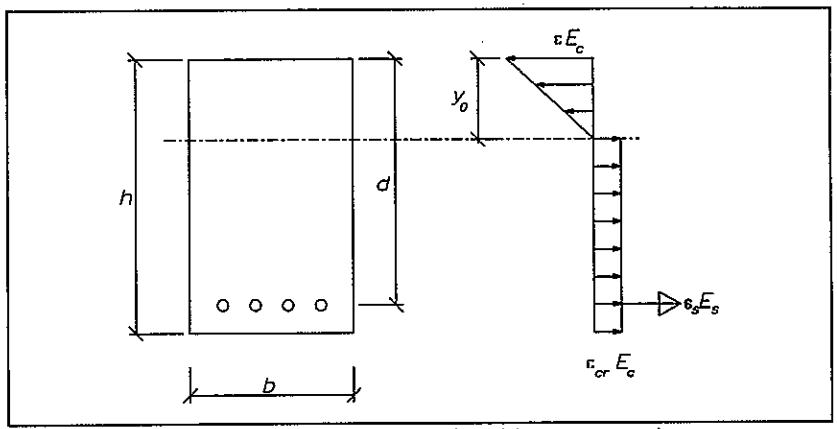

Figure 3.2: Stresses on a cracked fibre reinforced beam cross-section.

Because of the *crack arresting effect* from crossing fibres, the deflections are generally smaller for FRC beams than for plain concrete beams, i.e. the tension stiffening increases. Furthermore both the number of cracks and their widths are reduced considerably. A simple model meant to include the stiffening effect of fibres crossing a crack is outlined in figure 3.2.

The *linear-elastic* solution of pure bending is well-known. The depth y_0 of the neutral line and the moment of inertia are calculated as

$$\left.\begin{aligned} \frac{y_0}{d} &= \frac{1}{2}\frac{(h/d)^2 + 2\alpha\phi}{h/d + \alpha\phi} \\ \frac{I}{bd^3} &= \frac{1}{3}\left(\frac{h}{d}\right)^3 - \frac{h}{d}\frac{y_0}{d}\left(\frac{h}{d} - \frac{y_0}{d}\right) + \alpha\phi\left(1 - \frac{y_0}{d}\right)^2 \end{aligned}\right| \quad \begin{aligned} \alpha &= \frac{E_s}{E_c} \\ \phi &= \frac{A_s}{bd} \end{aligned} \tag{3.2}$$

where the cross-sectional constants are normalized with respect to the beam width b and the effective depth d. The elasticity ratio and the reinforcement ratio are denoted α and ϕ respectively.

When the beam starts to *crack* the normal approach is to take account of only the compressive zone and the steel bars, i.e. the tensile concrete stresses in figure 3.2 are neglected. In that case y_0 corresponds to the position of the crack tip and the expressions in eq. (3.2) read

$$\begin{aligned} \frac{y_0}{d} &= \alpha\phi\left(\sqrt{1 + \frac{2}{\alpha\phi}} - 1\right) \\ \frac{I_{cr}}{bd^3} &= \frac{1}{3}\left(\frac{y_0}{d}\right)^3 + \alpha\phi\left(1 - \frac{y_0}{d}\right)^2 \end{aligned} \tag{3.3}$$

In case of FRC (and compresit matrix) it seems reasonably to utilize a *tensile strain limit*, where the matrix material starts to crack. The following cracking happens under constant tensile stresses provided by the crossing fibres, see figure 3.2. The cracking strain of the matrix is denoted ε_{cr} and until this value is exceeded the expressions in eq. (3.2) are valid.

After first cracking the depth y_0 of the compression zone depends on the compressive strain ε of the upper beam side, see figure 3.2. The equality between the compressive and the tensile forces on the cross-section yields a second order polynomium, that should be solved in order to determine y_0:

$$\left(1 + 2\frac{\epsilon_{cr}}{\epsilon}\right)\left(\frac{y_0}{d}\right)^2 + 2\left(\alpha\phi - \frac{h}{d}\frac{\epsilon_{cr}}{\epsilon}\right)\frac{y_0}{d} - 2\alpha\phi = 0 \tag{3.4}$$

and the corresponding moment of inertia reads

$$\frac{I_{FRC}}{bd^3} = \frac{1}{3}\left(\frac{y_0}{d}\right)^3 + \frac{1}{2}\frac{\epsilon_{cr}}{\epsilon}\left(\frac{h}{d} - \frac{y_0}{d}\right)^2\frac{y_0}{d} + \alpha\phi\left(1 - \frac{y_0}{d}\right)^2 \tag{3.5}$$

In case of normalized parameters the constitutive relation in eq. (3.1) reads

$$\frac{M}{bd^2f_c} = m = \frac{E_c}{f_c}\frac{I}{bd^3}\kappa d, \qquad \kappa d = \frac{\epsilon}{y_0/d} \tag{3.6}$$

where m denotes the normalized bending moment. In figure 3.3 a normalized moment - curvature relationship is depicted, where both the uncracked line, the cracked line and the FRC line are shown.

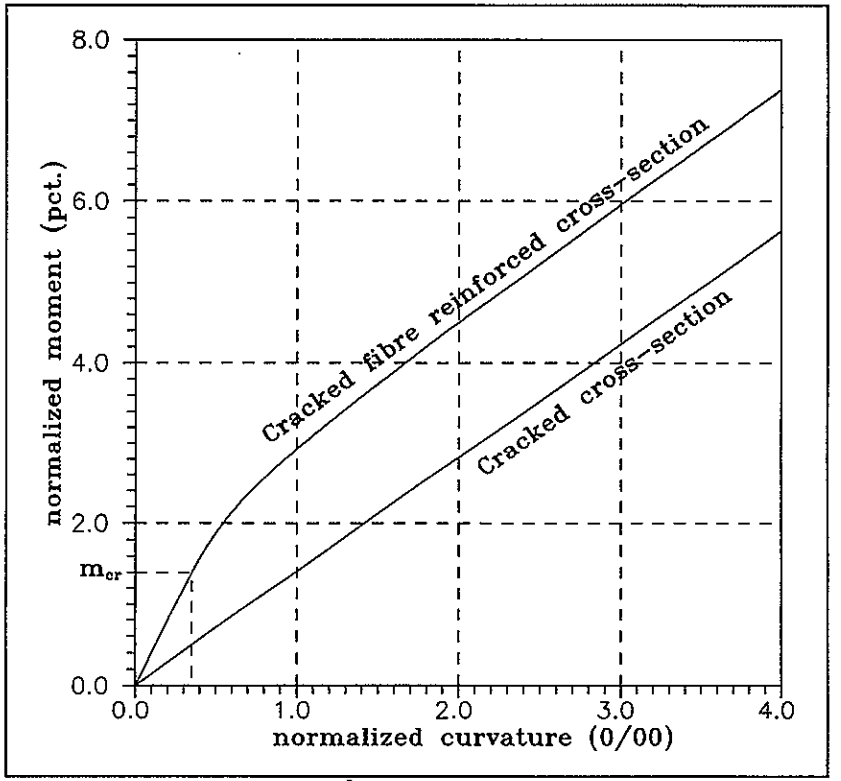

Figure 3.3: Characteristic $M/(bd^2f_c)$ - κd relationship for FRC beam.

At first cracking the *slope* of the FRC curve decreases slowly from the uncracked slope of eq. (3.2) towards the cracked slope of eq. (3.3). This also appears from letting $\varepsilon_{cr}/\varepsilon \to 0$ in eqs. (3.4) and (3.5), which makes the values go towards those of eq. (3.3). Thus, the horizontal distance between the FRC line and the cracked line (the tension stiffening in

figure 3.3) tends towards a constant value. At sufficiently high values of the curvature the vertical distance between the two lines in figure 3.3 is calculated as

$$\frac{\Delta M}{bd^2 f_c} = \Delta m = \frac{\epsilon_{cr}}{2}\left(\frac{h}{d} - \frac{y_0}{d}\right)^2 \frac{E_c}{f_c} \tag{3.7}$$

where y_0/d is taken from eq. (3.3). The *tension stiffening* due to the fibres is estimated as Δm divided by the moment of inertia from eq. (3.3):

$$\Delta\kappa d = \frac{3\epsilon_{cr}}{2} \frac{(h/d - y_0/d)^2}{(y_0/d)^3 + 3\alpha\phi(1 - y_0/d)^2} \tag{3.8}$$

The magnitude of this tension stiffening is proportional to the tensile strength of the concrete through the value ϵ_{cr}, but it decreases significantly with increasing $\alpha\phi$. Thus, the tension stiffening effect of the fibre bridging stresses over the tension zone of figure 3.2 is only significant in case of beams with relatively low contents of conventional reinforcement like it is expected.

In Alsayed (1993) an empirical model is proposed to take the tension stiffening effect of fibres into account. The model proposes a contribution to the bending stiffness, that depends on the square of the fibre reinforcement index and decreases with increasing bending moments. A 3-parameter fitting of test data from both the author's own investigation and data from Swamy & Al-Ta'an (1981) is included. It is recalled, that the fibre reinforcement index is defined by $V_f(L_f/d_f)$.

In Heshe (1988) several compresit beams with 6 % fibres are tested under four-point bending. These beams are reinforced longitudinally with the geometrical reinforcement ratios ϕ exceeding 5 %. A moment - curvature model is applied to the experimental load - deflection data, where the tensile stresses of the matrix are neglected. This simple model seems to fit the experiments satisfactorily even though some experimental scatter exists.

3.1.2 Rectangular stress block

In figure 3.5 both the stress and the strain distribution on a beam cross-section in the ULS are outlined. The normal approach to describe the compressive stress distribution in the compression zone is to assume similarity with the experimental uniaxial stress - strain curve of concrete. From the Bernoulli assumption it is given, that the strains vary linearly from the tensile *steel strain* ϵ_s at the position of the steel reinforcement to the *ultimate compressive strain* ϵ_{cu} at the upper beam side.

The uniaxial stress - strain relationship for concrete under compression is observed in numerous tests and several attempts to describe it analytically are found for instance in

Sargin (1971), cf. Chapter 3 in Part I of the thesis[1]. For design purposes most codes use simplified stress distributions such as the *parabolic - rectangular* stress - strain diagram, see e.g. the eurocode *EC2 (1992)*. Thus, the stresses increase parabolically up to the peak value f_c followed by constant stresses until the strains reach the prescribed compressive strain ϵ_{cu}.

Another popular simplification is to prescribe a *rectangular stress block* as a substitute for the physically correct stress - strain curve, see e.g. the Danish concrete code *DS 411 (1984)* or the American code *ACI 318-89 (1989)*. The principle is to equivalent the correct stress - strain curve with a rigid-plastic rectangular stress block, so that both the resultant compressive force and its position are identical with the actual values.

The two constants c_1 and c_2 determine the rectangular stress block completely. The former constant is defined as the ratio between the actual area under the correct uniaxial stress - strain curve and the area of a rigid-plastic stress block. The rigid-plastic area equals $f_c\,\epsilon_{cu}$, while the actual area is obtained by integration.

The latter constant c_2 is the relative distance from the neutral axis to the centre of gravity of the stress block, divided with the strain corresponding to the *peak stress* ϵ_c.

If the stresses and strains, *normalized* with respect to their values at the peak point, are denoted Y and X respectively, then we get the following expressions for c_1 and c_2:

$$c_1 = \frac{\int_0^{X_{cu}} Y(X)\,dX}{X_{cu}}, \qquad c_2 = \frac{\int_0^{X_{cu}} X\cdot Y(X)\,dX}{\int_0^{X_{cu}} Y(X)\,dX}, \qquad \begin{cases} X = \dfrac{\epsilon}{\epsilon_c} \\ Y = \dfrac{\sigma}{f_c} \end{cases} \tag{3.9}$$

where $X_{cu} = \epsilon_{cu}/\epsilon_c$ is the normalized strain along the upper beam side, which is also the upper limit of the integrations. The analytical stress - strain curve is given by the function $Y(X)$. When the values of c_1 and c_2 are calculated according to a given value of X_{cu}, the moment capacity of an *under reinforced rectangular beam* is given by

$$m = \frac{M}{bd^2 f_c} = \Phi\left(1 - \frac{1 - c_2/X_{cu}\Phi}{c_1}\right) \tag{3.10}$$

where the reinforcement degree Φ is defined in eq. (3.11). The term *under reinforced* means, that the steel bars yield during failure, contrary to the term *over reinforced*, where the compression zone crushes, while the reinforcement steel acts linear-elastic.

[1]Basic Strength Properties of Compresit Matrix.

$$\Phi = \frac{A_s f_y}{bdf_c} = \phi\frac{f_y}{f_c} \tag{3.11}$$

For a given value of the reinforcement degree Φ the moment capacity m in eq. (3.10) varies with X_{cu} and the correct value of X_{cu} is recognized as the one, that maximizes m. This corresponds to the assumption, that the material produces maximum resistance against failure.

In *Exner (1983)* a uniaxial stress - strain relationship of the socalled Sargin type, which includes 4 parameters, is occupied, cf. Sargin (1971), Wang et al. (1978), or see also eq. (3.3) in Part I of the thesis. This relationship is also suggested by the model code CEB (1990). According to the characteristics of a *rigid-plastic* material the ultimate moment capacity in pure bending is given by $m_p = \Phi(1 - \Phi/2)$, assuming that both the concrete and the steel yield under constant stresses until the compression depth $y_0/d = \Phi$ reaches the reinforcement level (i.e. until $y_0 = d$), where the normalized plastic moment capacity m_p equals 1/2.

The investigation reported in Exner (1983) solves the above problem of maximizing m in eq. (3.10) with respect to X_{cu}. Furthermore Exner performs a fitting of the effectiveness factor ν, to be multiplied with f_c in the rigid-plastic solution, in order to obtain the capacity corresponding to the correct stress distribution. The results are included in both Exner (1983) and Nielsen (1984). In the case of *over reinforced beams* Exner concludes, that the correct value of X_{cu} increases compared with the under reinforced case.

Numerical calculations of the rectangular stress block. In order to perform an analysis of the stress distribution for compresit matrix the following simple analytical expression of uniaxial stress - strain relation is applied

$$Y(X) = \frac{\beta X}{\beta - 1 + X^{\beta}}, \qquad \beta \geq 1 \tag{3.12}$$

where the normalized stresses and strains are defined in eq. (3.9). The expresion describes both the ascending and the descending branch, see *Carreira & Chu (1985)* or Section 3.1.1 of Part I for further details. This model is chosen for its simplicity and ability to model most concrete types satisfactorily with only one parameter. The parameter β primarily controls the descending branch, where increasing values increases the steepness of the post peak behaviour.

Table 3.1 summarizes the input parameters to be used for various concrete types and qualities. The values are taken from Chapter 3 of Part I of the thesis and it is emphasized, that because of the experimental scatter on the test results, they should be used with care. However the accuracy is assumed to be sufficient for practical use.

Concrete type	Strength f_c (MPa)	Peak strain ε_c (‰)	Parameter β
NSC	< 40	2	2
HSC	up to 100	2 - 3	8
Compresit matrix	150	4 - 5	4

Table 3.1: Suggested input parameters to the analytical expression of the uniaxial compressive stress - strain curve defined in eq. (3.12).

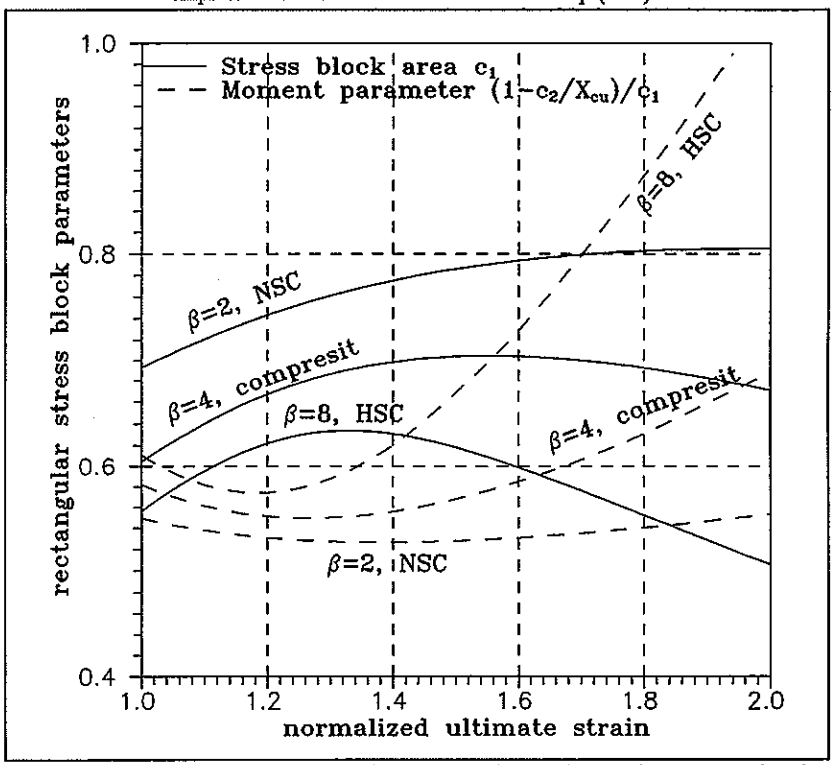

Figure 3.4: Variation of stress block parameters in eqs. (3.9) and (3.10) as a function of $X_{cu} = \varepsilon_{cu}/\varepsilon_c$ for 3 different types of concretes, cf. table 3.1.

In *figure 3.4* the constant c_1 of eq. (3.9) is calculated by means of numerical integration for the 3 values of β in table 3.1 together with values of the parameter $(1 - c_2/X_{cu})/c_1$ of eq.

(3.10). The latter controls the moment capacity and it shows a minimum value, when m has its maximum.

For NSC the *Danish code DS 411 (1984)* prescribes a stress block of magnitude f_c acting over 80 % of the compression depth. The ultimate strain ε_{cu} is prescribed at a constant value of 3.5 ‰, i.e. $X_{cu} \approx 3.5/2 = 1.75$ for NSC according to DS 411 (1984). From figure 3.4 the minimum for $(1 - c_2/X_{cu})/c_1$ is not found to be very distinct for NSC and the error introduced by not choosing the value of X_{cu}, that corresponds to the exact minimum value is minor. The code values of $X_{cu} = 1.75$ and $c_1 = 0.8$ seem reasonably from the NSC curves with $\beta = 2$ in figure 3.4.

For the compresit and the HSC curves in figure 3.4 the minimum for $(1 - c_2/X_{cu})/c_1$ gets more pronounced as β increases. In case of *HSC*, where the peak strain ε_c is only increased slightly compared to NSC, the minimum occurs at $X_{cu} \approx 1.2$ (i.e. $\varepsilon_{cu} \approx 2$ - 3 ‰) and c_1 should be in the vicinity of 0.65.

For the *compresit* curves in figure 3.4 a value of $X_{cu} \approx 1.5$ (i.e. $\varepsilon_{cu} \approx 6$ ‰) seems appropriate together with $c_1 = 0.7$. However, the presence of steel fibres in the compresit matrix, which ensures its coherence, makes it plausible to suggest a full utilization of the compression zone (i.e. $c_1 = 1$) without the risk of sudden failures caused by explosive spalling.

Finally it is noted, that *ACI 318-89 (1989)* only permits rectangular stress blocks of magnitude $0.85f_c$ acting over 65 - 85 % of the compression zone. The extent of the stress block decreases with increasing concrete strength. Furthermore a constant value of $\varepsilon_{cu} = 3$ ‰ is prescribed. The effect of limiting the magnitude of the stresses is to make the centre of gravity of the stress block and the actual stress distribution correlate better.

In the following ULS expressions for the bending carrying capacity the rectangular stress block method is applied with the parameters suggested in the present section. Thus, the approach does not strictly follow the theory of plasticity, or includes the effectiveness factor ν on the uniaxial compressive strength.

3.2 Ultimate limit state

3.2.1 Ultimate moment capacity of T-beam cross-section

In figure 3.5 the geometrical and statical conditions for a cross-section, subjected to an ultimate combination of moment and normal force, are outlined. It is assumed, that the moment M and the normal force N are positive as shown and they act in the mid-point of the cross-section. Like it is previously described the compressive stresses of the concrete are assumed to be equivalent to its uniaxial stress - strain curve. The maximum compressive

strain at the upper side is denoted ε_{cu} and by means of geometrical equivalence the tensile strains of the steel bars in depth d are given by

$$\epsilon_s = (d/y_0 - 1)\epsilon_{cu} \tag{3.13}$$

The following calculations assume a *rectangular stress block* of magnitude f_c, acting over the depth $c_1 y_0$, where y_0 is the depth of the compression zone, cf. the previous section. Furthermore an eventual *prestress* of the steel bars is included by means of an additional strain ε_{pre}, which is added to the strain ε_s originating from the bending action.

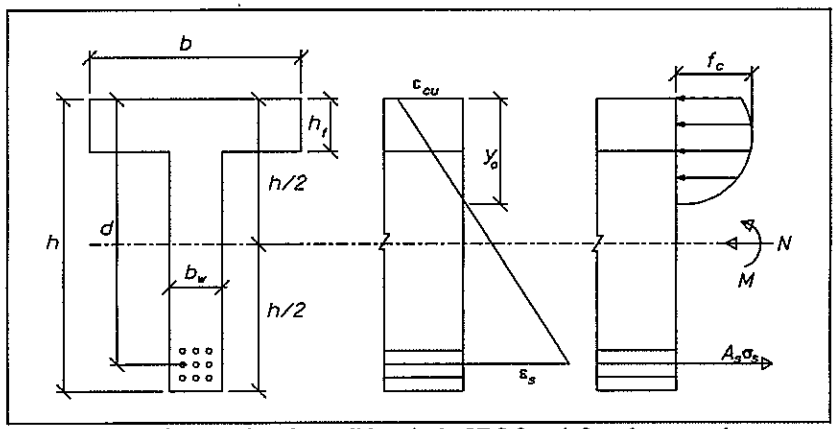

Figure 3.5: Stress and strain conditions in the ULS for reinforced concrete beam cross-section under combined bending and compression.

The *balanced situation*, which makes the transition from the under reinforced cross-section to the over reinforced cross-section, is given by

$$\epsilon_s + \epsilon_{pre} = \epsilon_{sy} \quad \Leftrightarrow \quad \frac{y_0}{d} = \frac{\epsilon_{cu}}{\epsilon_{cu} + \epsilon_{sy} - \epsilon_{pre}} \tag{3.14}$$

where ε_{sy} is the tensile yield strain of the steel bars. In the case of pure bending (i.e. $N = 0$) the socalled *balanced reinforcement degree* is found to equal

$$\Phi_{bal} = \left(1 - \frac{b_w}{b}\right)\frac{h_f}{d} + c_1 \frac{\epsilon_{cu}}{\epsilon_{cu} + \epsilon_{sy} - \epsilon_{pre}} \frac{b_w}{b} \tag{3.15}$$

It is noted that eq. (3.15) and the folowing formulas correspond to *rectangular cross-section*, when $b_w/b = 1$ and $h_f/d = 0$. The cross-sectional dimensions are shown in figure 3.5.

When the cross-section is *over reinforced* the reinforcement does not yield. It is assumed, that the steel bars follow a linear elastic stress - strain curve until yielding, i.e. the *constitutive conditions* for the reinforcement steel read

$$\sigma_s = \frac{f_y}{\epsilon_{sy}}(\epsilon_s + \epsilon_{pre}) \quad \text{for} \quad \epsilon_s + \epsilon_{pre} < \epsilon_{sy}\,, \qquad \sigma_s = f_y \quad \text{for} \quad \epsilon_s + \epsilon_{pre} \geq \epsilon_{sy} \tag{3.16}$$

For the *under reinforced* cross-section the equivalence between M, N and the normal stresses yields

$$\left.\begin{aligned} c_1\frac{y_0}{d} &= \frac{n + \Phi - \left(1-\frac{b_w}{b}\right)\frac{h_f}{d}}{b_w/b} \\ m &= \frac{1}{2}\frac{h}{d}n + \Phi - \frac{1}{2}\frac{b_w}{b}\left(c_1\frac{y_0}{d}\right)^2 - \frac{1}{2}\left(1-\frac{b_w}{b}\right)\left(\frac{h_f}{d}\right)^2 \end{aligned}\right\} \quad n+\Phi \leq \Phi_{bal} \tag{3.17}$$

where the moment and the normal force is normalized with respect to the compressive strength, the beam width and the effective depth according to $m = M/bd^2f_c$ and $n = N/bdf_c$.

For the *over reinforced* cross-section we obtain the compressive depth c_1y_0 as the highest root of a second order polynomium:

$$\frac{b_w}{b}\left(c_1\frac{y_0}{d}\right)^2 + \left[\left(1-\frac{b_w}{b}\right)\frac{h_f}{d} + \Phi\frac{\epsilon_{cu}-\epsilon_{pre}}{\epsilon_{sy}} - n\right]c_1\frac{y_0}{d} - c_1\Phi\frac{\epsilon_{cu}}{\epsilon_{sy}} = 0 \tag{3.18}$$

while the moment capacity is similar to eq. (3.17):

$$m = \frac{1}{2}\frac{h}{d}n + \Phi\frac{\epsilon_s+\epsilon_{pre}}{\epsilon_{sy}} - \frac{1}{2}\frac{b_w}{b}\left(c_1\frac{y_0}{d}\right)^2 - \frac{1}{2}\left(1-\frac{b_w}{b}\right)\left(\frac{h_f}{d}\right)^2\,, \quad \begin{cases} n+\Phi > \Phi_{bal} \\ \dfrac{y_0}{d} \leq 1 \end{cases} \tag{3.19}$$

where c_1y_0/d is the root from eq. (3.18) and ϵ_s is taken from eq. (3.13).

In table 3.2 a survey of the calculations necessary to determine the ultimate moment capacity for a T-beam is given. In the case of the normalized flange depth h_f/d being greater than Φ_{bal} for a rectangular cross-section, calculated by means of eq. (3.15), the balanced state occurs before the compression zone reaches below the flange.

The expressions are easily extended in order to include compression reinforcement. However, the number of restrictions to determine, whether the reinforcement yields or not is increased. The compressive strain ϵ_{sc} of any eventual compressive reinforcement is

determined similarly to eq. (3.13): $\epsilon_{sc} = \epsilon_{cu}(1 - d_c/y_0)$, where d_c is the depth to the compression reinforcement.

<table>
<tr><td colspan="4">Given cross-sectional dimensions and normal force N.</td></tr>
<tr><td colspan="4">Is $\Phi_{bal}(h_f/d = 0,\ b_w/b = 1) \leq h_f/d$?</td></tr>
<tr><td colspan="2">*Yes*, i.e. $\Phi_{bal} = \Phi_{bal}(h_f/d = 0,\ b_w/b = 1)$.</td><td colspan="2">*No*, i.e. $\Phi_{bal} = \Phi_{bal}$ in eq. (3.15).</td></tr>
<tr><td colspan="4">Is $n + \Phi \leq \Phi_{bal}$?</td></tr>
<tr><td colspan="2">*Yes*, i.e. under reinforced.</td><td colspan="2">*No*, i.e. over reinforced.</td></tr>
<tr><td colspan="2">Is $n + \Phi > h_f/d$?</td><td colspan="2">Is c_1y_0/d from eq. (3.18) $> h_f/d$?</td></tr>
<tr><td>*Yes*, i.e. T-beam.</td><td>*No*, i.e. rect. beam.</td><td>*Yes*, i.e. T-beam.</td><td>*No*, i.e. rect. beam.</td></tr>
<tr><td>Equation (3.17).</td><td>Equation (3.17) with $h_f/d = 0$ and $b_w/b = 1$.</td><td>Equations (3.18) and (3.19).</td><td>Equations (3.18) and (3.19) with $h_f/d = 0$ and $b_w/b = 1$.</td></tr>
</table>

Table 3.2: Calculation scheme for a T-beam under combined bending moment M and normal force N. Note that in case of a rectangular beam we have $h_f/d = 0$ and $b_w/b = 1$.

3.2.2 Parameter study of ULS

In figure 3.6 an illustration of the normalized ultimate moment capacity is given for four different beam dimensions (rectangular cross-section and $h_f/d = 0.1$ together with varying web widths b_w/b). The transition points from the under reinforced state to the over reinforced state are also indicated on the m - Φ curves. In the over reinforced state the slope of the curves decreases significantly compared with the under reinforced state. Thus, from an economical point of view it seems reasonably to consider under reinforced conditions in ULS design of beams. The effect of increasing the amount of steel bars is much higher than in the over reinforced case. Furthermore the under reinforced ULS design provides the structure with *safety* against sudden failure. The yielding of the steel bars gives warning of a total collapse.

Like it appears from the previous section the normal force and the reinforcement degree act together in governing the conditions for the ultimate moment capacity. If either the reinforcement degree or the normal force increases the conditions go towards the over reinforced case. Also the strain ϵ_{pre} originating from an eventual prestressing of the reinforcement influences the balanced conditions, see eq. (3.15). In table 3.3 examples of the *balanced reinforcement degrees* are given in case of typical NSC, HSC or compresit, according to the findings of Section 3.1.2.

Parameter	NSC	HSC	Compresit matrix
ε_{cu} (‰)	3.5	3	6
c_1	0.8	0.65	1
Φ_{bal} from eq. (3.15)	0.47	0.35	0.70

Table 3.3: Examples of balanced reinforcement degrees for rectangular cross-section subjected to pure bending. The reinforcement yield strain ε_{sy} equals 2.5 ‰, corresponding to reinforcement bars of mild steel with yield strength in the vicinity of 500 MPa. No prestress is applied.

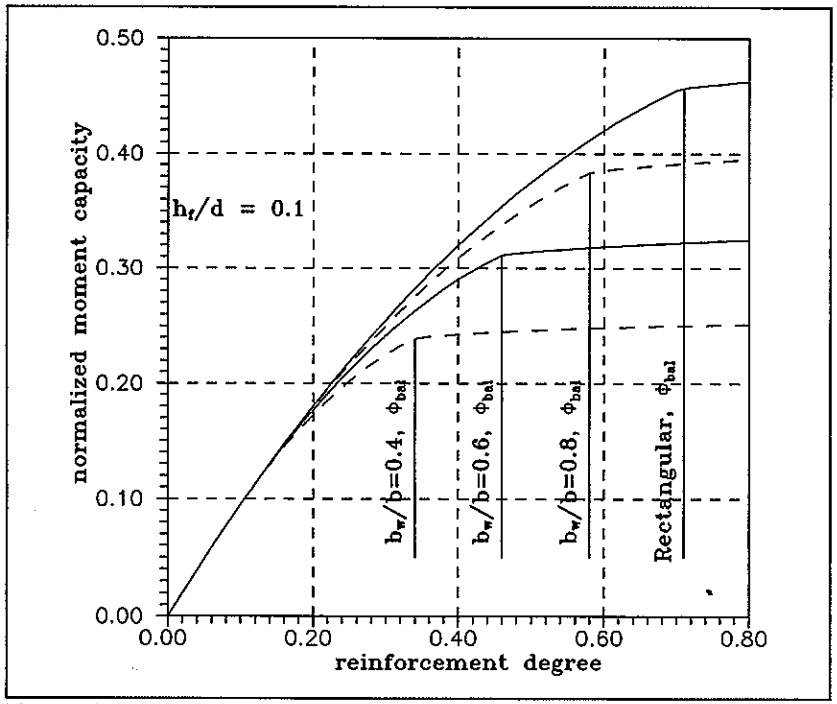

Figure 3.6: Normalized m - Φ relationship for a compresit T-beam with varying web width subjected to pure bending. The flange depth is $h_f = 0.1d$.

It is recalled from eq. (3.11), that the reinforcement degree Φ depends on the strength ratio f_y/f_c. Therefore identical reinforcement ratios for NSC and compresit result in different

values of Φ. The 3 examples of Φ_{bal} in table 3.3 correspond to reinforcement ratios ϕ equal to approximately 5, 7 and 28 % for NSC, HSC and compresit respectively. Like it is shown in the following example there is a need for stronger reinforcement in case of compresit matrix in order to match both its high compressive strength and its ductility.

Example 3.1: Effect of f_c on moment capacity. Consider two beams with identical cross-sections and reinforcement. The concrete strength f_c differs by a factor 4 and thus, the reinforcement degree also differs by a factor 4. In figure 3.7 the ratio between the moment capacities for the two beams is given as a function of realistic amounts of reinforcement (ϕ up to 5 %). Even though the reinforcement degree decreases from the low-strength beam to the high-strength beam, then the absolute value of the moment capacity of the high-strength beam still is higher, than that of the low-strength beam, because of its higher f_c.

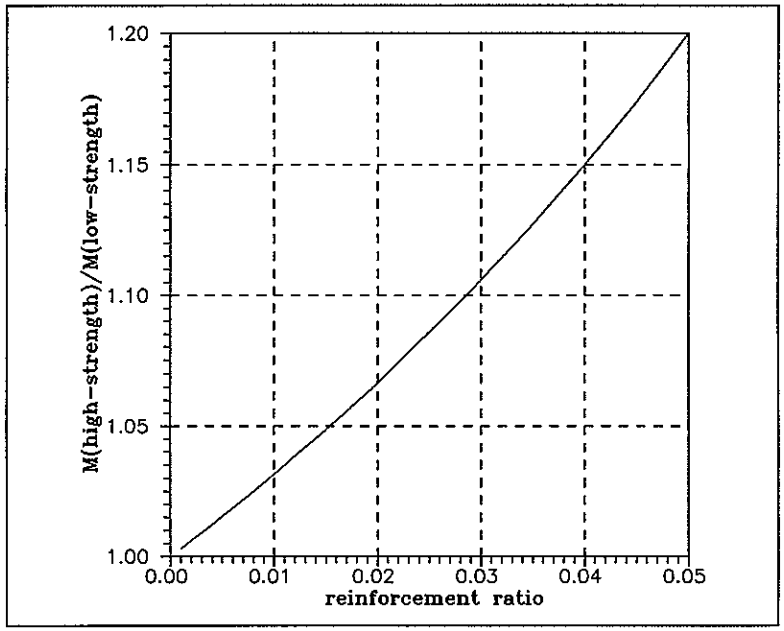

Figure 3.7: Ratio between moment capacities of two beams with f_c differing by a factor 4.

Bearing in mind, that the bending moments in a beam increase with the square of the beam span, it seems obviously, that an increase of the moment capacity of 10-20 % only enables

a marginal increase of the beam span. Thus, no significant strength increase is obtained by simply replacing a low-strength concrete with HSC unless also the reinforcement is changed. A significant increase of the moment capacity (and thereby the beam span) by means of an increase of f_c requires either additional reinforcement, i.e. increased ϕ, or higher steel strength, i.e. increased f_y/f_c. If the reinforcement degrees are identical for two beams the moment capacity increases proportional to the compressive strength increase, i.e. with a factor 4, which enables a doubling of the beam span.

3.3 Serviceability limit state

In the SLS the demands concern both the *maximum deflections* and the *cracking* of the concrete beams. These demands are governed by both *aesthetics* and *durability reasons*. For instance it is required from the Danish Road Directorate, that the maximum deflections of a road bridge should not exceed 1/400 of its span, when it is subjected to the live loads. The dead loads, which are the permanent loads, result in time dependent deflections due to e.g. the creep characteristics of concrete. These *long-term* deflections are often counteracted by means of an initial *upward-directed deflection*, which is slowly reduced. The live loads cause *short-time* deflections to be added to the deflections from the dead loads. It is these additional short-time deflections, that are limited by 1/400 of the span in order to ensure the proper bending stiffness.

The presence of *cracks* in the tensile regions of a beam has several negative effects. For instance the risk of corrosion of the embedded reinforcement steel is increased in cracked concrete. This may be dangerous, especially in aggressive environments, i.e. cracks cause *durability* problems. Furthermore, the presence of cracks has a psychological effect on its users, even though the capacity of the beam is not threatened.

From the constitutive relation in eq. (3.1) it is recalled, that the beam curvature κ depends on the bending stiffness $E_c I$ for a given bending moment. It is known that the concrete *modulus of elasticity* does not increase with the same rate as the compressive strength. In figure 3.8 the dependency of E_c on f_c is taken from DS 411 (1984) and compared with the measurements on compresit matrix, cf. Section 3.2.2 of Part I of the thesis. The modulus of elasticity is only doubled, while the compressive strength is quadrupled from NSC to compresit. Therefore we have reason to believe, that in order to utilize the compressive strength of compresit in the ULS and increase the beam span, the deflections get too high to fulfil the demands in the SLS, if no precautions such as prestressing are taken.

In the following sections various aspects concerning the SLS conditions are treated. A simply supported beam subjected to a *prestress force P* is investigated. It is expected that both concrete and steel act *linear-elastic* in the SLS and that the cross-sectional constants are transformed to take the stiffness of the reinforcement into account.

The prestress force acts horizontally along the beam axis, see figure 3.9, i.e. the case of curved prestress tendons is not included. Furthermore the question whether the tensioning of the tendons is performed before or after casting is not included in the study.

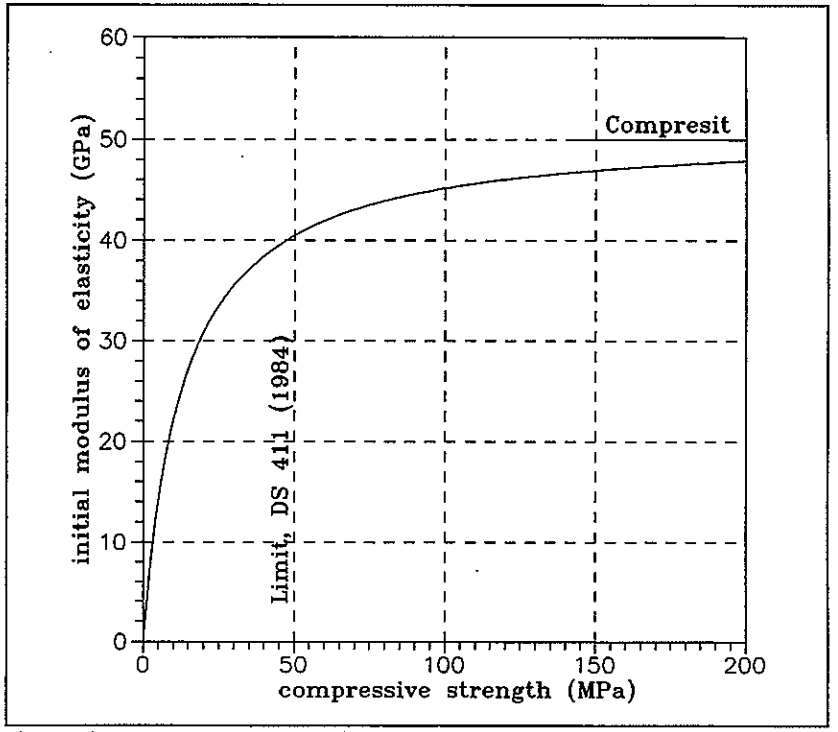

Figure 3.8: Proposed E_c - f_c relationship from DS 411 (1984). Note that the relationship is extrapolated beyond the code limit of f_c = 50 MPa.

3.3.1 Deflections of a simply supported beam

The curvature κ is defined as the negative *second derivative* of the beam deflection δ, i.e. $\kappa = -d^2\delta/dx^2$. The negative sign is due to the assumption, that positive deflections are downward-directed, while positive bending moments give compression in the upper beam side. The constitutive equation in eq. (3.1) gives the relationship between the bending moment and the deflections. When the bending moments within a beam are known the deflection, corresponding to a certain position along the beam axis, is calculated by integrating $M/(E_c I)$ twice and applying the proper boundary conditions.

With a constant load p per unit length of the beam span L we obtain the maximum moment $M_p = pL^2/8$ at mid-span of the simply supported beam. The linear-elastic mid-span *deflection* δ is calculated as

$$\delta = \frac{5}{48}\frac{M_p}{E_c I}L^2 \approx \frac{\kappa L^2}{10}, \quad M_p = \frac{pL^2}{8} \tag{3.20}$$

Uncracked cross-sectional constants for a T-beam. Like in Section 3.1.1 it is assumed, that the reinforcement bars deform according to the surrounding concrete. The *elasticity ratio* between the moduli of elasticity for steel and concrete is denoted $\alpha = E_s/E_c$. The steel stresses are determined by multiplying the concrete stresses, corresponding to the Navier stresses at the position of the steel bars, with the ratio α.

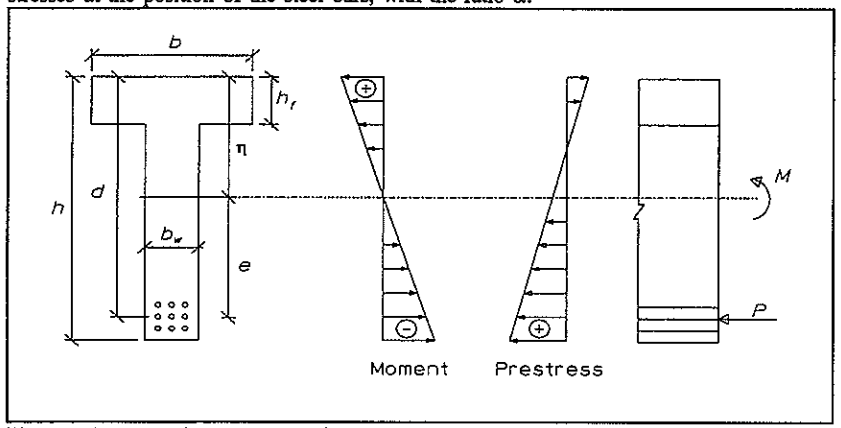

Figure 3.9: T-beam cross-section subjected to the bending moment M and the prestress force P with corresponding stress distributions.

In figure 3.9 a T-beam cross-section is depicted under pure bending with a prestress force P acting from the reinforcement bars. The external moment M acts at the *geometrical center of gravity* of the cross-section, while the prestress force P acts at a distance e from this center. The distance η from the upper beam side to the center of gravity, which is also termed the beam axis, is calculated as

$$\frac{\eta}{d} = \frac{\frac{1}{2}\left(\frac{h}{d}\right)^2\frac{b_w}{b} + \left(1-\frac{b_w}{b}\right)\left(\frac{h_f}{d}\right)^2 + 2\alpha\phi}{\frac{h}{d}\frac{b_w}{b} + \left(1-\frac{b_w}{b}\right)\frac{h_f}{d} + \alpha\phi} \tag{3.21}$$

By comparing η with the depth y_0 of the neutral line in eq. (3.2) it is obvious, that the special case of the rectangular cross-section is obtained with $h_f/d = 0$ and $b_w/b = 1$. The

distance η is not identical with the position of the neutral line because P gives a compressive stress of magnitude P/A_c at the beam axis, cf. figure 3.9.

The geometrical *moment of inertia* around the center of gravity is given by eq. (3.22), which is also found to equal the rectangular case in eq. (3.2), when $h_f/d = 0$ and $b_w/b = 1$:

$$\frac{I}{bd^3} = \frac{1}{12}\left(\frac{h_f}{d}\right)^3 + \frac{1}{3}\frac{b_w}{b}\left(\frac{h}{d}-\frac{h_f}{d}\right)^3 + \frac{h_f}{d}\left(\frac{\eta}{d}-\frac{1}{2}\frac{h_f}{d}\right)^2 - \frac{b_w}{b}\left(\frac{h}{d}-\frac{h_f}{d}\right)\left(\frac{h}{d}-\frac{\eta}{d}-\frac{h_f}{d}\right)\frac{\eta}{d} + \alpha\phi\left(1-\frac{\eta}{d}\right)^2 \tag{3.22}$$

The vertical y-axis is directed downwards from its origin at the beam axis, which goes through the geometrical center of gravity. The normal stresses are calculated by means of the *Navier equation* with contributions from both the bending moment M and the prestress force P:

$$\sigma(y) = \frac{P}{A_c} - \frac{M - Pe}{I}y \tag{3.23}$$

The numerically highest normal stresses, which occur at the upper and the lower beam sides, are calculated by means of the *moment of resistance*. This is denoted W and defined by dividing the moment of inertia with the distance from the beam axis to the beam side in question. In terms of the normalized moment of inertia in eq. (3.22) we get

$$\frac{W_{low}}{bd^2} = w_{low} = \frac{I}{bd^3}\frac{d}{h-\eta}, \quad \frac{W_{up}}{bd^2} = w_{up} = \frac{I}{bd^3}\frac{d}{\eta} \tag{3.24}$$

where the terms w_{low} and w_{up} denote the normalized moments of resistance, corresponding to the lower and the upper beam side respectively. The *core radii* are defined as the moment of resistance divided by the transformed cross-sctional area, i.e. by means of the expressions $k_{low} = W_{low}/A_c$ and $k_{up} = W_{up}/A_c$. If a compressive normal force acts within the core, limited by k_{low} and k_{up} around the beam axis, then the corresponding normal stresses are solely compressive.

Under the assumption, that the cross-sections remain uncracked, the mid-span deflection of eq. (3.20) depends on the *curvature* represented by $\kappa = (M\text{-}Pe)/E_c I$. Thus, the mid-span deflection decreases proportional with the prestress force. However, if the prestressing is too high or low there is a risk, that the cross-section starts to crack. This situation depends on the loads, which are analyzed in the following section.

In case of the uncracked linear-elastic behaviour is assured by means of a proper prestressing, then the SLS deflection demand of maximum $L/400$ from the live loads becomes a rather simple calculation. The *live load* per unit length is denoted q and the

corresponding mid-span bending moment is denoted M_q. Similarly the *dead load p* and the corresponding M_p are defined. The *SLS deflection demand* is written

$$\frac{1}{10}\frac{M_q}{E_c I}L^2 \le \frac{L}{400} \Rightarrow m_q \le \frac{1}{40}\frac{E_c}{f_c}\frac{I}{bd^3}\frac{d}{L}, \qquad m_q = \frac{M_q}{bd^2 f_c} \tag{3.25}$$

where E_c corresponds to the short-term modulus of elasticity. A discussion of both the short-term and the long-term stiffnesses is given in Section 3.3.3.

The inequality in eq. (3.25) shows, that the magnitude of the the prestressing force is not included in the criterion. Only the bending stiffness of the beam is important.

3.3.2 Valid prestress range

There are four demands for the SLS stresses in a beam, corresponding to the upper beam side and the lower beam side subjected to either compression or tension respectively. Like it is previously described the bending moment, corresponding to the dead load p, is denoted M_p and the live load q per unit length gives rise to M_q. The maximum allowable tensile and compressive normal stresses are denoted r_t and r_c respectively in the SLS. First the 4 demands are given in terms of upper and lower bounds for the prestress force P.

Lower beam side. The tensile stresses, corresponding to the total loads M_p, M_q and P, should not exceed r_t to avoid cracking of the concrete:

$$P(k_{low} + e) - (M_p + M_q) \ge -W_{low} r_t \tag{3.26}$$

which gives a *lower bound* for the prestress force.

The compressive stresses, corresponding to the permanent loads M_p and P, should not exceed r_c, which gives an *upper bound* for the prestress force:

$$P(k_{low} + e) - M_p \le W_{low} r_c \tag{3.27}$$

Upper beam side. The tensile stresses, corresponding to the permanent loads M_p and P, should not exceed r_t:

$$P(k_{up} - e) + M_p \ge -W_{up} r_t \tag{3.28}$$

which gives an *upper bound* for the prestress force because the core radius k_{up} is less than e in most practical cases. If on the other hand $k_{up} > e$, then P gives rise to compressive stresses all over the cross-section and the demand is transferred into a lower bound for P.

Finally the compressive stresses, corresponding to the total loads M_p, M_q and P, should not exceed r_c, which gives a lower bound for the prestress force:

$$P(k_{up} - e) + (M_p + M_q) \le W_{up} r_c \tag{3.29}$$

In table 3.4 the 4 demands in eqs. (3.26) - (3.29) are given in terms of the nomalized cross-sectional constants in eq. (3.24). Furthermore the prestress force is normalized according to P/bdf_c.

$\phi\sigma_{pre}/f_c$	Lower bound	Upper bound
Lower beam side	$(m_p + m_q - w_{low} r_t/f_c)/(k_{low}/d + e/d)$	$(m_p + w_{low} r_c/f_c)/(k_{low}/d + e/d)$
Upper beam side	$(w_{up} r_c/f_c - (m_p + m_q))/(k_{up}/d - e/d)$	$-(m_p + w_{up} r_t/f_c)/(k_{up}/d - e/d)$

Table 3.4: Bounds for the normalized prestress force $P/(bdf_c) = \phi\sigma_{pre}/f_c$ in order to avoid concrete crushing and cracking in the SLS. Both w_{up} and w_{low} are defined in eq. (3.24). The normalized mid-span bending moments m_p and m_q correspond to the dead load and the live load respectively.

3.3.3 Parameter study of SLS

Bending stiffness. The *creep characteristics* of concrete result in continuous deformations beyond the initial deformations. If concrete is loaded constantly it continues to deform slowly, i.e. only the permanent loads result in creep. Instead of applying the initial modulus of elasticity, observed from a short-term compression test, to describe the bending stiffness, a reduced *long-term modulus* is suggested to take the creep deformations into account. The elasticity ratio, defined by $\alpha = E_s/E_c$, increases from short-term to long-term conditions, denoted by α_0 and α_∞.

The long-term *creep coefficient* Ψ for concrete denotes the ratio between the long-term deformations and the initial ditto. The increase of α from short-term to long-term conditions is given by $\alpha_\infty = (1+\Psi)\alpha_0$. For *NSC* the short-term elasticity ratio α_0 ranges from 7 to 10 according to DS 411 (1984). Under long-term conditions E_c is reduced to approximately one fourth, i.e. $\Psi \approx 3$ and $\alpha_\infty \approx 30$ for NSC.

For *compresit matrix* the modulus of elasticity is experimentally determined to approximately 50 GPa, see Section 3.2.2 of Part I of the thesis and figure 3.8. There exist only

preliminary creep reults on compresit matrix[2]. The long-term creep coefficient seems to be about one half of what is found for NSC. These findings correspond to those of the two *State-of-the-Art reports ACI 363 (1984)* and *FIP/CEB (1990)* on HSC. They conclude that HSC seems to show *reduced creep strains* compared to NSC, but the test results are rather few. With the short-term modulus E_c ranging from 40 to 50 GPa for *compresit matrix* we have α_0 within the range 4 - 5. A creep coefficient of $\Psi = 1.5$ gives a long-term value of $\alpha_\infty \approx 10$.

The stiffness calculations above use a *steel modulus of elasticity* $E_s = 200$ GPa. It is noted, that steel experiences socalled *relaxation*, when subjected to a constant extension for a long period. Thus, the tensile stresses within a prestress tendon decreases slightly in time. This effect is however not included in the present analysis.

Prestress limits. For a given beam with prescribed cross-section, loading and reinforcement, the limits in table 3.4 depend on the beam span L and on the mechanical properties α, r_t/f_c and r_c/f_c. For each L a valid range for the *normalized prestress force* $\phi\sigma_{pre}/f_c$ exists. In *figure 3.10* a numerical example of these ranges is given, where the valid region determines the combinations of prestressing and beam span, that fulfil the criteria from eqs. (3.26)-(3.29). The lines in figure 3.10 are drawn according to the following parameter values: f_c = 40 MPa, f_y = 1600 MPa, $r_t/f_c = 0.01$, $r_c/f_c = 1$, $\phi = 2.8$ % and $p/q = 1.6$. The horizontal line in figure 3.10 represents the *maximum allowable prestress*, which is chosen as 80 % of the reinforcement yield strength f_y. The socalled *prestress degree* σ_{pre}/f_y, which is the magnitude of the prestresses in the tendons in percent of their yield strength, is related to the normalized prestress force through the expression: $\phi\sigma_{pre}/f_c = \Phi\sigma_{pre}/f_y$.

From the curves in figure 3.10 it appears, that in order to obtain high values of the beam span, the following situations exist:

- The tensile stresses in the lower beam side exceed r_t at $L \approx 3d$, when no prestress is applied. Thus the cracking criterion is very restrictive.

- In order to increase L without violating the *cracking* criterion we impose some prestress. By increasing this prestress to $\Phi\sigma_{pre}/f_y \approx 0.7$ we obtain $L \approx 30d$. At this point the *crushing* criterion at the upper beam side starts to govern the beam span instead of the cracking criterion.

- After this point any further increase of $\Phi\sigma_{pre}/f_y$ has a relatively small effect on the beam span in order to avoid crushing of the upper beam side.

- Finally the amount of prestress is limited by the upper bound for the *prestress degree* σ_{pre}/f_y.

[2]Brite EuRam project Ministruct.

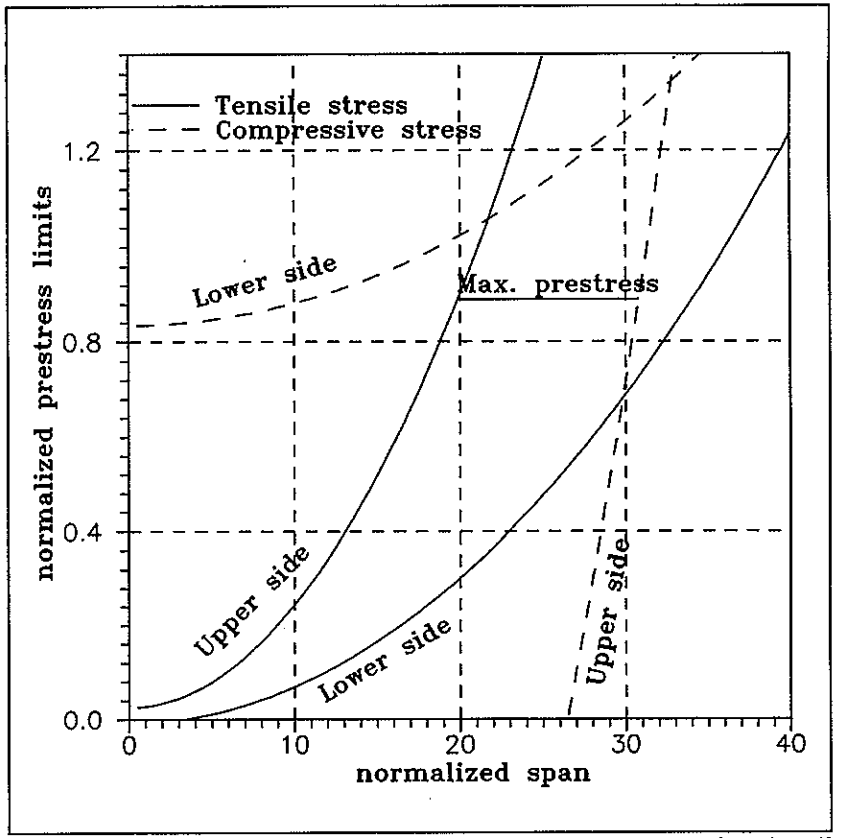

Figure 3.10: Qualitative illustration of limits for the normalized prestress force $\phi\sigma_{pre}/f_c = \Phi\sigma_{pre}/f_y$ as a function of L/d according to table 3.4.

It is noted, that the quantities in figure 3.10 are not general values. They depend on the beam geometry and material properties. However, the curves represent the qualitatively correct behaviour.

The various limits, that exist on the combinations of $\phi\sigma_{pre}/f_c$ and L/d depend on the material parameters according to the following

- The *deflection* demand $u/L \leq 1/400$ in eq. (3.25) gives an upper bound for the span L under a given load situation. It is directly altered by the short-term E_c, but also the reinforcement ratio ϕ influences the demand through the moment of inertia.

- The *stress criteria* for the upper and lower beam side are primarily altered by the allowable SLS stresses r_c and r_t to avoid crushing and cracking. If these stresses are increased the valid region is widened. The reinforcement ratio ϕ and E_c also have some influence through the moment of inertia.

- When q/p increases, e.g. the live load increases, the maximum allowable span gets smaller.

- The *maximum prestress level* depends on the allowable prestress degree and the reinforcement degree Φ, i.e. the reinforcement strength f_y.

3.3.4 Comparison of compresit and NSC in the SLS

As a consequence of the fact, that the brittleness of concrete increases with the compressive strength, the tensile concrete strength f_t is often modelled as being proportional to the *square root* of f_c (DS 411 (1984) prescribes the expression $f_t = \sqrt{(0.1 f_c/\text{MPa})}$). However, for compresit matrix with its high amount of fibres this is not necessarily true. The ratio between f_t and f_c is found to be almost identical for NSC and compresit, even though f_c increases by a factor 4, cf. Section 2.4 of Part I of the thesis. Therefore the tensile stress criteria in table 3.4 are not expected to differ significantly for NSC and compresit (r_t/f_c is practically identical). In the following example two identical beams made from NSC and compresit are compared. The maximum SLS stresses are assumed to be $r_c = f_c$ and $r_t = 0.05 f_c$.

Example 3.2: Numerical calculations of the prestress ranges. In order to observe the main differences between a NSC beam and a compresit beam two geometrically identical beams are considered. A rectangular simply supported beam with $b \times d = 200 \times 900$ mm is loaded by a dead load of $p = 10$ kN/m and a live load of $q = 10$ kN/m. The prestressing reinforcement ratio is $\phi = 2.8$ % for both beams, which is obtained by means of 4 × 4 ø20 mm strands. These strands have a yield strength of approximately 1600 MPa, cf. table 3.5. The long-term elasticity ratios α_∞ are chosen to the values 30 and 10 for the NSC and the compresit beam respectively, cf. Section 3.3.3.

Beam	Stress criteria			Geometry		
	$r_c = f_c$ (MPa)	r_t/f_c	f_y/f_c	b (mm)	h (mm)	d (mm)
NSC	40	0.05	40	200	1100	900
Compresit	160	0.05	10			

Table 3.5: Allowable stresses and geometry of NSC beam and compresit beam.

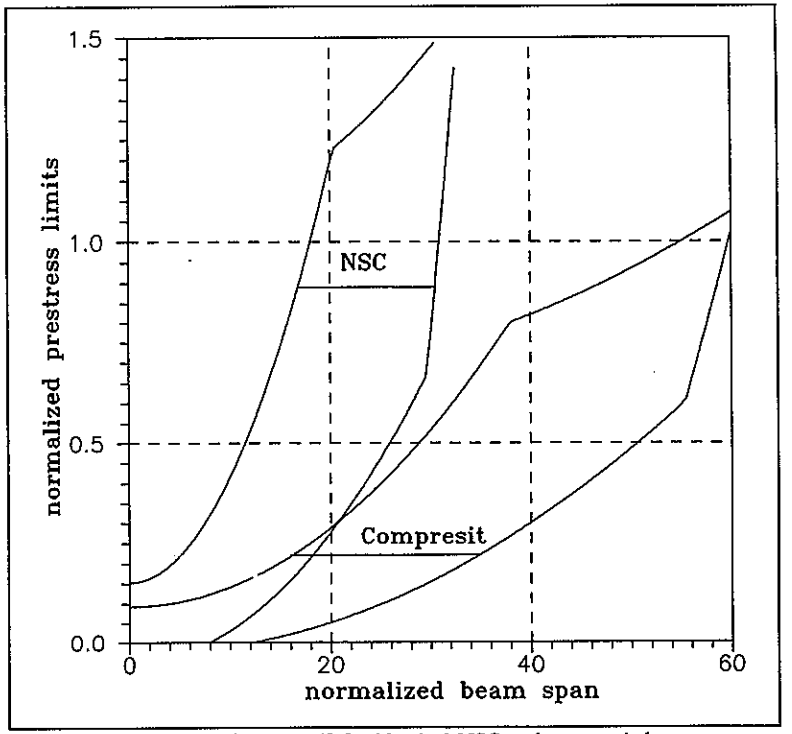

Figure 3.11: Limits for $\Phi\sigma_{pre}/f_y$ for identical NSC and compresit beams.

In figure 3.11 the valid prestress regions are depicted for the two beams, termed NSC and compresit. The curves are similar with those in figure 3.10. The maximum *prestress degree* is chosen to $\sigma_{pre}/f_y = 80$ %. It is obvious, that the maximum obtainable span only increases marginally for the *compresit* beam compared with the NSC beam. This is because the amount and type of reinforcement are identical and thus, the maximum prestress level limits the obtainable beam span. If however this level (= 0.8Φ) is raised by either increasing the reinforcement strength, or by increasing the reinforcement ratio the effect on the compresit beam span would be much more significant, than for the NSC beam span. In fact the NSC beam hardly suffers any span reduction, if the reinforcement ratio is reduced by a third.

In *Jobse & Moustafa (1984)* the use of HSC for highway bridges in the USA is analyzed. Standard prestressed bridge girders are compared under the assumption, that the concrete strength is increased from 42 to 70 MPa. Under identical loading, geometry and reinforcement the girder length is increased together with the compressive strength. The

length increase is about 20 - 30 % from NSC to HSC, but the effect is limited by the maximum prestress force. From these results *Shah & Ahmad (1985)* conclude, that "..if the design is governed by serviceability limit states, then high strength concrete can be beneficial". Furthermore Shah & Ahmad state, that the use of HSC speed up construction in general because a given strength level is attained earlier.

These observations basically are in agreement with the findings of Example 3.2 and those of Section 3.2.2. In order to utilize the high compressive strength of compresit we have to increase the reinforcement degree, either through the reinforcement ratio ϕ, or through the strength f_y. Thus, it is not enough simply to replace the conventional concrete in a beam design with a HSC mix or with compresit, if a significant mechanical effect is wanted beside the improved durability.

A way to increase the reinforcement content ϕ is to place the steel bars closer within the same beam dimensions. The distance/*spacing* between steel bars is governed by design rules to ensure proper embedment without air voids, to provide protection against corrosion and to provide the necessary anchorage capacity. The minimum bar spacing depends on aggregate size, bar diameter and the aggressiveness of the external environment. Like it is recalled from Chapter 1, one of the purposes of the compresit concept is to apply a *compact* steel bar reinforcement to the structure. The relatively small aggregate size of 4 mm makes it possible to reduce the bar spacing. Furthermore the increased bond strength between the matrix - bar interface, that is experimentally observed for compresit matrix, enables smaller bar spacings. However, a lower limit of these spacings is taken as one fibre length in order to ensure a homogeneous fibre distribution between the bars.

In DS 411 (1984) a concrete cover of magnitude 2 bar diameters is recommended and so is the horizontal spacing between mild steel bars in a layer. If n_b is the number of bars per layer and d_b is the bar diameter, then the beam width is limited by $b \geq (2+3n_b)d_b$.

In compresit however, both the cover depth and the bar spacing are expected to be reduced to about one bar diameter, i.e. $b \geq (1+2n_b)d_b$. This halving of the bar spacing is only found to enable 2 or 3 extra bars into each reinforcement layer for typical values of b/d_b, which is a rather modest increase of the reinforcement content. Instead of adding more reinforcement to an existing reinforcement arrangement it seems more advantageous to increase the size of the tensile zone of the cross-section. Thus, by considering a lower flange, where the tensile reinforcement is embedded, or by considering external reinforcement. These considerations are of course strongly dependent on the actual situation.

3.4 Concluding remarks

Ultimate limit state. The observations in Section 3.1.2, concerning a *rectangular stress block* to describe the compressive concrete stresses in the compression zone, of a beam at failure are

- The sensitivity of the analytical bending strength toward the ultimate compression strain seems to increase with the compressive strength. This is due to the brittle nature of high-strength concretes. Thus, it becomes more important to incorporate a proper stress distribution, when HSC is considered.

- Because of the extensive steel fibre reinforcement of compresit matrix it is expected, that the complete compression zone is utilized by the rectangular stress block. This is due to the high ductility of compresit matrix, contrary to the explosive failure behaviour of plain HSC.

The findings of Section 3.1.2 is summarized in table 3.6, where c_1 is the extent of the rectangular stress block of magnitude f_c, within the compression zone. Furthermore the ultimate compression strain ε_{cu} is given for NSC, HSC and compresit.

Concrete type	NSC	HSC	Compresit
ε_{cu} (‰)	3.5†	3	6
c_1	0.8†	0.65	1
Mild steel reinforcement: $\varepsilon_{sy} \approx 2.5$ ‰, $\varepsilon_{pre} = 0$			
Φ_{bal} (%)	47	36	71
ϕ_{bal} (%)	4	6	20
Prestressing reinforcement: $\varepsilon_{sy} \approx 10$ ‰, $\varepsilon_{pre} = 6$ ‰			
Φ_{bal} (%)	38	28	60
ϕ_{bal} (%)	1	1	5

†According to DS 411 (1984).

Table 3.6: Approximate values for the balanced reinforcement degrees and corresponding reinforcement ratios for various types of concrete and 2 types of reinforcement. The prestress degree is chosen at 60 %. It is recalled, that the relationship between reinforcement degrees and ratios is $\Phi = \phi f_y / f_c$.

Table 3.6 also contains calculations of the balanced values of the reinforcement degree Φ and the ratio ϕ for two different types of reinforcement (f_y = 500 and 1600 MPa). The *balanced reinforcement degrees* are calculated from eq. (3.15) for a *rectangular* beam cross-section. The importance of Φ_{bal} in structural design is obvious, because it is advantageous from an economical point of view and for the sake of structural safety, to consider *under reinforced design* of concrete structures.

Like it is concluded in Section 3.2.2, a significant effect of increasing the moment capacity, by means of higher compressive strengths, is obtained by keeping the reinforcement degree constant. From table 3.6 it appears, that compresit has high values of the balanced reinforcement degree and ratio, compared with the other concrete types, both in case of mild steel reinforcement and prestressing reinforcement. Therefore it is possible to add high amounts of reinforcement to compresit beams and at the same time maintain the *under reinforced* cross-section. This property is utilized to make the best possible use of the high compressive strength of compresit.

Serviceability limit state. The analysis in Section 3.3 is based on a compresit beam with prestressed strands. The prestress is necessary in order to utilize the uncracked bending stiffness. Several criteria exist in order to limit the prestressing force, so that the stresses do not exceed certain critical values. These criteria are given in Section 3.3.2. The SLS demands, concerning cracking and deflection, are found to limit the possibility of long beam spans.

In conventional concrete bridges the dead load is often dominant, compared with the live load, which gives them certain cross-sectional dimensions to ensure the proper bending stiffness. Figure 3.8 shows, that the *modulus of elasticity* is only increased about 25 % from the case of a good NSC to compresit matrix, while the compressive strength increases 3 to 4 times. For beams made out of HSC or compresit the cross-sectional dimensions are minimized due to the high strength. Thus, also the self-weight and the bending stiffness are reduced. The SLS demand for bending stiffness is related to the live load, which remains unaltered from the conventional design and therefore the long spans need an improved SLS design.

Preliminary test results show reduced *creep* characteristics for compresit and give reason to believe, that the *elasticity ratio* $\alpha = E_s/E_c$ decreases from its short-term value of $\alpha_0 \approx 4$ to a long-term value of $\alpha_\infty \approx 10$.

A subject that still needs research, is the influence of fibres on the bending cracks with respect to both crack widths and mutual crack distances. In Section 2.4 of Part I of the thesis[3], results from tensile tests on mild steel bars, embedded in compresit matrix, are given. These results show, that no visible cracks occur for tensile strains up to 1 ‰. Thus,

[3]Basic Strength Properties of Compresit Matrix.

it seems that even though the cracking strain of the matrix is exceeded several times ($\varepsilon_{cr} \approx$ 0.2 ‰), then the fibres seem to provide a very effective dispersing of the cracks. However, it is also observed, that the matrix looses its stiffness, when ε_{cr} is exceeded. Therefore the tensile stress criteria, given in Section 3.3.2, is meant to ensure the uncracked bending stiffness of the cross-section.

Finally it is summarized, that the bending analysis shows a possibility to make use of the high compressive strength of compresit, but this utilization is closely connected with the presence of steel fibres to provide enough ductility. Compared to NSC, where the compressive strength about one fourth of the compresit strength, we can double the beam span with compresit roughly speaking. Thus, it seems possible to dispense with a column support for instance. However, the lack of bending stiffness makes it necessary to rectify the SLS demands by means of e.g. prestressing.

3.5 References

ACI 363 (1984), 'State-of-the-Art Report on High-Strength Concrete', ACI Committee 363, *ACI Journal*, Vol. 81, pp. 364-411.

ACI 318-89 (1989), *Building Requirements for Reinforced Concrete and Commentary*, American Concrete Institute, Detroit, Michigan, 353 pp.

Alsayed, S.H. (1993), 'Flexural Deflection of Reinforced Fibrous Concrete Beams', *ACI Structural Journal*, Vol. 90, pp. 72-76.

Carreira, D.J. & K.-H. Chu (1985), 'Stress - Strain Relationship for Plain Concrete in Compression', *ACI Journal*, Vol. 82, pp. 797-804.

CEB (1990), *CEB - FIP Model Code*, CEB Bulletin D'information No. 213/214, Thomas Telford, London, 437 pp.

DS 411 (1984), *Danish Code of Practice for the Structural Use of Concrete*, 3rd Ed., Dansk Ingeniørforening, 98 pp.

EC2 (1992), *Eurocode 2: Design of Concrete Structures - Part 1: General Rules and Rules for Buildings*, European Prestandard ENV 1992-1-1:1991, 1st Ed., May 1992, Dansk Standardiseringsråd, Copenhagen, 253 pp.

Exner, H. (1983), *Betonbjælkers Bøjningsbæreevne*, in Danish, Serie R, No. 176, Department of Structural Engineering, Technical University of Denmark, Lyngby, 62 pp.

Favre, R. & H. Charif (1994), 'Basis Model and Simplified Calculations of Deformations According to the CEB-FIP Model Code 1990', *ACI Structural Journal*, Vol. 91, pp. 169-177.

FIP/CEB (1990), *High Strength Concrete, State of the Art Report*, CEB Bulletin d'Information No 197, 61 pp.

Henager, C.H. & T.J. Doherty (1976), 'Analysis of Reinforced Fibrous Concrete Beams', *Journal of the Structural Division*, ASCE, Vol. 102, No. ST1, pp. 177-188.

Heshe, G. (1988), 'Experimental Research on Compact Reinforced Composite (CRC)', *Bygningsstatiske Meddelelser*, Vol. 59, No. 1, Danish Society for Structural Science and Engineering, 79 pp.

Jobse, H.J. & S.E. Moustafa (1984), 'Applications of High Strength Concrete for Highway Bridges', *PCI Journal*, Vol. 29, No. 3, pp. 44-73.

Nielsen, M.P. (1984), *Limit Analysis and Concrete Plasticity*, Prentice-Hall Inc., Englewood Cliffs, New Jersey, xii + 420 pp.

Sargin, M. (1971), *Stress - Strain Relationships for Concrete and the Analysis of Structural Concrete Sections*, Study No. 4, Solid Mechanics Division, University of Waterloo, Canada, xxvi + 167 pp.

Shah, S.P. & S.H. Ahmad (1985), 'Structural Properties of High Strength Concrete and its Implications for Precast Prestressed Concrete', *PCI Journal*, Vol. 30, No. 6, pp. 92-119.

Swamy, R.N. & S. Al-Ta'an (1981), 'Deformation and Ultimate Strength in Flexure of Reinforced Concrete Beams Made with Steel Fiber Concrete', *ACI Journal*, Vol. 78, pp. 395-405.

Wang, P.T., S.P. Shah & A.E. Naaman (1978), 'Stress - Strain Curves of Normal and Lightweight Concrete in Compression', *ACI Journal*, Vol. 75, pp. 603-611.

4. Shear strength of beams

The shear failure of reinforced concrete beams is very *complex* compared with the bending failure, where the mechanism is better known. Thus, the shear strength is rather difficult to predict because it depends on a lot of parameters such as the shear span, the amount of both longitudinal and vertical reinforcement, the concrete strength and also the beam size. The normal code-like approach is to divide the shear capacity into a sum of contributions from the concrete (aggregate interlock), the reinforcement bars (dowel action), etc. These contributions are analytically described by means of empirical expressions.

In the present investigation however, basis is taken in the theoretical *plastic upper-bound solution* to the shear capacity of beams subjected to *4-point loading*. This solution is summarized in the following section for a rigid-plastic *Coulomb material* with zero tension cut-off. It is expected that the plastic solution is going to dominate the code recommendations in the future, especially in Europe.

The plastic approach to the shear strength of beams has proven to be a good design tool for reinforced concrete structures. The work mainly took place at the Department of Structural Engineering, Technical University of Denmark, during the seventies, see e.g. *Nielsen (1984)*, pp. 205-235, for a thorough description of this work including several references. In *Nielsen & Brœstrup (1978)* the solution of non-shear reinforced beams is first published and in *Jensen (1981)* a great effort is made to obtain a complete exact plastic solution. Recently *Chen (1988)* has included the concrete tensile strength in the plastic solutions for beams with or without prestressing, deep beams and corbels.

In order to fit the plastic solution to laboratory test results an *effectiveness factor* ν is introduced. This factor is considered to fall within the range 0 - 1 and it is multiplied to the uniaxial compressive strength to obtain the plastic strength $\nu f_c \leq f_c$. An extensive *experimental fitting* of this factor exists in Roikjær et al. (1979) and in Chen (1988). The effectiveness factor is often interpreted to reflect the concrete *brittleness*, where smaller values of ν give a more brittle material, i.e. ν decreases with increasing f_c. In case of beams without shear reinforcement the effectiveness factor depends on many parameters. It is found to increase with the reinforcement ratio, while it decreases with shear span and beam size. In case of shear reinforced beams ν is only considered to vary with the concrete strength. Thus, the presence of shear reinforcement makes the other effects secondary.

The present investigation does not include any fitting with respect to the various parameters, but instead it is an analysis of the fibre effect on the shear strength. Furthermore the basic upper bound plastic solution is considered without taking the influence of the tensile strength of concrete into account. It is believed, that the fibres improve the concrete ductility and therefore increases the effectiveness factor significantly. The fact that shear failure normally happens under the formation of a diagonal shear crack gives reason to believe, that the fibres have a positive effect by providing increased ductility and energy dissipation.

4.1 Theoretical plastic solution

The plastic solution is based on a horizontal simply supported rectangular beam subjected to 2 vertical loads, symmetrically placed with respect to the beam mid-span. The clear distance between the support and the load is denoted the shear span a. The beam dimensions are similar to those applied in Chapter 3, cf. figure 4.1.

The basis for an exact plastic solution is an upper bound and a lower bound yield load, that coincide, see Section 2.1.1. The solution, that is applied in this chapter, is a simple one, where the most important parameters are included. In *Jensen (1981)* the exact solution is given with identical upper and lower bound yield loads. However, these exact expressions include both the width of the load plate, the width of the support plate and the position of the longitudinal reinforcement beside the reinforcement degree and of course the shear span. Thus, the exact solution is rather complex and involves a lot of parameters.

The simple solution, shown in eq. (4.2), is only exact, when a certain relationship exists between the position of the reinforcement d and the width of the support plate, cf. Jensen (1981). This solution corresponds to an upper bound failure mode with *pure translation*, while the complete solution requires *rotations* as well. In Jensen (1981) the complete solution is briefly compared with the work by *Roikjær et al. (1979)* on the experimental fitting of ν. His conclusion is, that the differences between the complete solution and the simple solution is only marginal. Therefore it seems reasonably to consider the simple expression for practical purposes instead of the more complex solution.

There exist various opinions of which beam dimensions, that are significant in describing the shear strength. The most common method is to consider the nominal shear stress defined as the shear force V divided by the effective cross-sectional area bd. Similarly the shear span a is often normalized with respect to the effective beam depth d. In figure 4.1 a diagonal discontinuity line, representing a shear crack, is depicted between the edges of the load plates and the distance between these edges is considered as the shear span in the following.

The reinforcement may consist of both longitudinal tensile steel bars at the depth d and vertical stirrups with spacing a_w. The corresponding reinforcement ratios and degrees are defined by

$$\phi = \frac{A_s}{bd}, \quad \Phi = \phi\frac{f_y}{f_c}, \quad \phi_w = \frac{A_{sw}}{ba_w}, \quad \Phi_w = \phi_w\frac{f_{yw}}{f_c} \tag{4.1}$$

where the subscript w denotes the web reinforcement.

In figure 4.1 the displacement discontinuity line, that is assumed in the upper-bound solution, is shown. The stresses in the beam are assumed to be *plane stresses* and the

Coulomb failure criterion with *zero tension cut-off* is applied. This corresponds to the *square yield locus*, cf. figure 2.6, and the angle of friction has no influence on the solution.

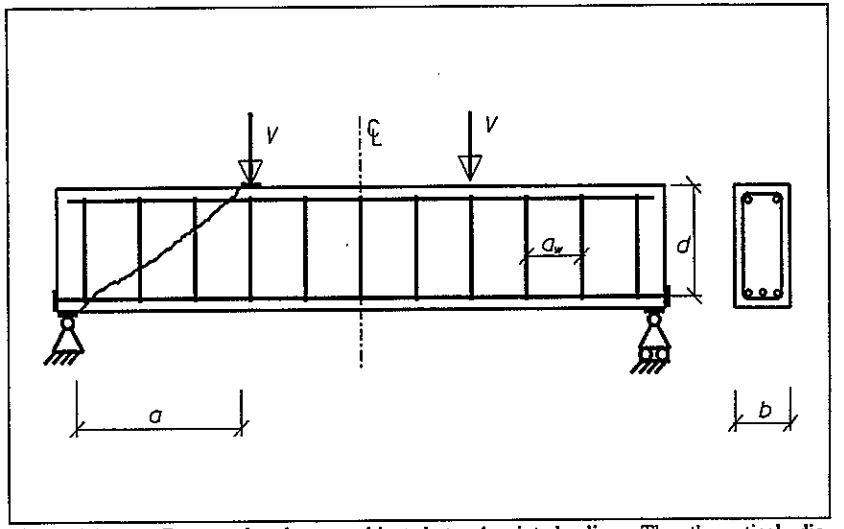

Figure 4.1: Rectangular beam subjected to 4-point loading. The theoretical displacement discontinuity line is also shown.

The shear capacity is written as a function of the vertical and horizontal reinforcement degrees, see e.g. Chen (1988). If either one of the reinforcement degrees Φ or Φ_w exceeds their maximum values ($(\nu/2)(h/d)$ and $\nu/2$ respectively) these maximum values are used in the expressions below. This is indicated by the conditions $\Phi \neq (\nu/2)(h/d)$ and $\Phi_w \neq \nu/2$.

$$\frac{V}{bdf_c} = \frac{\tau}{f_c} = \begin{cases} \frac{\nu}{2}\left(\sqrt{(a/d)^2 + 4(h/d - \Phi/\nu)\Phi/\nu} - a/d\right) + \frac{a}{d}\Phi_w, & 0 \le \Phi_w < \Phi_{w0} \\ \frac{2}{\nu}\sqrt{\Phi(\nu h/d - \Phi)\Phi_w(\nu - \Phi_w)}, & \Phi_{w0} \le \Phi_w \neq \frac{\nu}{2} \end{cases} \tag{4.2}$$

where the limit Φ_{w0} is defined by

$$\Phi_{w0} = \frac{\nu}{2}\frac{\sqrt{(a/d)^2 + 4(h/d - \Phi/\nu)\Phi/\nu} - a/d}{\sqrt{(a/d)^2 + 4(h/d - \Phi/\nu)\Phi/\nu}}, \quad 0 \le \Phi \neq \frac{\nu}{2}\frac{h}{d} \tag{4.3}$$

The maximum values for the reinforcement degrees corresponds to the situation, where the reinforcement stops yielding. If Φ_w is below Φ_{w0} then the theoretical discontinuity line runs all along the shear span, i.e. the capacity depends on a.

4.1.1 Shear strength without stirrups

In this section several test results are compared with the plastic solution in eq. (4.2). Emphasis is put on HSC beams without shear reinforcement. The number of test results on high-strength beams is still limited, making a parameter fitting rather difficulty. Furthermore most test series only includes one test beam for each parameter combination, so that the *experimental scatter* is difficulty to evaluate.

In *Zhang (1994)* some new ideas, concerning the shear strength of NSC beams without stirrup reinforcement, are stated. These ideas are briefly summarized here. Like previously mentioned the effectiveness factor is found to decrease with the shear span a for short spans and then increase again, when the shear span exceeds a value of approximately $3d$. This dependency of ν on a/d is modelled by a second order polynomium in Roikjær et al. (1979). However Zhang tries to eliminate this dependency by means of the socalled *cracked shear strength.*

The various phenomena during a shear failure under 4-point loading is summarized as

- Vertical bending cracks initiate in the mid-span of the beam, where the bending moment is constant and the shear force is zero.
- At a certain load level bending cracks also appear in the shear spans. These cracks tend to flatten off to form inclined shear cracks. The cracks run towards the load plates at the upper beam side.
- Suddenly a final diagonal shear crack propagates through the entire depth of the beam together with a splitting crack along the longitudinal reinforcement towards the support.
- Finally the load capacity is reached with the formation of this diagonal crack, or eventually further load is sustained until crushing of the compression zone under the load plate.

In her analysis Zhang (1994) assumes, that the position of the final diagonal crack is determined by the tensile bending strength of the beam and that *sliding* occurs in this diagonal crack. Thus, it is the cracked shear strength, that governs the shear strength of the beam instead of the monolithic strength. The plastic solution states, that the theoretical yield line runs from the load plate to the support plate, when the tensile concrete strength is neglected and *no stirrups* exist. Instead the tensile bending strength of the concrete is used to determine the actual position of the diagonal shear crack (and with it the modified

position of the yield line). This modified shear span, which is shorter than the actual span, is inserted in the plastic solution together with the cracked sliding strength. Zhang estimates the cracked sliding strength to be about half the monolithic strength on basis of push-off tests. For relatively *small shear spans* the concrete acts monolithic with a crack running from the load plate to the support plate.

The expressions are not repeated her but Zhang (1994) finds good agreement between several classical test results on NSC beams and her modified shear strength without including any dependency of the shear span on the effectiveness factor. For further details the reader is referred to her thesis.

It seems reasonable to apply this modified plastic solution to HSC beams, in particular because it is a brittle material, which makes it very sensitive to the presence of cracks. Thus, the difference between cracked and monolithic strength is expected to be much more distinct for HSC than for NSC.

HSC test results. In table 4.1 a survey of some of the shear tests on HSC beams is given. The results from these references are compared to the plastic solution in eq. (4.2) putting $\Phi_w = 0$ in the following diagrams. Both the dependency of the normalized shear strength τ/f_c on f_c, a/d and ϕ is treated, where it is recalled, that τ is defined by the shear force V divided by the effective cross-sectional area bd.

Investigation	Strength f_c (MPa)	Dimensions $b \times d$ (mm)	Shear span a/d	Reinf. ϕ (%)
Nielsen & Bræstrup (1978)	54	180 × 302	0.6 - 3.6	0.68
Mphonde & Frantz (1984)	20 - 100	152 × 298	1.5 - 3.6	3.36
Ahmad et al. (1986)	70	127 × 200	1 - 4	1.77 - 6.36
Thorenfeldt & Drangsholt (1990)	78, 98	150 × 250	2.3 - 4	3.23
Xie et al. (1994)	40, 104	127 × 215	1 - 3	2.07
Kim & Park (1994)	54	150 × 250	1.5 - 6	1.01 - 4.68

Table 4.1: Summary of existing shear tests on HSC beams without stirrups. Note that Mphonde & Frantz use 3-point loading instead of 4-point and Nielsen & Bræstrup use prestressed beams.

In Nielsen & Bræstrup (1978) the inverse expressions to eq. (4.2) are given in order to calculate ν when the shear capacity is experimentally determined. In case of $\Phi_w = 0$ the expressions in eq. (4.2) are rearranged into the following

$$\nu = \begin{cases} \dfrac{2\tau/f_c}{\sqrt{(a/d)^2 + (h/d)^2} - a/d} \le 2\Phi\dfrac{d}{h} \\ \dfrac{(\tau/f_c)^2 + \Phi^2}{\Phi h/d - (a/d)(\tau/f_c)} > 2\Phi\dfrac{d}{h} \end{cases} , \Phi_w = 0 \qquad (4.4)$$

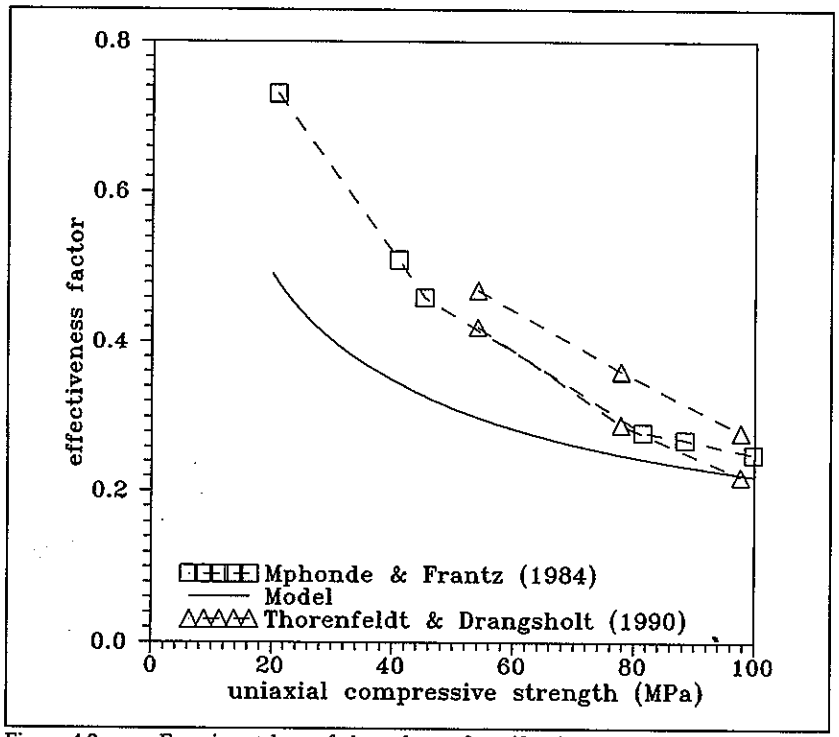

Figure 4.2: Experimental ν - f_c dependency for a/d = 3 - 4. Constant reinforcement ratio $\phi \approx 3.3$ % but varying concrete strength.

In figure 4.2 the effectiveness factors, calculated from some of the shear strengths in Mphonde & Frantz (1984) and Thorenfeldt & Drangsholt (1990), are depicted as a function

of f_c for relatively large values of the shear span. The expected decreasing ν - f_c relationship is significant. Furthermore, the model $\nu = 2.2/\sqrt{f_c}$ is inserted in figure 4.2. This type of relationship is often applied in order to model the influence of f_c. However, it does not seem to fit the test results properly along the whole strength range.

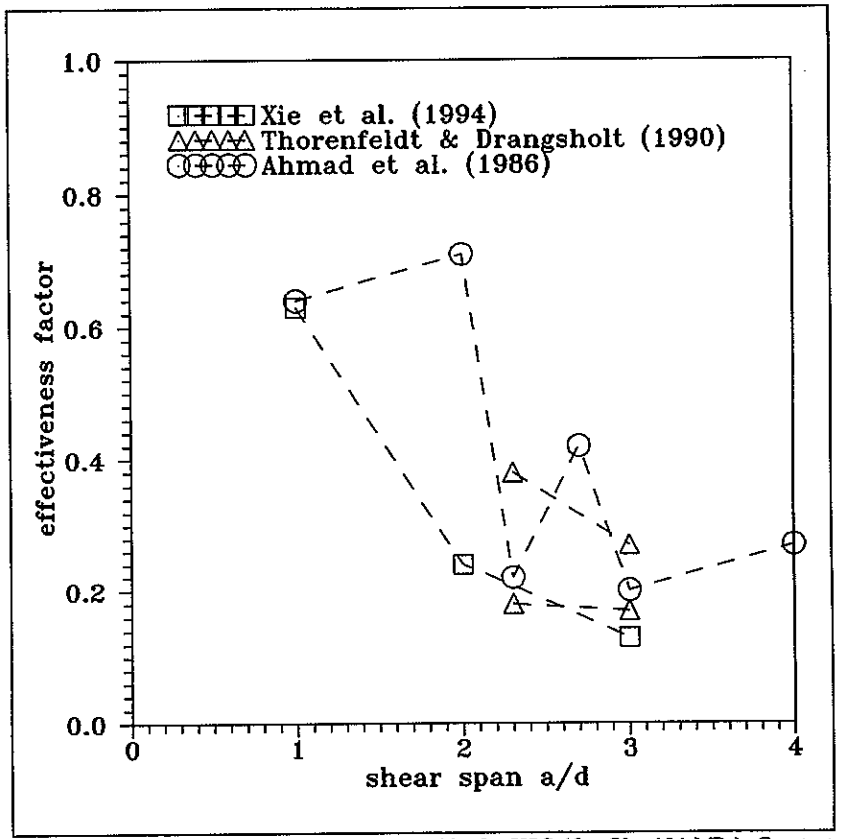

Figure 4.3: Experimental ν - a/d relationship for HSC (f_c = 70 - 104 MPa). Constant reinforcement ratio $\phi \approx 2$ %.

In *figure 4.3* a few examples of the fitted values of ν are given as a function of the shear span for 3 different test series. It is noted that the experimental scatter makes any clear conclusion difficult. From the HSC test results two trends seem to exist when the findings of Zhang (1994) are kept in mind:

- The effectiveness factor decreases, when the shear span increases.

- The shear strength seems to be independent of the shear span, when $a/d > 3$.

The first observation symbolizes the transition from monolithic strength to cracked strength. For *short shear spans* ($a/d < 1$) the plastic solution requires a rather high effectiveness factor because the failure passes through monolithic concrete. The fact that the experimental results sometimes exceed $\nu = 1$ for short spans may be connected with the plane stress assumption, which is violated.

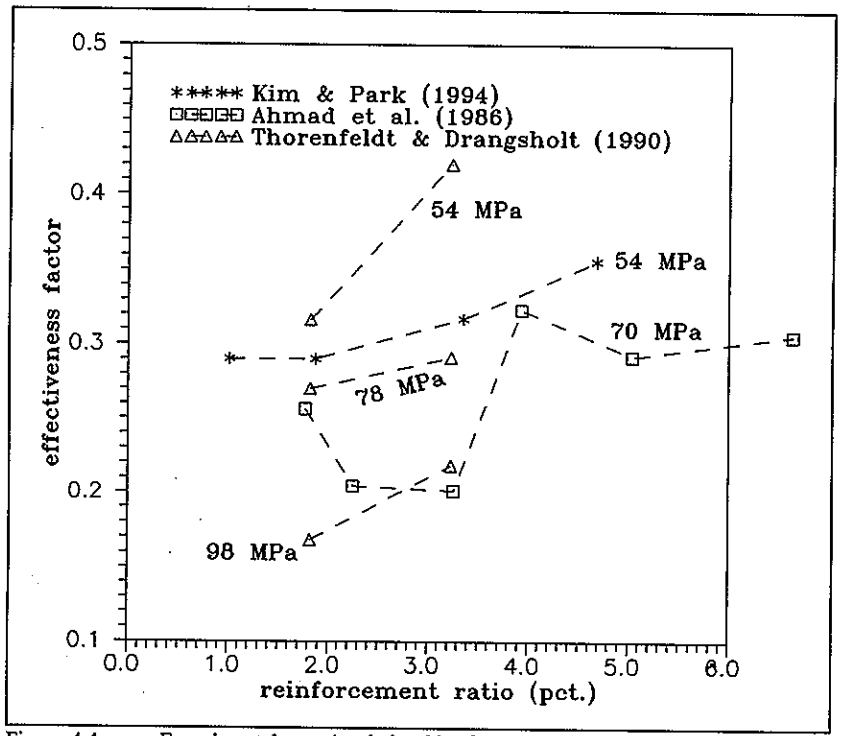

Figure 4.4: Experimental ν - ϕ relationship for $a/d = 3$. The numbers indicate the compressive concrete strengths.

For *moderate shear spans* ($1 \leq a/d \leq 3$) the sliding resistance of a bending related crack governs the shear capacity. Thus, the effectiveness factor decreases significantly in this range and the modified theory by Zhang (1994) should be applied.

Finally the *long shear spans* ($a/d > 3$) are recognized to give almost constant strengths independent of a/d. Thus, the plastic solution with continuously decreasing τ/f_c - a/d relationship is not valid. Instead the theoretical shear strength at $a/d = 3$ should be used for longer spans. The fact that the shear strength seems to be constant, when a/d exceeds 3 is often interpreted as the *tensile strength* of the concrete which is neglected in the simple solution.

The beam *size effect* on the shear strength is investigated by Kim & Park (1994). Four different beam cross-sections with effective depths ranging from 142 mm to 915 mm are tested, all having identical compressive strength ($f_c = 54$ MPa), reinforcement ratio ($\phi = 1.87$ % and $\Phi = 16.6$ %) and identical normalized shear span ($a/d = 3$). The effectiveness factors calculated by means of eq. (4.4) decrease from 0.29 to 0.21 from this increased beam depth, i.e. a decrease of approximately one third. A similar trend is observed from the results in Thorenfeldt & Drangsholt (1990), where the beam size is doubled.

The dependency of τ/f_c with respect to the amount of longitudinal reinforcement is depicted in figure 4.4. The effectiveness factor, calculated from eq. (4.4), is given as a function of the reinforcement ratio ϕ for the constant shear span $a/d = 3$. It seems that ν increases with the amount of reinforcement even though the effect is rather modest. Chen (1988) also observes an increasing effect of ϕ on the effectiveness factor, but only while $\phi \leq 2$ %, which is not supported by figure 4.4.

Investigation	Strength f_c (MPa)	Dimensions $b \times d$ (mm)	Shear span a/d	Reinf. ϕ (%)	Web reinf. $\phi_w f_{yw}$ (MPa)
Mphonde & Frantz (1985)	20 - 90	152 × 298	3.6	3.36	0.34 - 1.03
Sarsam & Al-Musawi (1992)	40, 75	180 × 233	2.5, 4	2.23 - 3.51	0.76 - 1.53
Xie et al. (1994)	42 100	127 × 203	1 - 4	3.2 4.54	1.58 1.65 - 2.53

Table 4.2: Summary of existing shear tests on HSC beams with stirrups. Note that both Mphonde & Frantz and Xie et al. use 3-point loading instead of 4-point.

4.1.2 Shear strength with stirrups

There exist scarcely any beam tests on HSC beams with stirrups. In table 4.2 three investigations are included, viz. *Mphonde & Frantz (1985), Sarsam & Al-Musawi (1992)* and *Xie et al. (1994)*, where concrete strengths up to 100 MPa are tested. The investigations by Mphonde & Frantz and Xie et al. use beams under 3-point loading, while Sarsam & Al-Musawi use 4-point bending.

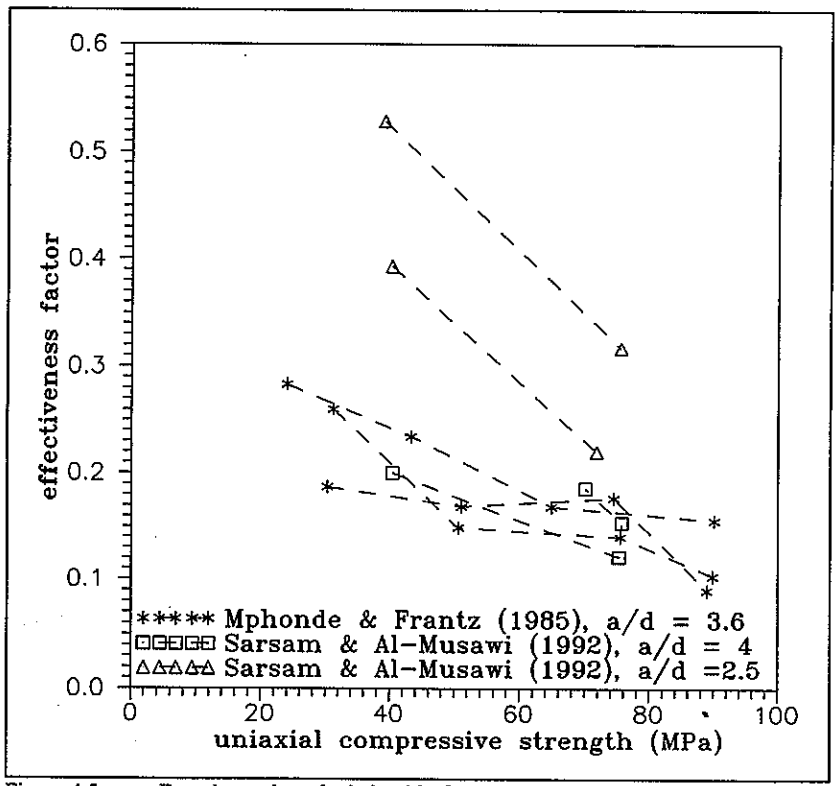

Figure 4.5: Experimental ν - f_c relationship from HSC beams with shear reinforcement. The connected symbols only include variation of f_c.

In figure 4.5 the effectiveness factors, calculated from two of the test series in table 4.2, are depicted as a function of the uniaxial strength. The data points in figure 4.6, that are connected by lines represent tests, where only the compressive strength of the concrete mix

is altered. The trend from beams without stirrups, where the effectiveness factor decreases, still exists, cf. figure 4.2. However, the effectiveness factor also seems to decrease with the shear span like in the case without stirrups. The lack of repetitions makes it impossible to include the experimental scatter in order to verify the significance.

In *Xie et al. (1994)* the *shear span* alone is varied for both NSC and HSC beams (a/d = 1, 2 and 3). The effectiveness factor equals 0.54, 0.21 and 0.13 respectively for the NSC beams and 0.34, 0.18 and 0.1 respectively for the HSC beams, when the shear span increases. Thus, there seems to be a significant influence from the shear span on ν.

Furthermore both Sarsam & Al-Musawi (1992) and Xie et al. (1994) vary the amount of shear reinforcement for constant values of a/d, f_c and Φ. Sarsam & Al-Musawi (a/d = 2.5 and f_c = 75 MPa) find a significantly decreasing ν, when the shear reinforcement ratio increases. Xie et al. (a/d = 3 and f_c = 100 MPa) find an almost constant effectiveness factor on the contrary.

The normal approach in case of shear reinforced NSC beams is to consider an influence of the compressive strength on the effectiveness factor only. The influence of the other parameters such as reinforcement ratios and shear span is often neglected. However, the test results on HSC beams may indicate, that this approach cannot be transferred directly to higher concrete strengths without also including the influence of especially the shear span. The scarce nature of the shear reinforced beam tests however, makes any proper conclusions impossible.

4.2 Steel fibre effect on shear strength

There exist several investigations, where steel fibres are added to concrete in order to evaluate their effect on the beam shear strength. Table 4.3 contains most of these investigations. Most of the research is based on comparisons between code expressions of the shear strength and test results with varying amounts of fibres. It seems that the concrete beam shear strength is one of the few strength properties, that is significantly altered by the presence of steel fibres.

Recently Batson & Youssef (1994) have compared shear test results with the plastic solution and found a significant increase of the effectiveness factor. This observation is further supported in the following section. Like it appears from table 4.3, the investigated fibre types and amounts vary significantly. Most researchers use fibre contents ranging from 0.25 to 1.5 % and normally a reference mix without fibres is included. A few of the investigations also include beams with shear reinforcement.

Investigation	Strength f_c (MPa)	Shear span a/d	Fibre content V_f (%)	Aspect ratio L_f/d_f	$V_f(L_f/d_f)$
Imam et al. (1994)	110	1.75 - 4.5	0, 0.75 hooked-end	75	0, 0.6
Shin et al. (1994)	80	2 - 6	0 - 1 straight	100	0 - 1
Swamy et al. (1993)†	40 - 50	2 - 4.9	0, 1 crimped	100	0, 1
Tan et al. (1993)†	35	1.5 - 2	0 - 1 hooked-end	60	0 - 0.6
Ashour et al. (1992)	92 - 100	1 - 6	0.5 - 1.5 hooked-end	75	0.4 - 1.1
Lim et al. (1987)	34	1.5 - 3.5	0 - 1 straight	60	0 - 0.6
Narayanan & Darwish (1987)	60 - 70	2 - 3.1	0 - 2 crimped	100, 133	0 - 1
Mansur et al. (1986)	30	2 - 4.4	0 - 0.75 hooked-end	60	0 - 0.5
Sharma (1986)	45	1.9	0, 1 deformed end	83	0, 0.8
Swamy & Bahia (1985)†	50	4.5	0 - 1.2 crimped	100	0 - 1.2
Williamson & Knab (1975)	30	4.7	0, 1.5 -	-	-
Batson et al. (1972)	33 - 40	1.2 - 5	0.2 - 1.8 crimped	60	0.1 - 1.1

† Svamy & Bahia, Swamy et al. and Tan et al. investigate thin-webbed I-beams

Table 4.3: Shear tests on FRC beams reinforced with only longitudinal bars and steel fibre reinforcement. Williamson & Knab test large beams, but they do not specify their fibres, while the others test laboratory-sized beams.

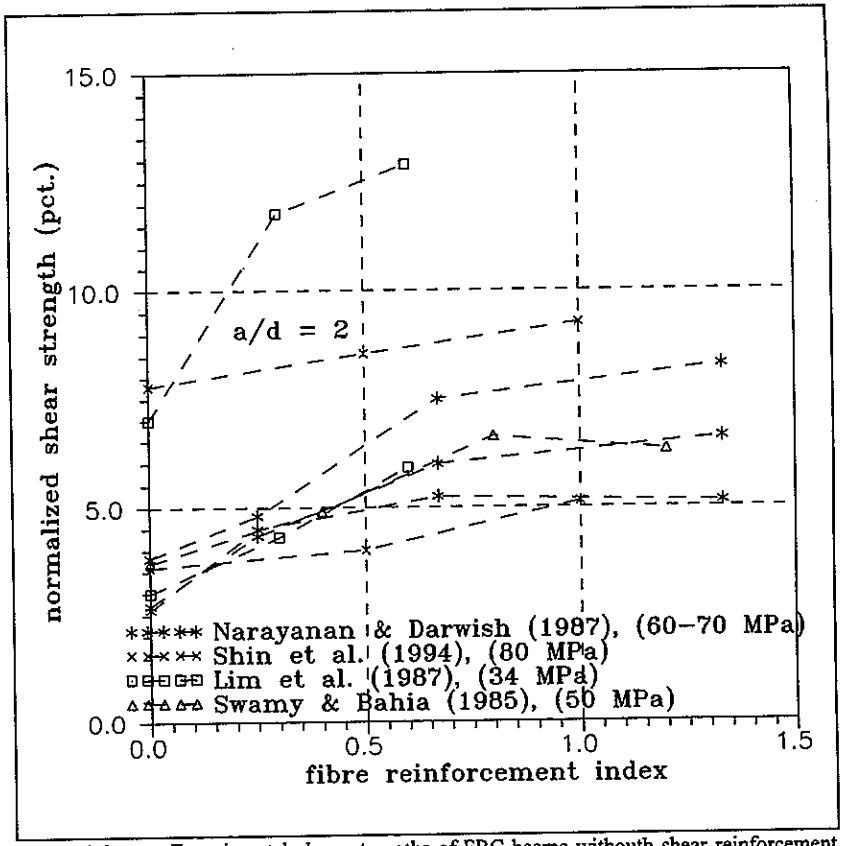

Figure 4.6: Experimental shear strengths of FRC beams withouth shear reinforcement in a τ/f_c - $V_f(L_f/d_f)$ diagram. Numbers in brackets are f_c.

4.2.1 Experimental shear strength of FRC

FRC beams without stirrups. The reported strength effect of adding steel fibres is not connected with increased compressive strengths, because the relatively small amounts of fibres hardly influence the uniaxial compressive strength. In figure 4.6 the normalized shear strengths τ/f_c are depicted as a function of the fibre reinforcement index $V_f(L_f/d_f)$. Only the amount and the geometry of the fibre reinforcement vary for the connected data points in

figure 4.6, while all other parameters such as shear span and reinforcement degree are kept constant.

Beside the experimental scatter, that is expected, the results in figure 4.6 seem to indicate an increasing strength effect for $V_f(L_f/d_f) < 0.75$. For higher values of the fibre reinforcement index no further strength increase seems possible.

In *Darwish & Narayanan (1990)* shear design recommendations are given for FRC beams based on both their own test results and others. The shear capacity is divided into a reinforcement contribution and a fibre contribution. The *fibre contribution* depends almost linearly on the fibre reinforcement index and the fibre effect on the compressive strength is also included by Darwish & Narayanan. The proposed *lower limit* for $V_f(L_f/d_f)$ is approximately 0.3 in order to include the fibre effect on the shear strength. The proposed *upper limit* of the fibre reinforcement index ranges from 2 to 3. These limits depend on the type of steel fibre. Within this range the fibre contribution to the shear strength is proportional to $V_f(L_f/d_f)$ according to Darwish & Narayanan. This design proposal is not in accordance with figure 4.6.

The FRC results are compared with the plastic solution in the previous section. In *figure 4.7* all FRC shear tests without stirrups are depicted in a diagram with the experimentally observed shear strengths, normalized with respect to f_c, along the ordiante and the rigid-plastic solution along the abscissa, i.e. eq. (4.2) with $\nu = 1$. The *diagonal line* in the diagram represents the condition, where the experimental results fit $\nu = 1$, while data points below this diagonal line represent effectiveness factors less than unity. In order to model the data points, that lie above the diagonal line with theory of plasticity, we have to expand the expressions in eq. (4.2) to include the tensile strength of the concrete. The latter is not included in the present analysis because it complicates the plastic solution strongly, cf. Chen (1988).

The data points in figure 4.7 are divided into 3 groups, viz. firstly the reference group without fibres (symbolized with the circles), secondly the beams with small amounts of fibres (having $V_f(L_f/d_f) < 0.75$ and symbolized with the asteriscs) and finally a group with fibre reinforcement indices $0.75 \le V_f(L_f/d_f) \le 1.3$ (symbolized with the boxes). The test results include normalized shear spans a/d from 1 to 6, compressive strengths f_c from 20 to 110 MPa and reinforcement degrees Φ from 15 to 70 % and various fibre geometries, cf. table 4.3.

Furthermore 3 test results on *compresit beams* with 6 % fibres are inserted in figure 4.7 corresponding to $V_f(L_f/d_f) = 2.4$ (straight Dramix fibres with $L_f = 6$ mm and $d_f = 0.15$ mm). A total of 5 compresit beams are described in Heshe (1988) with 3 different longitudinal reinforcement arrangements. The beams are reinforced strongly in order to avoid bending failure, i.e. with reinforcement degrees $\Phi > 60$ %. The cross-sectional dimensions are $b =$ 100 mm and $h = 200$ mm with the effective depth $d \approx 160$ mm. Three different shear spans give a/d = 4.1, 4.5 and 4.8, i.e. relatively large shear spans. The uniaxial compressive

strength is approximately 180 MPa. Unfortunately no beam tests on plain compresit matrix without fibres exist.

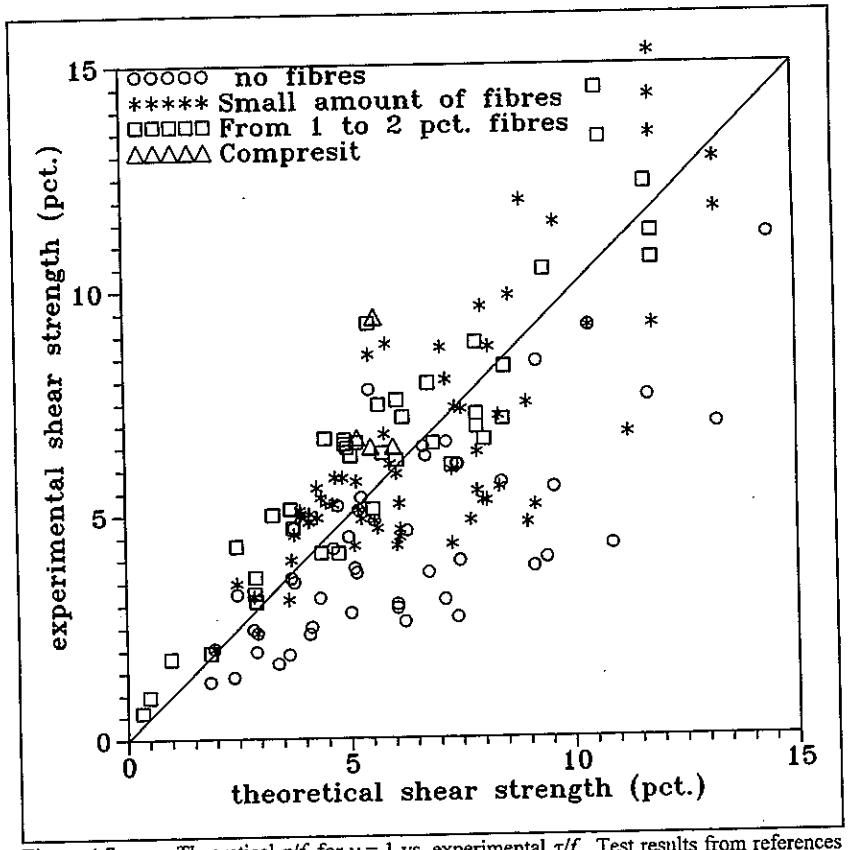

Figure 4.7: Theoretical τ/f_c for $\nu = 1$ vs. experimental τ/f_c. Test results from references in table 4.3. The compresit beams are taken from Heshe (1988).

The plain beam results without fibres are placed below the diagonal line like it is expected, i.e. $\nu < 1$. The fibre reinforced results lie much closer to the diagonal line, which means that the effectiveness factor is closer to unity. If the mean value of the ratios between the experimental and the theoretical shear strength is calculated we obtain the following sample means: $E[(\tau/f_c)_{ex}/(\tau/f_c)_{th}] = 0.755$, 1.03 and 1.20 respectively for the 3 groups of data points in figure 4.7. Of course the results show a large experimental scatter like it is expected.

The results of figure 4.8 show, that even though only a small amount of fibres is added to the concrete mix (< 1 %), then the FRC material acts like a plastic material in shear. Thus, the effectiveness factor on the compressive strength may be neglected. Recalling the ideas, concerning the *cracked shear strength* approach, described in Section 4.1.1, a reasonable explanation of the significant fibre effect exists. The sliding resistance of an existing bending crack consists both of aggregate interlock and of crossing fibres being pulled out, i.e. a crack through FRC does not reduce the shear strength as much as a crack through plain concrete. Furthermore the presence of fibres prevents the sudden failure of a single diagonal shear crack, so that the failure is notified like it is in case of shear reinforcement.

FRC beams with stirrups. The few test results, that exist, where both fibres and stirrups are applied, are not sufficient to make any clear conclusions. In *El-Niema (1991)* shear reinforced NSC beams with various fibre contents are tested under 4-point loading (a/d = 4.5). The compressive strength is $f_c \approx 25$ MPa and the longitudinal reinforcement corresponds to $\Phi > 50$ % and the web reinforcement $\phi_w f_{yw} = 1.1$ MPa. The steel fibres are crimped and they are applied to 9 different concrete mixes giving *fibre reinforcement indices* within the range 0.3 to 1.3, beside a reference mix without fibres. The normalized experimental shear strengths τ/f_c do not show any significant influence of the fibre reinforcement.

In *Sharma (1986)* a normalized shear span of $a/d = 1.9$ is used. A concrete mix with $f_c \approx$ 45 MPa is reinforced by 1 % fibres, corresponding to $V_f(L_f/d_f) = 0.8$, which results in a normalized shear strength increase of approximately 40 % compared to the reference mix. Unfortunately Sharma does not include the strength characteristics of the reinforcement steel implied so that a further analysis is difficult.

In *Shin et al. (1994)* HSC beams with $f_c = 80$ MPa are reinforced with both fibres and stirrups for $a/d = 3$. The amount of shear reinforcement is not reported, but a comparison with the reference beam without fibres indicates, that the fibres do not influence the shear strength, when stirrups are present. The fibre reinforcement index applied by Shin et al. has the values 0.5 and 1, cf. table 4.3.

Finally both *Lim et al. (1987)* and *Narayanan & Darwish (1987)* include reference test beams with stirrups, but no steel fibres, cf. table 4.3. The normalized shear spans are a/d = 1.5, 2.5 and 3.5 and a/d = 2, 2.5 and 3 respectively for the two investigations and the longitudinal reinforcement ratios ϕ are constantly 2.2 and 2 % respectively. Lim et al. apply NSC beams with $f_c = 34$ MPa, while Narayanan & Darwish use HSC beams with $f_c = 60$-70 MPa. The shear reinforcement consists of stirrups with $\phi_w f_{yw} = 0.8$ MPa in both cases. The conclusion in *Lim et al. (1987)* is, that the stirrups can be replaced by 0.5 % straight steel fibres to give identical shear capacity. In *Narayanan & Darwish (1987)* less than 0.25 % crimped steel fibres is enough to replace the stirrups.

These observations are validated by Lim et al. by means of the direct tensile strength of the FRC mix. This tensile strength is measured to correspond reasonably to $\phi_w f_{yw}$ from the stirrup reinforcement, when 0.5 % fibres are added.

4.3 Diagonal compression field theory

The ULS shear design, that is used in Denmark since 1983, is based on the theory of plasticity. A method to predict the necessary shear reinforcement in order to carry a given shear force is named the diagonal compression field theory, which is recommended in DS 411 (1984).

This method is based on a *lower bound* plastic solution, which is briefly summarized here, see also Nielsen (1984), pp. 205-235 for further details. The beam is considered to consist of a compressive and a tensile *stringer*. The distance between these stringers is termed the *internal moment lever* h_i. The nominal shear stress τ is calculated as the shear force V divided with bh_i. The value of h_i changes along the beam according to the variations of the bending moment. It is assumed, that the value of h_i corresponds to the maximum bending moment of the beam. The beam web, which is the region between the stringers, is assumed to be in uniaxial compression inclined θ with respect to the beam axis. The angle θ is termed the *crack angle* because it symbolizes diagonal cracks parallel with the compressive stresses. Both the compressive and the tensile stringer are assumed to be sufficiently strong in order to carry the bending action.

Failure is defined as a combination of web crushing, when the inclined uniaxial compression σ_c exceeds the effective strength νf_{cd}, and yielding of the stirrups under the stress f_{ywd}. Only *vertical stirrups* perpendicular to the beam axis are considered. It is noted, that the reduced material strengths f_{cd} and f_{ywd} are applied because of the ULS.

The equilibrium equations give the relationship between the shear stress τ, the diagonal compression σ_c and the crack angle:

$$\sigma_c = \tau(\tan\theta + \cot\theta) \le \nu f_{cd}, \qquad \tau = \frac{V}{bh_i} \tag{4.5}$$

In order to ensure equilibrium on a section parallel with the beam axis the tensile stresses σ_{sw} in the stirrups should should fulfil the relationship

$$\left.\begin{array}{l} \tau b a_w \tan\theta = A_{sw}\sigma_{sw} \le A_{sw} f_{ywd} \\ \$ \\ \phi_w f_{ywd} \ge \tau\tan\theta \end{array}\right. \tag{4.6}$$

The inequalities of eqs. (4.5) and (4.6) correspond to the basic principle of plastic lower bound solutions, where the stress state in equilibrium should be safe within the yield surface, cf. Section 2.1.1.

The combination of eqs. (4.5) and (4.6) gives the design method outlined in figure 4.8. For a given shear force (and stress) it is checked, whether the web crushing condition in eq.

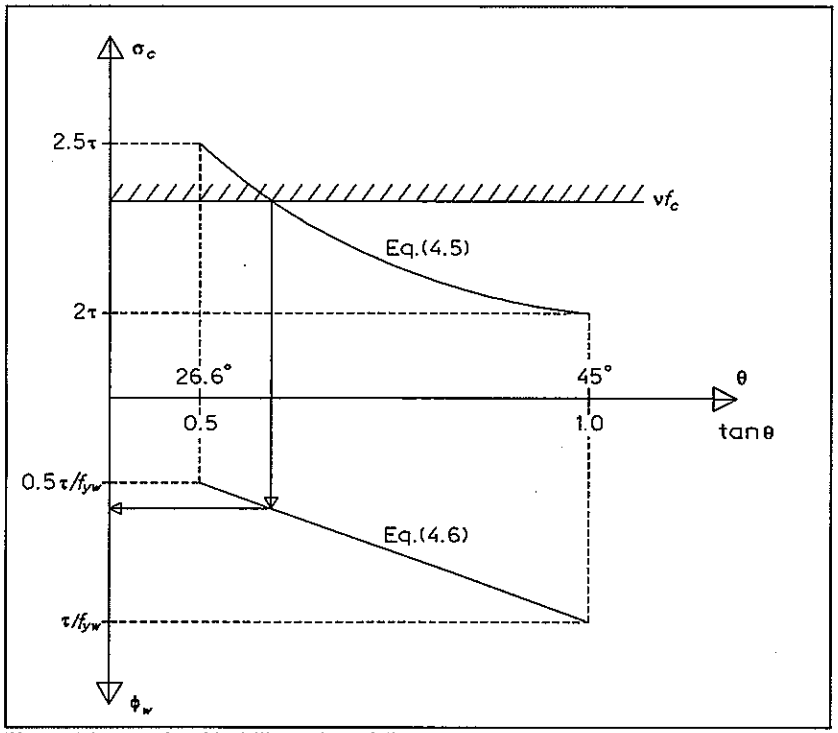

Figure 4.8: Graphical illustration of diagonal compression field theory for shear design of beams. Material strengths are reduced design values.

(4.5) is met. We wish to obtain the smallest possible crack angle in order to minimize the amount of shear reinforcement (ϕ_w in figure 4.8). It is theoretically possible to consider crack angles within the range $0 < \theta \leq 90°$, but the diagonal compression increases, when θ decreases. However, in order to ensure, that the shear cracks during the SLS is not to large, the Danish concrete code recommends the following range for θ

$$1 \geq \tan\theta \geq \begin{cases} 1/2 \\ 2/3 \end{cases} \quad \Rightarrow \quad 45° \geq \theta \geq \begin{cases} 26.6° \\ 33.7° \end{cases}, \text{ curtailed reinf.} \tag{4.7}$$

The value of the *effectiveness factor* to be used in eq. (4.5) is modelled as a decreasing function of the compressive strength:

$$\nu = 0.7 - \frac{f_c}{200 \text{ MPa}}, \quad f_c \leq 50 \text{ MPa} \tag{4.8}$$

Thus, the effectiveness factor decreases from almost 0.7 for a low-strength concrete to 0.45 for f_c = 50 MPa.

If the maximum allowable inclined compression stress $\sigma_c = \nu f_{cd}$ is less than 2τ, see figure 4.9, then it is impossible to reinforce the web sufficiently and a larger cross-sectional web area is needed. If instead νf_{cd} is higher than 2.5τ, then the lower limit of θ, see eq. (4.7), is chosen because it gives the smallest amount of shear reinforcement. However, the latter condition may be interpreted as the compressive strength of the web not being fully utilized.

The method described above corresponds to the solution in eq. (4.2) with sufficiently strong longitudinal reinforcement, i.e. $\Phi \geq (\nu/2)(h/d)$, and $\Phi_w \geq \Phi_{w0}$. Thus, an illustration of the relationship between the shear strength τ and the shear reinforcement degree $\Phi_w = \phi_w f_{ywd}/f_{cd}$ obtained by combining eqs. (4.5) and (4.6), reveals a quarter of a circle in a τ/f_{cd} - Φ_w diagram with its center at $(\tau/f_{cd}, \Phi_w) = (0, \nu/2)$ and radius equal to $\nu/2$.

It should be noted, that in order to fulfil the equilibrium equations the stringer forces are altered by the shear force on the cross-section. If the bending moment on the cross-section is denoted M, then both the compressive and the tensile stringer forces are M/h_i. The compressive stringer force is reduced by $0.5V\cot\theta$ and the tensile stringer force is increased with the same amount. Thus the longitudinal reinforcement should be designed with this additional tensile load in mind.

According to the design method the shear force in question for determining the necessary web reinforcement is defined as the *smallest* shear force along a length $h_i\cot\theta$ of the beam axis. Often the beam is divided in intervals of length $h_i\cot\theta$ and each interval is treated separately according to the lowest shear force within that interval, cf. Nielsen (1984).

4.3.1 Application to compresit and HSC

It is assumed, that the presence of *steel fibres* makes it possible to utilize the compression diagonal in the web completely, i.e. eq. (4.5) reads $\sigma_c \leq f_{cd}$. This assumption is based on the findings of Section 4.2, where relatively small amounts of steel fibres affect the shear capacity remarkably.

In *figure 4.9* the normalized shear strength is calculated according to the diagonal compression field theory with varying web reinforcement ratio. For NSC, HSC and compresit the compressive strengths are 40, 80 and 140 MPa respectively and the stirrup yield strength is f_{yw} = 300 MPa. The effectiveness factor is calculated from eq. (4.8) to 0.5 for NSC and this value is also used for HSC. For compresit the effectiveness factor ν = 0.7 is applied in order to compare realistic design strengths.

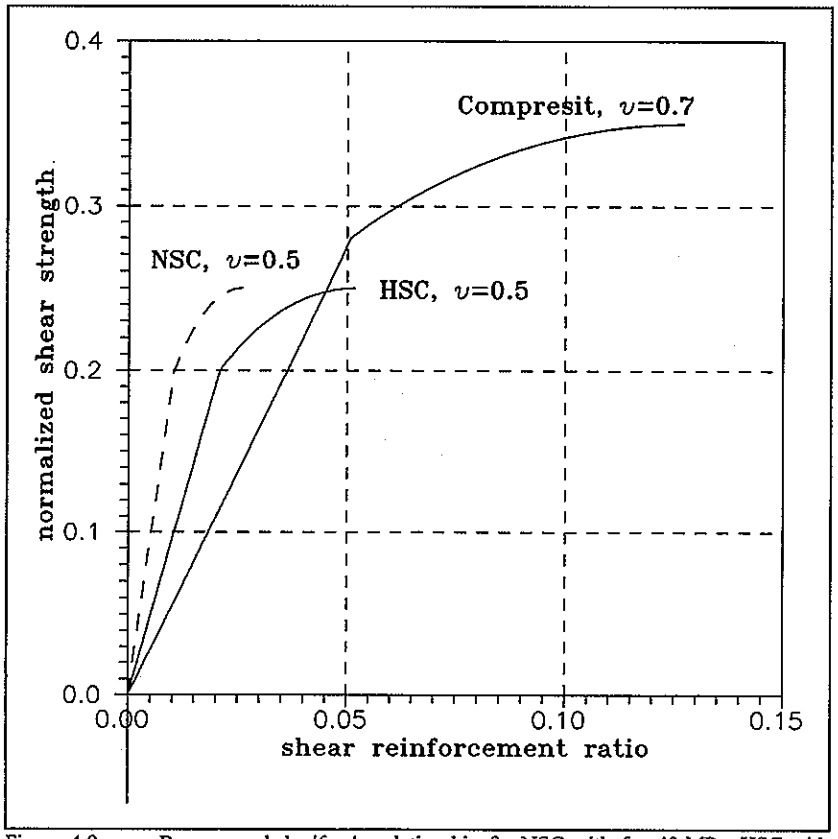

Figure 4.9: Recommended τ/f_c - ϕ_w relationship for NSC with f_c = 40 MPa, HSC with f_c = 80 MPa and compresit with f_c = 140 MPa.

The curved part of the relationships in figure 4.9 corresponds to the circular τ/f_c - Φ_w relationship mentioned in the previous section, i.e. combined web crushing and stirrup yielding. The initial part the curves are straight lines from the origin. This linear part represents the situation when the crack angle θ has reached its lower limit (26.6° given in eq. (4.7)). The circular curves are stopped when the slope gets zero, representing the over reinforced situation.

In figure 4.9 the strong effect of the effectiveness factor is obvious. For the *NSC beam* (dashed line) the web crushing criterion is met at $\phi_w \approx 1$ %. If, for instance steel fibres are

added to the NSC mix, increasing ν then the web crushing criterion gives significant higher shear strengths. The same trend applies for HSC in figure 4.9, but it also appears, that the higher compressive strength obtained in both HSC and compresit increases the need for stirrup reinforcement in order to utilize the compressive strength of the web.

4.3.2 Fibres as shear reinforcement

In figure 4.6 it is indicated, that steel fibres increases the normalized shear strength τ/f_c. For relatively large values of a/d (in the vicinity of 3) the results show a reasonably linear effect on τ/f_c with respect to the fibre reinforcement index. However, when $V_f(L_f/d_f)$ exceeds approximately 0.75 no further effect seems present. Like it is expected the fibre effect is strongest for the beam tests without any other shear reinforcement than steel fibres.

If the above-mentioned increasing effect from $V_f(L_f/d_f)$ on τ/f_c is compared with the stirrup effects in figure 4.9, then it is found, that $V_f(L_f/d_f) \approx 1$ corresponds to a rather modest shear reinforcement ratio $\phi_w \approx 0.2$ %. In the Danish concrete code the minimum shear reinforcement ratio is given as $\phi_w^{min} f_{yw} = 0.2 f_t$, where f_t is the concrete tensile strength (often taken as $f_t = \sqrt{(0.1 f_c)}$). For NSC this demand gives $\phi_w^{min} \approx 0.13$ %, i.e. the fibre effect corresponds approximately to the shear capacity obtained from the minimum required shear reinforcement ratio.

In *Feddersen (1989)* the design tool of the diagonal compression field theory from the previous section is extended to include the socalled compression *arch effect* of the concrete near the supports. The reader is referred to Feddersen (1989) for the details, but the solution in eq. (4.2) without shear reinforcement (Φ_w = 0) is combined with the diagonal compression field theory. If x denotes the distance from the support along the beam axis, then the shear strength from the arch effect is obtained by eq. (4.2), where the shear span a/d is replaced by the distance x/d. When steel fibres are added to the concrete beams the investigation in Section 4.2.1 show, that ν = 1 in eq. (4.2) is applicable. Thus, the arch effect is strongly affected by the fibres, contrary to the effect on a web reinforced beam.

4.4 Concluding remarks

The present analysis of the shear strength of HSC and FRC beams is mainly based on laboratory tests on beams subjected to 4-point loading. The beam failures are all recognized to happen as a consequence of the shear force within the shear span contrary to bending failure. The test results are compared with a theoretical plastic solution, which is summarized in Section 4.1. It is emphasized, that the practical experience with HSC and FRC beams is rather scarce compared with NSC beams, i.e. the conclusions reflect this fact. There are only a few available shear tests on *compresit beams*. They show that in order to

provoke a shear failure instead of a bending failure the beams have to be over reinforced considerably with respect to the longitudinal reinforcement. Unfortunately there exist no shear tests with plain compresit without fibres.

A common observation from all *FRC tests* is, that the shear failure gets much more *ductile*, when steel fibres are added. Instead of a single diagonal crack the failure may consist of several cracks originating from the bending cracks within the shear span. The steel fibres are also found to increase the *shear strength*. This effect is most pronounced in the FRC beams without any web reinforcement, cf. figure 4.7. The increased strength is significant for rather small amounts of steel fibres, e.g. when the fibre reinforcement index $V_f(L_f/d_f)$ is less than approximately 0.75. When $V_f(L_f/d_f)$ exceeds approximately 0.75 no further effect seems present. However, the number of existing tests with fibre reinforcement index beyond the value 1 is very limited. The fibre reinforcement may be equivalented to stirrup reinforcement, but a rough analysis shows, that the fibres hardly correspond to the shear capacity given by the required minimum shear reinforcement.

A comparison between the FRC test results *without stirrups* and the theoretical plastic solution shows, that the fibre effect is reasonably modelled by putting the effectiveness factor $\nu = 1$. This proposal is based on *typical values* of the longitudinal reinforcement degree, the shear span, the beam size and the concrete strength, cf. table 4.3. For values of the fibre reinforcement index $V_f(L_f/d_f) > 0.75$ the assumption $\nu = 1$ seems to give a *safe prediction* of the shear strength. Batson & Youssef (1994) also find, that steel fibres increase ν significantly, but no quantification is provided. It is expected, that a certain experimental relationship exists between the fibre parameters and the value of ν, but the experimental scatter together with the scarce number of tests make such a quantification impossible at the present time. Furthermore the variation of ν with respect to the different parameters of plain NSC beams is rather complex.

The quantification of the fibre effect on the beam shear strength may also be performed by taking the direct tensile strength into consideration in the plastic solution, cf. Chen (1988). However, it is the author's opinion, that this solution is much to complex for practical application. The fact that the shear strength becomes constant at a certain value of the shear span ($a/d = 3$) is actually an indication of the tensile strength of the concrete. Furthermore the tensile strength is difficulty to obtain experimentally.

An analysis of the design approach, given by the socalled *diagonal compression field theory*, which is applied by the Danish concrete code DS 411 (1984), is given in Section 4.3. This analysis shows, that in case of high compressive strengths (beyond the range of NSC), utilizing the web crushing criterion requires low crack angles (often lower than the minimum value of eq. (4.7)). The codes lower limit on θ is included in order to minimize the risk of large shear cracks in the SLS. Furthermore, utilizing the high compressive strength to its limit takes a large amount of web reinforcement which is difficult to contain in a beam web.

Therefore the increased effectiveness factors provided by the presence of steel fibres seems to be impossible to utilize in practice for high-strength concretes. However, the fibres may have a significant effect on the socalled *arch effect* near the supports of the beam, because the compressive strength governs the behaviour in these regions. If the effectiveness factor can be neglected due to a certain amount of fibres the calculations are also simplified remarkably.

4.5 References

Amad, S.H., A.R. Khaloo & A. Poveda (1986), 'Shear Capacity of Reinforced High-Strength Concrete Beams', *ACI Journal*, Vol. 83, pp. 297-305.

Ashour, S.A., G.S. Hasanain & F.F. Wafa (1992), 'Shear Behaviour of High-Strength Fiber Reinforced Concrete Beams', *ACI Structural Journal*, Vol. 89, pp. 176-184.

Batson, G.B., E. Jenkins & R. Spatney (1972), 'Steel Fibers as Shear Reinforcement in Beams', *ACI Journal*, Vol. 69, pp. 640-644.

Batson, G.B. & A.G. Youssef (1994), 'Shear Capacity of Fiber Reinforced Concrete Based on Plasticity of Concrete: A Review', *Fiber Reinforced Concrete, Developments and Innovations* (Eds. J.I. Daniel & S.P. Shah), ACI Special Publication, SP-142, pp. 141-165.

Chen, G. (1988), *Plastic Analysis of Shear in Beams, Deep Beams and Corbels*, Ph.D.-thesis, Serie R, No. 237, Department of Structural Engineering, Technical University of Denmark, 227 pp.

Darwish, I.Y.S. & R. Narayanan (1990), 'Design Charts for Reinforced and Prestressed Fibre Concrete Elements', *The Structural Engineer*, Vol. 68, No. 2, pp. 34-39.

DS 411 (1984), *Danish Code of Practice for the Structural Use of Concrete*, 3rd Ed., Dansk Ingeniørforening, 98 pp.

El-Niema, E.I. (1991), 'Reinforced Concrete Beams with Steel Fibers under Shear', *ACI Structural Journal*, Vol. 88, pp. 178-183.

Feddersen, B. (1989), 'Betonbjælkers Forskydningsbæreevne Under Hensyntagen til Buevirkning', in Danish, *Bygningsstatiske Meddelelser*, Vol. 60, No. 1, Danish Society for Structural Science and Engineering, 49 pp.

Heshe, G. (1988), 'Experimental Research on Compact Reinforced Composite (CRC)', *Bygningsstatiske Meddelelser*, Vol. 59, No. 1, Danish Society for Structural Science and Engineering, 79 pp.

Imam, M., L. Vandewalle & F. Mortelmans (1994), 'Shear Capacity of Steel Fiber High Strength Concrete Beams', *High-Performance Concrete* (Ed. V.M. Malhotra), ACI Special Publication, SP-149, pp. 227-241.

Jensen, J.F. (1981), *Plasticitetsteoretiske Løsninger for Skiver og Bjælker af Jernbeton*, in Danish, Ph.D.-thesis, Serie R, No. 141, Department of Structural Engineering, Technical University of Denmark, 153 pp.

Kim, J.-K. & Y.-D. Park (1994), 'Shear Strength of Reinforced High Strength Concrete Beams Without Web Reinforcement' *Magazine of Concrete Research*, Vol. 46, No. 166, pp. 7-16.

Lim, T.Y., P. Paramasivam & S.L. Lee (1987), 'Shear and Moment Capacity of Reinforced Steel-Fibre-Concrete Beams' *Magazine of Concrete Research*, Vol. 39, No. 140, pp. 148-160.

Mansur, M.A., K.C.G. Ong & P. Paramasivam (1986), 'Shear Strength of Fibrous Concrete Beams Without Stirrups', *Journal of Structural Engineering*, ASCE, Vol. 112, No. 9, pp. 2066-2079.

Mphonde, A.G. & G.C. Frantz (1984), 'Shear Tests of High- and Low-Strength Concrete Beams Without Stirrups', *ACI Journal*, Vol. 81, pp. 350-357.

Mphonde, A.G. & G.C. Frantz (1985), 'Shear Tests of High- and Low-Strength Concrete Beams With Stirrups', *High-Strength Concrete* (Ed. H. Russel), ACI Special Publication, SP-87, pp. 179-196.

Narayanan, R. & I.Y.S. Darwish (1987), 'Use of Steel Fibres as Shear Reinforcement', *ACI Structural Journal*, Vol. 84, pp. 216-227.

Nielsen, M.P. (1984), *Limit Analysis and Concrete Plasticity*, Prentice-Hall Inc., Englewood Cliffs, New Jersey, xii + 420 pp.

Nielsen, M.P. & M.W. Bræstrup (1978), 'Shear Strength of Prestressed Concrete Beams Without Web Reinforcement' *Magazine of Concrete Research*, Vol. 30, No. 104, pp. 119-128.

Roikjær, M., C. Pedersen, M.W. Bræstrup, M.P. Nielsen & F. Bach (1979), *Bestemmelse af Ikke-Forskydningsarmerede Bjælkers Forskydningsbæreevne*, in Danish, Serie I, No. 62, Structural Research Laboratory, Technical University of Denmark, 44 pp.

Sarsam, K.F. & J.M.S. Al-Musawi (1992), 'Shear Design of High- and Normal Strength Concrete Beams with Web Reinforcement', *ACI Structural Journal*, Vol. 89, pp. 658-664.

Sharma, A.K. (1986), 'Shear Strength of Steel Fiber Reinforced Concrete Beams', *ACI Journal*, Vol. 83, pp. 624-628.

Shin, S.W., J.G. Oh & S.K. Ghosh (1994), 'Shear Behaviour of Laboratory-Sized High Strength Concrete Beams Reinforced with Bars and Steel Fibers', *Fiber Reinforced Concrete, Developments and Innovations* (Eds. J.I. Daniel & S.P. Shah), ACI Special Publication, SP-142, pp. 181-190.

Swamy, R.N. & H.M. Bahia (1985), 'The Effectiveness of Steel Fibers as Shear Reinforcement', *Concrete International: Design & Construction*, Vol. 7, No. 3, pp. 35-40.

Swamy, R.N., R. Jones & A.T.P. Chiam (1993), 'Influence of Steel Fibres on the Shear Resistance of Lightweight Concrete I-Beams', *ACI Structural Journal*, Vol. 90, pp. 103-114.

Tan, K.H., K. Murugappan & P. Paramasivam (1993), 'Shear Behaviour of Steel Fiber Reinforced Concrete Beams', *ACI Structural Journal*, Vol. 90, pp. 3-11.

Thorenfeldt, E. & G. Drangsholt (1990), 'Shear Capacity of Reinforced High-Strength Concrete Beams', *High-Strength Concrete* (Ed. W.T. Hester), ACI Special Publication, SP-121, pp. 129-154.

Williamson, G.R. & L.I. Knab (1975), 'Full Scale Fibre Concrete Beam Tests', *RILEM Symposium on Fibre Reinforced Cement and Concrete*, The Construction Press, Lancaster, pp. 209-214.

Xie, Y., S.H. Ahmad, T. Yu, S. Hino & W. Chung (1994), 'Shear Ductility of Reinforced Concrete Beams of Normal and High-Strength Concrete', *ACI Structural Journal*, Vol. 91, pp. 140-149.

Zhang, J.-P. (1994), *Strength of Cracked Concrete, Part 1 - Shear Strength of Conventional Reinforced Concrete Beams, Deep Beams, Corbels and Prestressed Reinforced Concrete Beams Without Shear Reinforcement*, Part of Ph.D.-thesis, Serie R, No. 311, Department of Structural Engineering, Technical University of Denmark, 106 pp.

5. Example of compresit bridge design

In this chapter an actual bridge design is considered. An existing *footbridge*, that crosses a motorway, is analyzed and a compresit solution is suggested. This compresit solution is finally compared with the actual costs of the normal concrete solution. The presentation does not include a thorough analysis of the possibilities, but a single realistic solution is chosen and investigated further in order to get a preliminary design proposal.

The footbridge in question is crossing the Amager-motorway at position 61.08 km. It is built by the Danish Road Directorate[1] in 1985. The existing solution, which is termed the NSC solution, consists of a *prestressed* concrete bridge deck with 3 circular openings, where the cables run in between. The bridge deck has 2 spans and 3 column *supports* and it is continuously running over the mid-support. In figure 5.1 a front view and a cross-section of the NSC solution is given. The bridge *spans* are 30 and 28.7 m respectively and the total length is 66.5 m. The bridge deck has a total height of 1.15 m, which gives the bridge a span - depth ratio of approximately 26, which is relatively *slender* for a normal concrete bridge.

A solution is proposed, where the concrete girder is replaced by a *box girder* design of compresit. Two variations are considered in Section 5.2: *solution A* keeps the column design from figure 5.1 unchanged with 2 spans and *solution B* investigates the possibility of dispensing with the mid-support and considering a single simply supported span. In order to minimize the material consumption of the box girder, the webs are designed as *truss structures* with compressive members of compresit and tensile members based on prestressing *tendons*. It is believed that the good bond properties of compresit make it possible to minimize the truss dimensions and still provide sufficient anchorage capacity of the strands.

The compresit solution is inspired by the HSC structures, that are designed by the French engineering company Bouygues amongst others, see e.g. *Valenchon (1992)* and *Podolny & Mireles (1983)*. The *Bubiyan bridge* in Kuwait is designed with a 3-dimensional truss structure to carry the bridge deck. The trusses are precast as equilateral triangles and then the deck is cast in-situ on the truss structure. External tendons are placed along the lower side of the girder to balance the permanent loads.

The *Sylans viaduct* also applies a truss structure to carry the bridge deck. The webs of the two-cell box girder consist of X-shaped trusses. These X-elements are precast and post-tensioned. Then a segment of the bridge girder is cast by means of 8 X-elements, that are cast into the bridge deck and a lower flange. The longitudinal reinforcement is partially external, see Valenchon (1992). The concrete used for the Sylans viaduct has characteristic compressive strength of 60 MPa.

[1]Bridge no. 3-0093, crossing of cycle path and footpath at 61.08 km, Amager motorway.

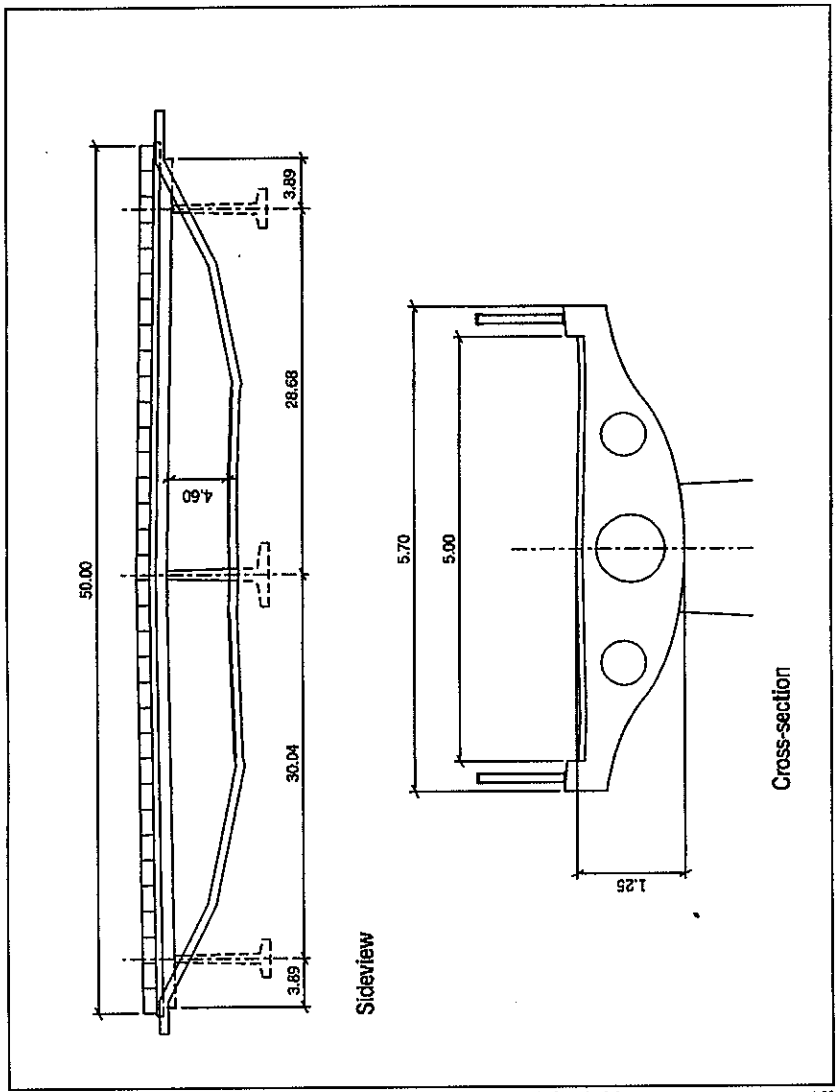

Figure 5.1: Existing prestressed concrete solution of footbridge over motorway. All measures are in m.

It is a general characteristic of these bridge designs, where an extensive minimization of the concrete is performed, that external prestressing tendons are needed. The reduced cross-sections simply make it impossible to contain the steel reinforcement.

The compresit solution is also inspired by the HSC footbridge design for the 100 years anniversary of the Danish Society of Engineers (DIF) in 1992. This bridge is situated at Lunderskov railway station crossing the railway track and it is owned by the Danish State Railways (DSB). The background for the concrete mix, applied to this design, is a part of the Danish research programme "*High-Quality Concrete in the 90ies*", which was carried out from 1988 to 1992. An innovative bridge design is used, where the bridge deck spans 30 m and makes the lower flange of the girder. In each side of the bridge deck a vertical plane truss beam is placed, i.e. a U-shaped cross-section being precast in sections of 3 m each. Underneath the bridge deck both external and embedded prestressing tendons are placed. The concrete strength for this bridge design is 75 MPa, which is used in both the ULS and the SLS.

5.1 Basic assumptions and background

In the following sections the various aspects of the compresit solution are discussed in details. It is assumed, that the compresit bridge deck is durable enough to ensure protection of the embedded reinforcement. Thus, the layer of insulation against water is omitted. This design helps both to reduce the self-weight and the costs connected with the installation of these pavement layers. These principles have been tested in Denmark by the Danish Road Directorate on both the Ryå bridge and the Madum bridge since the early 1980ies, where the effect on the durability of micro silica and fly ash respectively are tested.

In figure 5.2 the structural system is sketched with two simply supported truss beams, acting together with the *upper flange* (the bridge deck) and the *lower flange*. The cross-section of the box girder is considered to have right angles, but a more detailed investigation may suggest inclined webs. The distance between the box girder webs is chosen to 2 m and even though figure 5.2 does not show any edge beams, they are expected to be there. It is chosen to consider a truss model with vertical compressive trusses and inclined tensile trusses. The solution of inclining both the tensile and the compressive trusses is not investigated at present.

It is assumed, that the truss beams are *precast* together with the lower flange. The girder is assembled on site from the precast elements by means of prestressing and the bridge deck is cast *in-situ*. In figure 5.2 the prestressing tendons are indicated in the lower flange, but they need not necessarily to be embedded totally in compresit. Along the upper flange of each box girder web a longitudinal beam is placed. These beams also include the possibility

of prestressing reinforcement. Furthermore they act as connection between the bridge deck and the underlying precast structure.

For calculation purpose the truss system in figure 5.2 is considered to act as an ideal truss beam with pure compression or tension in its elements. However, the actual structure contains several *restraints*, that cause bending of the trusses, but these effects are not included in the present analysis. The *lower flange* is subjected to tension and in order to fulfil the deflection demand in SLS we consider *prestressing* of the lower flange. In the *upper flange* the truss beams are assumed to act together with the bridge deck in compression. The *vertical trusses* are subjected to compression and the *inclined trusses* are in tension. In figure A2.1 of *Appendix 2* the calculation model of the truss beam is shown and the internal forces of the trusses are calculated in Section A2.1.

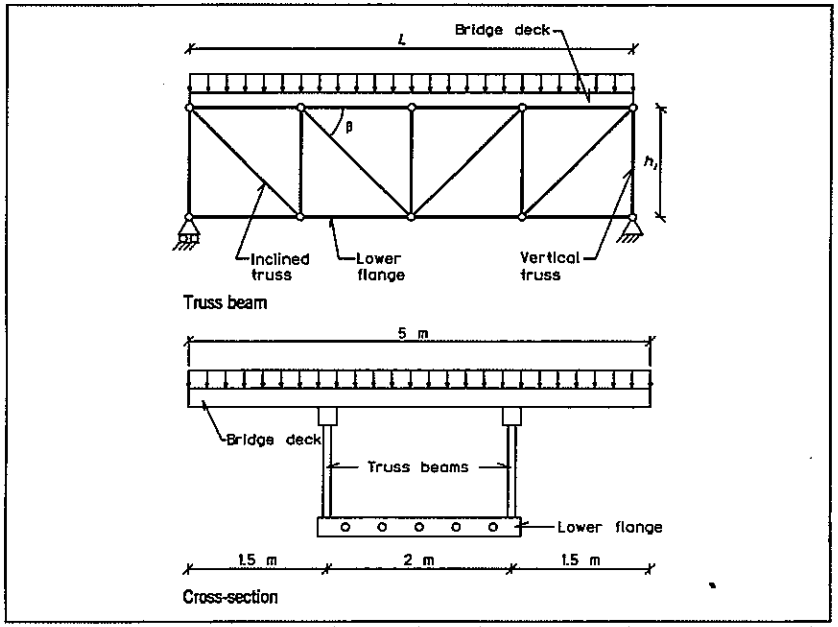

Figure 5.2: Structural model of compresit solution. The webs of the box girder consist of plane truss beams.

The existing NSC solution is prestressed with *Freyssinet tendons* of the type 12T15, i.e. a bundle of 12 strands (T15). Each strand has a nominal diameter of 15.2 mm and a nominal cross-sectional area of 139 mm^2. This type of strands are also used in the compresit solution. The *number of tendons* used in the NSC solution is 10 tendons in the lower beam side at mid-span and 16 tendons in the upper beam side over the mid-support, cf. figure 5.1. A total

of 4 tendons run through the entire length of the bridge, while 6 tendons only run 3/4 of the length from each end. All the tendons run in between the 3 openings of the cross-section.

Material parameters and loading. In the following the material strengths and stiffnesses to be used in the design are given. The values are partly based on *DS 411 (1984)* and on the experimentally determined material properties of compresit matrix with approximately 6 % steel fibres, that are reported in Part I of the thesis[2].

The *characteristic compresit strength* is chosen to f_c = 140 MPa and with the partial coefficient γ_c = 1.8 we obtain f_{cd} = 78 MPa.

For the steel reinforcement we use a partial coefficient of γ_s = 1.4 according to DS 411 (1984). In case of *conventional* reinforcement bars a characteristic *yield strength* of f_y = 400 MPa is applied, which gives f_{yd} = 286 MPa. In case of the *prestressing* strands, which consist of high-strength steel, a characteristic *yield strength* of f_y = 1600 MPa is utilized, which gives f_{yd} = 1143 MPa. The characteristic *modulus of elasticity* of the steel is E_s = 200 GPa for both types of steel.

The characteristic *short-term stiffness* of the compresit matrix is based on a modulus of elasticity of E_c = 50 GPa, i.e. α_0 = 200/50 = 4. The *long-term stiffness* is based on E_c = 20 GPa, i.e. α_∞ = 10, cf. Section 3.3.3.

Two types of loads are considered on the footbridge. The *dead load* per unit length is denoted p and the *live load* is denoted q. According to the *load rules* prescribed by the Danish Road Directorate the characteristic live load on a footbridge is a constant load per unit area of 5 kN/m^2. It is assumed, that the traffic is restricted by a bar at each end so that no vehicles can enter the bridge. The dead load consists of the self-weight of the bridge deck and the girder. The weight of hand rails, signs and lighting columns are included in p.

In DS 411 (1984) the normal *load combination* to use in *ULS* is the dead loads together with the live load increased from its characteristic value with 30 %. Thus the *ULS load combination* is written

$$q_d = p + 1.3q \tag{5.1}$$

If the width of the traffic area is 5 m like in figure 5.1, then the *live load* is found to q = 25 kN/m. The *self-weight* of the compresit bridge deck and girder is estimated to approximately p = 30 kN/m, which is justified later on. The existing concrete solution in figure 5.1 has a girder self-weight of approximately 54 kN/m.

[2]Basic Strength Properties of Compresit Matrix.

Centrally loaded column. The vertical compression trusses are designed according to DS 411 (1984), taking the risk of buckling into consideration. The method is briefly summarized here. The method is based on the *Engesser theory*, where the *tangent modulus of elasticity* of the uniaxial compressive concrete stress - strain curve is used.

The description is based on a *square column* with cross-sectional width b. The critical stress σ_{cr} is defined as

$$\frac{\sigma_{cr}}{f_{cd}} = \frac{1}{1 + \frac{f_{cd}}{E_{cd}}\left(\frac{l_s}{\pi i}\right)^2}, \qquad \frac{l_s}{\pi i} = \frac{\sqrt{12}\, l_s}{\pi\ b} \tag{5.2}$$

where l_s is the *buckling length* and the radius of inertia $i = \sqrt{(I_c/A_c)}$. Normally no contributions from the reinforcement are included in the cross-sectional constants. It is noted that the reduced strengths, corresponding to the ULS, are applied. DS 411 (1984) recommends that E_{cd} in eq. (5.2) is set to 75 % of the initial compressive modulus of elasticity. For NSC with characteristic strength f_c = 40 MPa we obtain $E_{cd}/f_{cd} \approx 710$, while this ratio equals approximately 270 for compresit matrix with f_c = 140 MPa.

The central compressive load C on the column is restricted by the following 3 criteria:

$$\frac{C}{A_c \sigma_{cr}} \le \begin{cases} 1 + \alpha\phi\ , & \alpha = E_{sd}/E_{cd}\ , \quad \phi = A_s/A_c \\ 1 + \Phi\ , & \Phi = \phi f_{yd}/f_{cd} \\ 2 \end{cases} \tag{5.3}$$

where the first criterion represents the situation without yielding of the reinforcement bars and the second criterion includes yielding. The third criterion ensures, that the reinforcement bars do not carry more load than the concrete, that surrounds them. It is demanded in DS 411 (1984), that the reinforcement bars must be properly confined against buckling by means of stirrups. It is noted that the yield strength f_{yd} corresponds to yielding under compression.

The *short-term elasticity ratio* α_0 for a good NSC is approximately equal to 10. For *compresit matrix* it is assumed, that the elasticity ratio in eq. (5.3) equals approximately 4. For mild steel reinforcement bars with a characteristic yield strength in compression of approximately 400 MPa we obtain $f_{yd}/f_{cd} \approx 7$ for NSC and $f_{yd}/f_{cd} \approx 4$ for compresit. It is assumed, that the design expressions in eqs. (5.2) and (5.3) are applicable to compresit with the parameters described above. It appears that the two first criteria in eq. (5.3) are practically identical for compresit because $\alpha \approx f_{yd}/f_{cd}$.

In figure 5.3 a normalized version of eq. (5.3) is shown with typical compresit data inserted. For constant values of the normalized load $C/b^2 f_{cd}$ the necessary *reinforcement ratio* ϕ is given as a function of the normalized buckling length l_s/b. When the column length

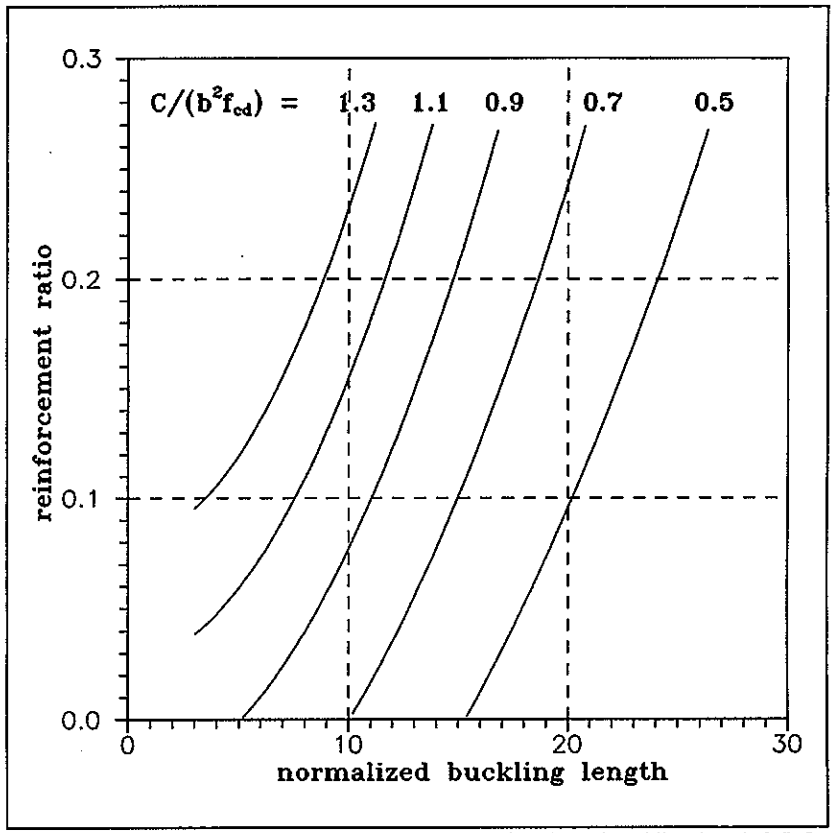

Figure 5.3: Necessary reinforcement ratio ϕ as a function of buckling length l_s/b for a compresit column. Note that reduced material strengths are applied according to ULS.

increases the necessary reinforcement ratio also increases, but at a certain point the third criterion in eq. (5.3) is met and no further reinforcement helps. In this case a larger cross-section is needed in order to carry the specified load C.

For a given load C the minimum column width b_{min} to carry this load is calculated from

$$b_{min}^2 = \frac{1}{4}\frac{C}{f_{cd}}\left(1 + \sqrt{1 + 9.73\frac{(f_{cd} l_s)^2}{C E_{cd}}}\right) \tag{5.4}$$

where eq. (5.2) is inserted into the third criterion of eq. (5.3). From figure 5.3 it appears, that the reinforcement ratio necessary to obtain this minimum width is approximately 27 %, which is rather high for practical considerations. Even though the concept of compresit includes high amounts of reinforcement then 27 % is too high in practice.

5.2 Compresit solution

The analysis in this section are based on the calculations performed in *Appendix 2*. Section A2.1 includes expressions for the *internal forces* in the trusses of the beam. In figure A2.1 of Appendix 2 the calculation model is outlined. Like it appears a rather simple model is chosen for the analysis, which also reflects the rough nature of the analysis.

The optimum truss configuration. In order to determine the *configuration* of the truss beam the *material consumption* is analyzed in Section A2.2 of Appendix 2. When the truss angle β in figure 5.2 is varied the necessary amount of steel reinforcement and compresit vary. In the following the optimum truss angle is evaluated in order to obtain *minimum material costs* of the truss beam.

The tensile forces in both the lower flange and in the inclined trusses are assumed to be carried by *prestressing tendons*. The vertical compressive trusses are compresit columns reinforced by means of *mild reinforcement steel*. The upper flange, which consists primarily of the bridge deck, is not included because its dimensions do not depend on the truss angle. The *buckling length* l_i in eq. (5.4) of the vertical trusses is assumed to equal the depth h_i, which is a safe value, because these trusses are actually restrained to a certain degree by the upper and lower flanges.

For a given set of parameters such as the beam span L, the depth h_i and the load q, the number of sections n together with β vary through $n\cot\beta = L/h_i$. The necessary steel volume is given in eqs. (A2.5) and (A2.6) of Appendix 2 and the compresit volume in the vertical trusses is given in eq. (A2.7). In order to obtain a reasonable comparison the material volumes are converted into *material costs*.

The *material price* for reinforced compresit is estimated to DKK 20,000 per m^3 compresit and for prestressing steel it is estimated to DKK 30 per kg, which gives DKK 234,000 per m^3 steel. These estimates are only used for comparative matters in the present analysis, but they are further discussed in Section 5.3. In *figure 5.4* a comparison of 3 different beam geometries is given ($L/h_i = 15$, 30 and 45). The total material costs in the figure are divided with the parameter qL^2/f_{yd}, which has the unit m^3.

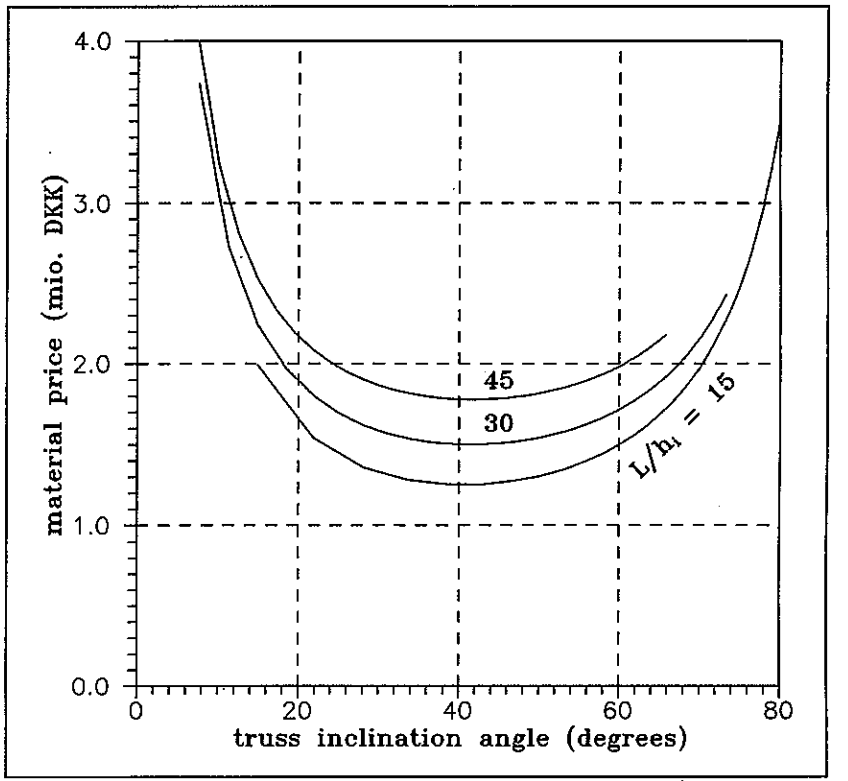

Figure 5.4: Theoretical material price normalized with respect to qL^2/f_{yd} versus truss angle β. Three different beam geometries $L/h_i = 15$, 30 and 45.

It is evident from figure 5.4, that the optimum is rather shallow, which is often found in structural optimization problems. However it seems reasonable, that β should be chosen in the vicinity of 40° to obtain a satisfactory solution.

Compresit configurations. Two different compresit solutions are presented. In each situation it is tried to put the compresit material to its limit. From an *architectural point of view* it seems desirably to reduce the truss angle β from its optimum value of approximately 40° because this gives a lighter appearance of the truss structure. Because the optimum in figure 5.4 is not so well-defined it is decided to choose a value of β nearer to 30° than 40°. The two compresit solutions are termed solution A and B:

- *Solution A* consists of *two* simply supported girders each spanning $L = 30$ m between the existing supports, cf. figure 5.1. The bridge girder is not considered to be continuous over the mid-support, even though it probably is in an actual design situation. The internal moment lever distance is taken as $h_i = 1$ m and each truss beam is divided into $n = 18$ sections, which gives $\beta = 31°$.

- *Solution B* consists of a *single span* girder simply supported with $L = 60$ m. Thus, the mid-support in figure 5.1 is dispensed with. In order to test the possibility of very slender beams we set $h_i = 1.5$ m and $n = 24$, which gives $\beta = 31°$.

In the following sections these two solutions are treated with respect to both the SLS and the ULS, according to the material data given in the previous section.

5.2.1 ULS design

In this section the cross-sectional dimensions of the two solutions are determined together with the reinforcement requirements. It is noted that the calculations do not include all details required for a final design. The load q_d, given in eq. (5.1), is applied to the girder. The dead load is estimated to $p = 30$ kN/m and the live load equals $q = 25$ kN/m, because the lane width is 5 m, cf. figure 5.1 and 5.2. This gives a total *ULS load* per unit length, that equals $q_d = (30 + 1.3 \cdot 25)$ kN/m = 62.5 kN/m.

Vertical compressive trusses. Equation (5.4) is used to determine the smallest possible width of the square compresit trusses. The compressive load corresponding to the outermost truss is applied, i.e. $C = 0.25 q_d L$. The reason for the factor 0.25 is that the load q_d is divided on 2 truss beams. The results of the calculations are *minimum column widths* b_{min} equal to 74 mm for solution A and 107 mm for solution B.

	Solution A	Solution B
Length $l_s = h_i$ (mm)	1000	1500
Width b (mm)	80	120
l_s/b	12.5	
$C/(b^2 f_{cd})$	0.94	0.84
Necessary ϕ (%)	15	12

Table 5.1: Necessary width and reinforcement ratio of vertical trusses according to the curves of figure 5.3. Calculated from the outermost vertical truss in the beam.

The necessary reinforcement ratios under these minimum dimensions are rather high ($\phi >$ 25 % from figure 5.3). If these widths are increased slightly the need for reinforcement decreases. In table 5.1 the conditions are shown, when b is increased from its minimum value to 80 and 120 mm for solution A and B respectively. It appears that this increase of widths reduces the necessary reinforcement ratio to about half.

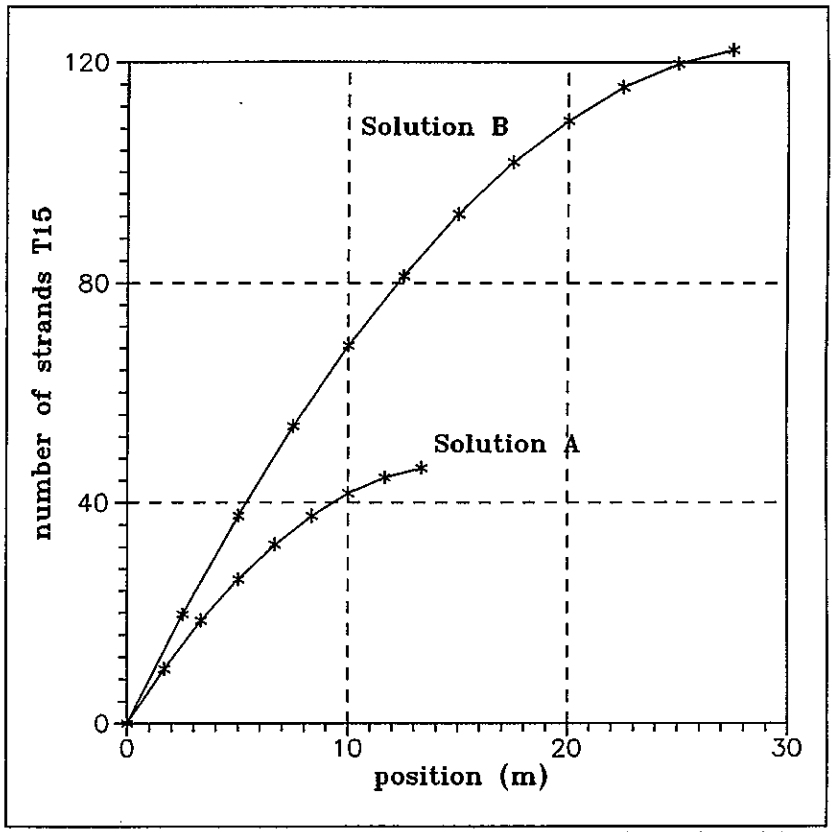

Figure 5.5: Necessary number of prestressing strands in lower flange of box girder as a function of the position from the simply supported end.

It is obvious, that a more detailed analysis should include the variation in compressive internal forces throughout the truss beam together with the restraints from the bridge deck and the lower flange, i.e. include the correct buckling length, but this analysis is not performed here.

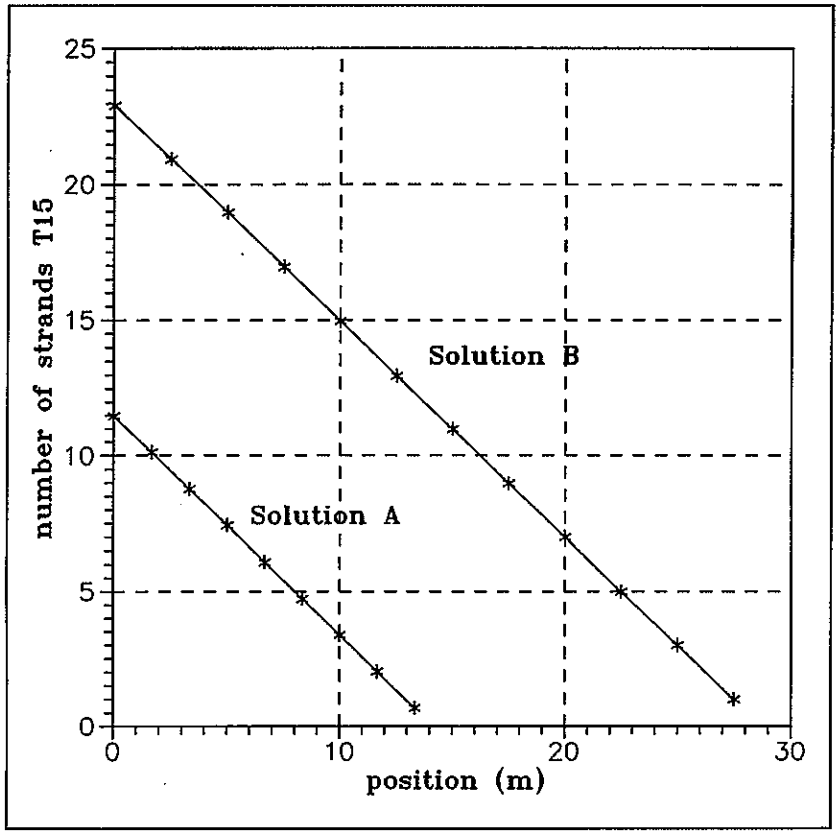

Figure 5.6: Necessary number of prestressing strands in the inclined trusses as a function of the position from the simply supported end. Note that the strands should be divided between two truss beams.

Prestressing tendons. Based on the expressions in eqs. (A2.1) and (A2.2) of Appendix 2 the necessary amount of prestressing steel is evaluated. The amount is presented as the number of *Freyssinet strands T15*, each having a nominal cross-sectional area of 139 mm^2. In *figure 5.5 and 5.6* the necessary number of strands is shown, corresponding to the lower flange of the box girder and the inclined trusses respectively. The axis of abscissas in the diagrams gives the position from the simply supported end of the girder. The curves only apply for one half of the span in each case because of the symmetry. Each mark on the

curves corresponds to a section of the truss beam. It is not surprising, that the curves are similar to the variation of the bending moments and the shear forces within the girder.

In the *lower flange* we need 4 tendons 12T15, i.e. 48 strands, in *solution A* to carry the tensile force at mid-span, while *solution B* needs 10 tendons at mid-span, cf. figure 5.5. It turns out that the SLS gets most restrictive than the ULS, so that the tendon arrangement of the lower flange is treated further in the following section.

Figure 5.6 shows, that the *outermost inclined trusses* need 7 strands in *solution A* and 12 strands in *solution B*. Note that the values in figure 5.6 are the total number of strands, which apply to both truss beams. The necessary amount of strands reduces to only a few strands towards the girder mid-span. The actual choice of reinforcement arrangement in the inclined trusses depends on several conditions. In the calculations to follow it is assumed, that the amount of prestress reinforcement in the inclined trusses corresponds with the curves in figure 5.6.

Bridge deck slab. The bridge deck is supported by the box girder webs, see figure 5.2. *Edge beams* run along both edges of the deck to ensure sufficient stiffness and to carry the hand rail of the footbridge. The beams, that run along the upper flanges of the truss beams, are precast together with the trusses and the lower flange and they primarily serve to anchor the reinforcement from both the vertical and the inclined trusses.

The cross-section of the bridge deck is modelled as a *cantilever beam* in the present analysis. The cantilever length is approximately 1.5 m and the maximum bending moment occurs above the supports from the truss beams. The constant *thickness* of the slab is estimated to 100 mm, which is a value chosen from practical considerations concerning in-situ casting, rather than the result of an optimization. The reinforcement of the slab consists of *deformed mild steel bars* in both longitudinal and transversal directions. A preliminary calculation shows, that a reinforcement ratio of ϕ = 1 % is enough to carry the ULS load.

The bridge deck also acts as the compressive upper flange of the box girder. In both solution A and B the maximum compressive force at mid-span does not result in any problems, but care must be taken in making the slab act together with the precast trusses. It is emphasized, that the ULS design of the bridge deck is only meant to guide a more detailed approach, which is not performed in this thesis. It is obvious that possibilities exist to save material in the deck slab. For instance by varying the slab thickness.

5.2.2 SLS design

The SLS design is performed according to the *downward-directed deflections* δ of the bridge at mid-span. The dead load p gives *long-term* deformations, that are counteracted by an initial upward-directed deflection δ_{inf}, i.e. a certain camber of the girder. The deflections corresponding to the live load q should not exceed 1/400 of the span L in order to ensure

suffient *bending stiffness* of the bridge, cf. Broteknik (1984). The possible SLS load q_s, that is considered, lies within the dead load p = 30 kN/m and the maximum SLS load q_{smax} = $p+q$ = (30+25) kN/m = 55 kN/m.

In Section A2.3 of Appendix 2, expressions for the mid-span deflection δ of the bridge girder are given. The deflection is considered to be a sum of 4 contributions, viz. $\delta = \delta_F + \delta_T + \delta_K + \delta_C$, where

- δ_F originates from the inclined trusses,
- δ_T originates from the lower flange,
- δ_K originates from the upper flange and
- δ_C originates from the vertical trusses.

Equations (A2.13) - (A2.17) give expressions for these 4 separate deflection contributions. Note that downward-directed deflections are considered positive.

The deflections depend on the *prestressing* of the lower flange, according to the *prestress degree* σ_{pre}/f_{yd}, where σ_{pre} is the prestress of the tendons and f_{yd} is their strength. In the analysis only a constant value of σ_{pre}/f_{yd} is considered.

	Solution A	Solution B
Span L and depth h_t (m)	30 and 1	60 and 1.5
Sections n, β, l	18, 31°, 1.67 m	24, 31°, 2.5 m
Through tendons (12T15)	2 tendons	6 tendons
Extra tendons (12T15)	2 tendons from each end of length 28 m.	4 tendons from each end of length 45 m. 2 tendons in the central part of length 15 m.

Table 5.2: Necessary number of prestressed tendons (Freyssinet 12T15) in lower flange in order to ensure compression in the SLS. The constant prestress degree is σ_{pre}/f_{yd} = 0.6. Notation taken from figure A2.1.

Tendons in lower flange. The amount of strands in figure 5.5 is necessary to ensure the ULS carrying capacity, but it is not enough to ensure the SLS demands. The number of prestressed tendons in the lower flange is chosen so that the flange is under compression during its service life. Thus, with a given prestress degree and the maximum service load $p+q$ = 55 kN/m applied, the lower flange should be in compression. The constant prestress

degree is chosen to σ_{pre}/f_{yd} = 60 %. No effects of steel relaxation or frictional losses are included in the present investigation. In table 5.2 the necessary number of tendons (Freyssinet 12T15) is given.

The reason for ensuring compression of the lower flange is in order to apply its compressive stiffness which is much larger than the tensile stiffness of the tendons alone. It would be possible to allow tensile stresses if only the cracking criterion of the SLS is considered because compresit matrix has a large tensile strain capacity without discrete cracking. However, the deflection criterion is more strict than the cracking criterion.

Short-term deflections. When compression is ensured in the lower flange of the girder due to prestressing and the deflection calculations are linear-elastic, then the deflections increase linearly with the SLS load q_s. In table A2.1 of Appendix 2 the calculated deflections are listed for each of the above-mentioned contributions. The following assumptions concerning the stiffnesses of the trusses are applied in the calculations:

- The *inclined trusses* are reinforced by means of prestressing strands, according to figure 5.6, i.e. exactly enough to fulfil the ULS demands.
- The cross-sectional dimensions of the compresit *lower flange* are estimated to equal 2 × 0.2 m, cf. figure 5.2.
- The *upper flange* cross-sectional dimensions are taken as those of the bridge deck, i.e. 5 × 0.1 m.
- The square cross-sections of the *vertical trusses* have dimensions $(80\ mm)^2$ and $(150\ mm)^2$ for solution A and B respectively, cf. table 5.1.

The *upper limit* for the short-term deflections from the *live load* q = 25 kN/m, is $L/400$, which equals 75 and 150 mm respectively for solution A and B in order to ensure sufficient bending stiffness. The calculations show, that the increments in deflections, corresponding to the live load, are equal to 104 mm and 316 mm for solution A and B respectively. Thus, neither of the compresit solutions fulfils the SLS demand unless the girder is stiffened further.

For *solution A* the deflection demand is fulfilled by increasing the stiffness of the inclined trusses, i.e. by reducing the term δ_F in table A2.1. It is recalled, that the reinforcement of the inclined trusses corresponds precisely to the number of prestressing strands given in figure 5.6. However, the actual number of strands will be higher of practical reasons and therefore the stiffness of the inclined trusses is underestimated in the calculations. The analysis in eq. (A2.20) of Appendix 2 shows that, if the number of prestressing strands in each inclined truss is *increased by 60 %*, then the sufficient stiffness of the bridge girder is obtained.

For *solution B* the beam span is relatively higher, than in solution A (L/h_l = 40 and 30 respectively), which causes problems in the SLS. The calculations in Section A2.3 show, that it is not sufficient to increase the stiffness of the inclined trusses alone, cf. eq. (A2.22). In order to fulfil the condition $\delta(p+q) - \delta(p) \leq L/400 = 150$ mm we have to prestress the inclined trusses as well as the lower flange. In the previous considerations the inclined trusses have only contributed to the stiffness by the reinforcement steel. It is assumed, that the prestressing strands are embedded in compresit, but its stiffness is not included under tension. If however, the inclined trusses are in compression, for instance due to prestressing, then the compresit cross-sections get active.

In eqs. (A2.17) and (A2.23) of Appendix 2 a simple method to increase the stiffness is given, by means of prestressing the embedded strands in the inclined trusses. For instance, the strands are prestressed before casting. The model assumes, that each truss is prestressed according to its maximum tensile force during its service life, which means compression at all times and involves the total compresit cross-section instead of just the reinforcement. The cross-sectional dimensions of the square trusses are assumed to equal (150 mm)^2. By means of this prestressing of the inclined trusses their stiffness is increased by a factor 3.

Finally it is assumed, that the stiffness of the *upper flange* (bridge deck) can be increased with 50 %, if the contributions from the steel reinforcement and the edge beams are included in the stiffness calculations. In eq. (A2.24) the expression for the deflections is given, where both the prestressed inclined trusses and the increased upper flange stiffness are included. The deflection increment, corresponding to the live load, is now reduced to 178 mm, which is a little higher than the limit of 150 mm.

It is emphasized that the investigation of solution B is mainly performed in order to evaluate the possibilities of increasing the beam span at a higher rate than the beam depth. Therefore we have not performed any increase of the depth h_l from 1.5 m in order to obtain a sufficient bending stiffness of the bridge girder. However, this possibility also exists.

Long-term deflections. In the previous analysis of the short-term deflections the initial modulus of elasticity E_c = 50 GPa is applied for compresit matrix in the calculations. When the dead load alone is considered, the deflections increase as a function of time because of the *creep characteristics* of the compresit matrix. The *relaxation* of the prestressing steel also causes time dependent deflections. These various time dependent effects are included in the *long-term modulus of elasticity* equal to 20 GPa, cf. Section 3.3.3.

In table A2.2 of Appendix 2, the expressions for long-term deflections are given for the two compresit solutions. From the expressions in this table we calculate the long-term deflections δ_∞ under the dead load p = 30 kN/m. In table 5.3 both the short-term deflections and the long-term deflections are listed.

It is generally accepted, that a bridge looks best with a small camber at all times. Therefore it is chosen to provide the solutions in table 5.3 with an initial upward-directed deflection

δ_{ini} during construction. The value δ_{ini} = 150 mm is chosen for both solutions. For solution A this camber value ensures, that not even the maximum SLS load results in positive deflections. For solution B the dead load alone is unable to produce positive deflections. As in solution A the initial deflection δ_{ini} = 150 mm ensures, that the maximum SLS load does not result in positive deflections.

	Solution A	Solution B
Span L, depth h_l	30 m, 1 m	60 m, 1.5 m
Sections n, β, l	18, 31°, 1.67 m	24, 31°, 2.5 m
Short-term δ_0 (mm)	60	-51
Long-term δ_∞ (mm)	68	-65
Initial δ_{ini} (mm)	150	150

Table 5.3: Deflections calculated for the dead load p = 30 kN/m. Note that the camber δ_{ini} is upward-directed, while the other deflections are positive as downward-directed. Notation taken from figure A2.1.

5.3 Price comparison with existing concrete solution

The two compresit solutions A and B from the previous section are compared with the existing concrete solution. This comparison is based on the *price estimate* from the contractor. In fact the prices are taken from the cheapest bid out of 4 different bids. The analysis only concerns the structural elements, that are expected to cause differences between the solutions. The topics that are considered in the price comparison are the following:

- Primarily the amount of concrete/compresit and reinforcement steel differs between the various solutions.
- The top-layers of insulation against water on the bridge deck together with the top-layer to resist abrasion are omitted in the two compresit solutions.
- The mid-support column is dispensed with in solution B. For solution A the columns are assumed identical to those in the existing concrete solution.
- The form work is assumed identical for the solutions, because the widths of the bridge deck are identical.

- The amount of scaffolding for the compresit solutions are less than for the existing concrete solution, because the precast truss beams act as scaffolding for the bridge deck mould. However, these differences between the solutions are assumed to balance, because the truss beam involves transportation and assembling on site.

- The *moulds* for the circular openings of the existing concrete solution are not included in the compresit solutions. These moulds consist of corrugated steel tubes.

In Section A2.4 of Appendix 2 the amounts of compresit matrix, prestressing tendons and mild steel reinforcement are calculated for solution A and B. From these amounts the total material costs for the bridge girder are calculated. The prices of the reinforcement steel are taken from the estimate.

	Prices in 1,000 DKK		
	Existing concrete solution	Compresit solution A	Compresit solution B
Bridge deck, top layer	91	0	0
Bridge deck, moisture insulation	180	0	0
Prestressing reinforcement	275	162	357
Mild steel reinforcement	190	111	111
Mould for openings	43	0	0
Supports	243	243	162
Sum in 1985-DKK	1,022	516	630
Sum in 1995-DKK	1,345	679	829
Concrete/compresit price in 1995-DKK	484	890	890
Total sum in 1995-DKK	1,829	1,569	1,719

Table 5.4: Price comparison between the existing concrete solution, compresit solution A and compresit solution B (without mid-support). The price index for 1985 and 1995 is 509 and 670 respectively. The content of the table only treats the elements, that are changed in case of the compresit solution.

It is assumed, that the consumption of compresit is divided into the bridge deck, which is cast in-situ, and the truss beams being precast. The *compresit prices* for these two applications are estimated to DKK 6,000 per m^3 and DKK 17,000 per m^3 respectively. The cost of compresit matrix for the in-situ casting is more or less based on the raw material cost including 6 % steel fibres of type Dramix OL 12/.4 (L_f = 12 mm and d_f = 0.4 mm). The precast compresit cost is based on experiences obtained from the prefabrication of 40,000 compresit slabs to serve as drainage covers in the bottom of the Great Belt tunnel.

In table 5.4 the total prices are calculated from the amounts in Section A2.4 of Appendix 2 for the various elements of the bridge. The amount of *Freyssinet tendons* vary for the 3 solutions with solution A being cheapest. It is recalled, that solution A is treated as two separate simply supported girders, while the existing concrete solution is a continuous girder. The existing solution applies 727 m of tendons, while solution A and B apply 400 and 980 m respectively.

The *column supports* are included in table 5.4, because solution B does not include the mid-span column. In Section A2.4 the total price of the 3 columns is evaluated from the estimate. The costs for the existing concrete solution and solution A are assumed identical, while solution B is taken as 2/3 of this price. Thus, no investigation is performed to control whether the supports and the foundations need to be enlarged or reduced because of the changes in loading and self-weight.

The comparison does not include any eventual differences in the *earthworks* between the 3 solutions. It seems reasonably, that solution A is made similar to the existing solution with respect to the foundations, the columns and the embankments, because the depth of the girders are almost identical. However, for *solution B* the beam depth is increased by approximately 0.5 m and therefore the embankments need to be higher, i.e. higher costs of the earthworks. A very rough calculation of this extra cost from buying and adding more soil and gravel to raise the two embankments 0.5 m gives an amount of approximately 1995-DKK 250,000. If this amount is added to solution B in table 5.4 it exceeds the cost for the existing solution by about 100,000.

5.4 Concluding remarks

This section concludes the numerical calculations of a small footbridge made of compresit. The existing concrete bridge has a length of approximately 60 m with two continuous spans, see figure 5.1. This prestressed bridge girder is replaced by a compresit single-box girder with a plane truss system in each of its two webs. In figure 5.7 to 5.10 the appearance of the two compresit solutions are outlined in order to give the reader a better impression of the suggestions. The details of the compresit design are not treated in the present analysis, but a reasonable estimate of the outer dimensions and the necessary reinforcement are

provided in Section 5.2. The next step of the analysis is to model the structure more accurate, for instance by means of a finite element model. Furthermore the design of the nodes, where the trusses meet, still needs extensive calculations. Another topic that needs further investigation is the conditions during the assembling of the precast sections together with the prestressing procedure, which are important issues.

In Section 5.3 the solutions are compared from an *economic* point of view. The result is found in table 5.4 in terms of 1,000 DKK. It is noted, that the prices in table 5.4 are not the total cost for a complete bridge, but only includes the elements, where obvious differences exist between the 3 solutions. The table shows, that the price of compresit solution A is almost DKK 300,000 less than the concrete solution, while the price of solution B is almost equal with the concrete solution. Thus, it seems justified, that the compresit material, which is a rather expensive material, is considered to be *competitive* with normal concrete. Note that the compresit solutions are even more slender, than the existing concrete solution.

The analysis on the ULS and the SLS in Section 5.2 shows, that the slender design makes it difficult to fulfil the SLS demands. The bending stiffness of the bridge girder requires a certain amount of compresit material in both the compressive upper flange and in the lower flange, which is also compressed as a result of the prestressing. Thus, even though it seems possibly to minimize the dimensions of the lower flange, due to the ULS, then the dimensions are necessary to ensure the proper bending stiffness.

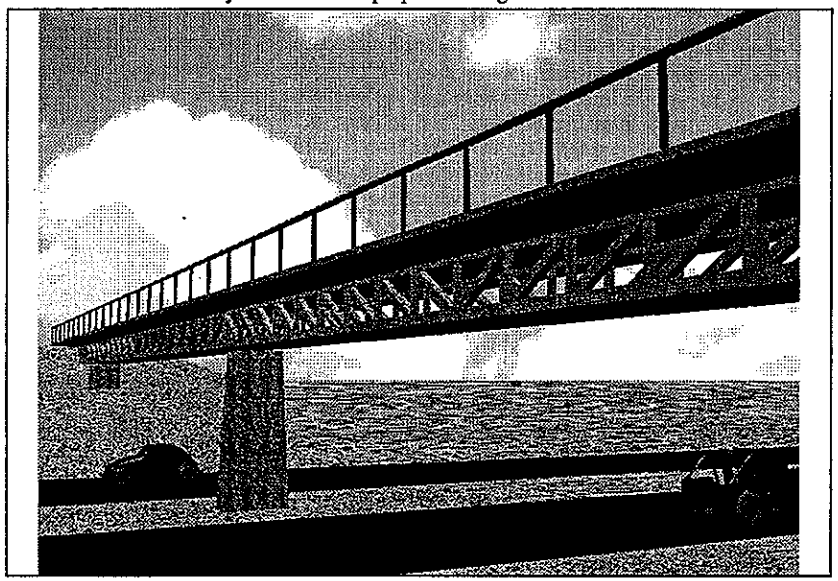

Figure 5.7: Illustration of compresit solution A.

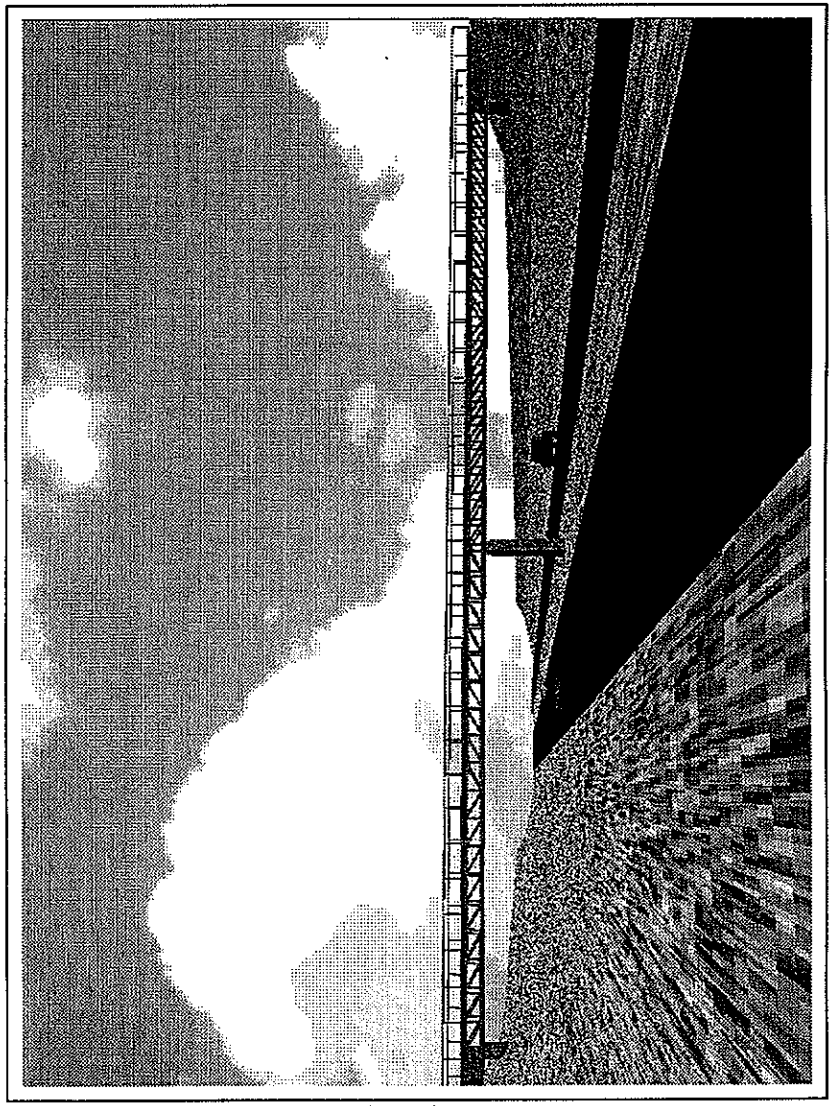

Figure 5.8: Front view of compresit solution A.

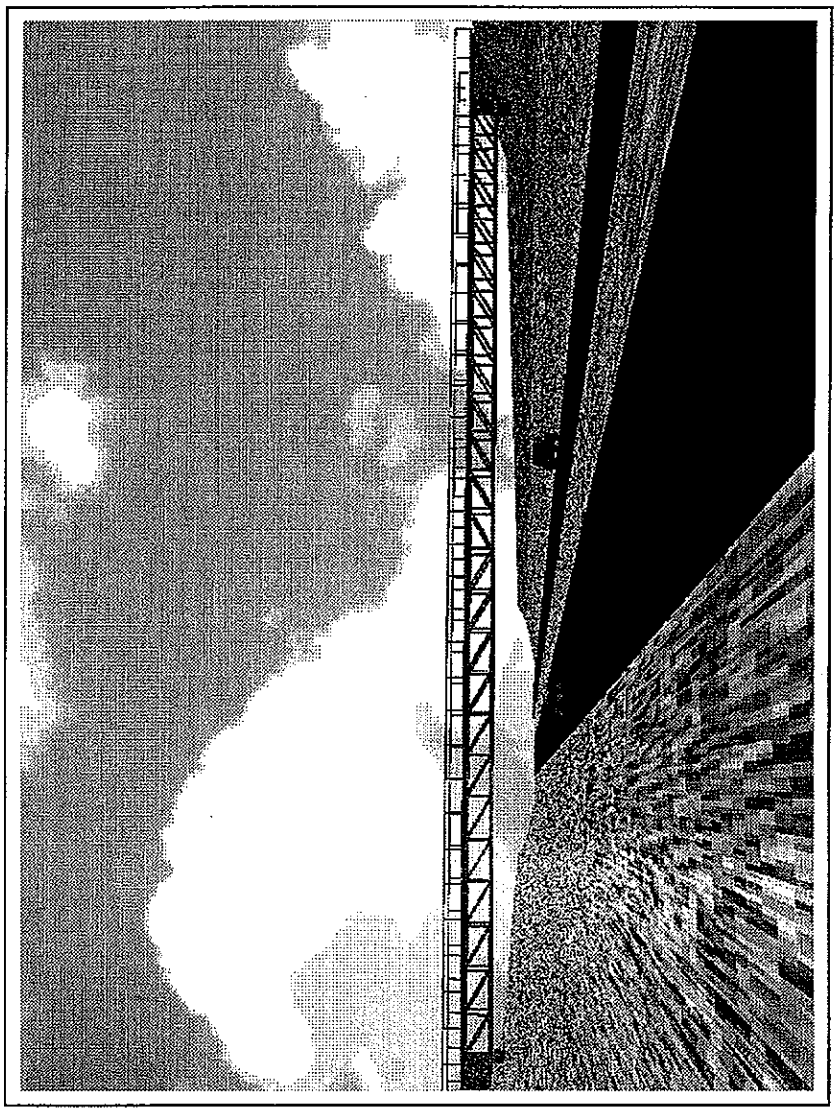

Figure 5.9: Front view of the compresit solution B.

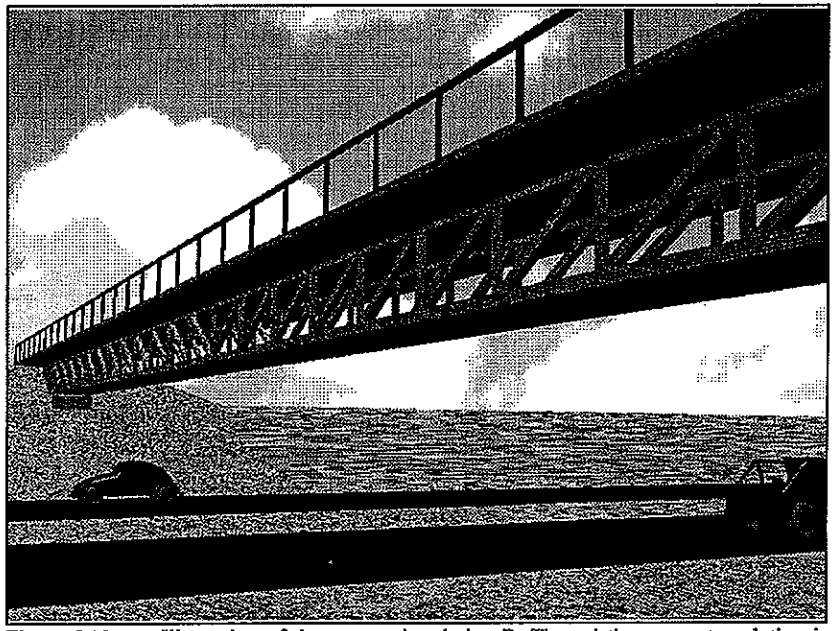

Figure 5.10: Illustration of the compresit solution B. The existing concrete solution is outlined in figure 5.1.

5.5 References

Broteknik (1984), *Belastninger, Beregnings- og Belastningsregler for Vejbroer*, in Danish, Vejdirektoratet, Vejregeludvalget, 29 pp.

DS 411 (1984), *Danish Code of Practice for the Structural Use of Concrete*, 3rd Ed., Dansk Ingeniørforening, 98 pp.

Podolny, W. & A.A. Mireles (1983), 'Kuwaits Bubiyan Bridge - a 3-d Precast Segmental Space Frame', *PCI Journal*, Vol. 28, pp. 68-107.

Valenchon, C. (1992), 'Offshore Application of High Performance Concrete Space Frame', *High Performance Concrete, From Material to Structure* (Ed. Y. Malier), E & FN Spon, London, pp. 477-494.

6. Conclusions

The technical conclusions of the research are given in Section 6.1, while Section 6.2 concerns the needs for further research. The conclusions include the work of both the present report (Part II) and Part I of the thesis[1]. It is emphasized that each chapter of both reports contains a separate section titled *concluding remarks*, summarizing the most important results. The reader is referred to these sections for more detailed conclusions on the various topics.

The *scopes* of the project are mainly:

- The scientific scope was primarily to establish the triaxial failure criterion for compresit matrix. Furthermore to investigate the most important material properties with respect to e.g. the fibre characteristics.

- The technological developments should be achieved concerning the structural behaviour of compresit. Furthermore the effect of steel fibres on the plastic effectiveness factors is investigated.

- The scope for practical applications was to establish design tools for the consulting engineers.

The method to provide the *material properties* of compresit matrix as a function of fibre content and type is several experiments performed at the Department of Structural Engineering, Technical University of Denmark. In Part I these compresit experiments are reported, and a better knowledge of the basic properties such as uniaxial compression and tension is obtained. The *triaxial failure criterion*, which is very important for the theory of plasticity, is established for compresit matrix, and parallels are drawn to the behaviour of high-strength concrete in general.

Part II of the thesis, includes primarily an investigation of the structural applications of compresit. This investigation is closely compared with similar concrete materials, both plain concrete of various strengths and fibre reinforced concrete. The *design tools* for structural engineering with compresit are not provided in a complete code-like manner. However, the bridge design example, that ends the present report, introduces design principles and ideas that are expected to be used in the future. The establishing of design rules for these new concrete materials takes further experiments on structural members in order to become generally accepted.

[1]Basic Strength Properties of Compresit Matrix.

6.1 Main conclusions

Strength properties. The experimental material properties in Part I concern the uniaxial compressive and tensile stress - strain curves, the triaxial compressive strength (failure criterion) and the fracture energy (energy dissipation per unit crack area). The tests include a variation of the fibre content (V_f = 0, 3, 6 and 9 %) and the fibre geometry (aspect ratios L_f/d_f = 30, 40 and 87). The fibres in question are straight Dramix fibres. It turns out that the *fibre reinforcement index*, which is defined as $V_f(L_f/d_f)$, is a very important parameter together with the interfacial fibre - matrix *bond strength*.

Both the uniaxial compressive and tensile strengths are observed to be *linear functions* of the product of the bond strength and the fibre reinforcement index. The values are not repeated here, but it appears that the fibres tend to act as confinement of the compression cylinders. Furthermore Part I contains a simple one-parameter analytical model of the uniaxial compressive stress - strain curve for compresit matrix. This model includes both the ascending and the descending part.

An observation from the *uniaxial tensile tests* is that a reinforcement index of approximately 1 marks an important transition. For smaller fibre reinforcement indices, the tensile stresses, transferred across a crack by means of fibres, do not exceed the matrix cracking strength. However, when $V_f(L_f/d_f)$ exceeds approximately 1 the possibility exists for a subsequent cracks to be formed, because the stresses transferred by the fibres are bigger than the matrix cracking strength.

Furthermore the tensile tests show, which fibre type and geometry, that should be preferred. In order to *avoid breaking* of the steel fibres instead of *pull-out failure*, an upper limit exists for the aspect ratio L_f/d_f. A total of 3 different Dramix fibres have been tested with compresit matrix, but they only represent 2 qualitatively different fibres:

- One is a brass-coated fibre of type OL 6/.15 HC, which has L_f/d_f = 40 and diameter d_f = 0.15 mm. This fibre has a critical aspect ratio of approximately 157, i.e. the fibre length may be almost 4 times higher than it actually is without breaking.

- The other fibre type is OL 12/.4 with L_f/d_f = 30 and diameter d_f = 0.4 mm. This fibre has a critical aspect ratio of approximately 43, i.e. the fibre length may be increased by almost 50 % without breaking.

The former fibre type is much more expensive than the latter, showing a price difference of approximately factor 3. Fortunately it seems that it is the cheapest steel fibre (OL 12/.4) that is closest to its optimum length in order to utilize its capacity completely. Of course, other fibre geometries exist with hooks or deformations in order to improve their bond strength to the matrix. Preliminary tests with some of these fibre types show no significant

improvements of the mechanical properties. Therefore only straight steel fibres are applied to compresit.

The *triaxial tests* result in detailed information, concerning a proper failure criterion for compresit matrix and similar high-strength concretes. The normal Coulomb friction criterion, which states, that the triaxial strength increases linearly with the confinement pressure, is applied to the results. Generally, a *reduced angle of friction* is found like it is in various other investigations on high-strength concrete, viz. an angle φ of approximately 30° instead of 37°, which is normally applied to normal-strength concrete. This reduction in the coefficient of friction is explained by *smoother crack surfaces* in high-strength concrete, where the aggregate is cracked as well as the binder.

However, the triaxial tests also show that for small values of the confinement pressure there seems to exist a rather high angle of friction ($\varphi \approx 51°$). This value is directly connected with the increased *brittleness* of high-strength concretes. A *bi-linear* version of the Coulomb failure criterion is given, which seems to apply to compresit matrix and to other high-strength concretes. It is interesting that even though the compresit matrix contains a rather high fibre content, it still seems to act as other high-strength concretes.

From the information in Part I of the thesis, we have listed some of the most important compresit characteristics for structural application in table 6.1.

Compressive strength f_c (MPa)	Compressive strain ε_{cu} (‰)	Modulus of elasticity E_c (GPa)	Long-term modulus E_∞ (GPa)
140	6	50	20

Table 6.1: Characteristic material properties for fibre reinforced compresit. The long-term modulus of elasticity is based on a creep coefficient of 1.5.

Structural applications. One of the questions, that arises, when fibre reinforced concrete is discussed, is the effect of fibres on the ultimate carrying capacity. Do the fibres make it possible to include the tensile strength in the ULS calculations? The answer to this question is not unambiguous, but depends on many different things:

- Firstly the *experimental scatter*, that is recognized on the tensile properties of concrete in general, makes it necessary to consider relatively high amounts of fibres, in order to detect any significant effect on the load capacity.

- Even though it is possible to alter the *post-cracking* behaviour of the concrete by means of adding steel fibres, the tensile strength is still limited to a few per cent of the compressive strength.

- Keeping in mind that steel fibres are a rather expensive component of a concrete mix, it is obvious that the fibre content should be minimized. Therefore it seems unlikely for the fibres to carry a significant part of the tensile stresses on a cross-section, compared with conventional steel reinforcement in structures.

Keeping these statements in mind it is emphasized that the investigation indicates a significant effect of steel fibres on the beam *shear strength*, which is elaborated further in the following.

However, no doubt exists, whether the fibres improve the *serviceability* behaviour of a concrete structure. Both the cracking behaviour and the bending stiffness are improved by the presence of fibres, even when the fibre content is modest. These observations are common for all investigations concerning fibre reinforced concrete.

The design of long span beams of compresit, with applications for instance in bridge design, is treated theoretically with the main conclusions being discussed below.

The *ultimate bending capacity* can utilize the compressive strength of compresit, but it requires high amounts of mild reinforcement steel, or application of high-strength steel to get an improvement of the beam span. The compressive ductility of the fibre reinforced compresit matrix gives a very wide range for the reinforcement degree without the risk of over reinforcing the beam.

The high strengths give rise to minimizing the cross-sectional beam dimensions and thereby also the *bending stiffness*. The modulus of elasticity does not increase by more than approximately 25 % for compresit compared with normal-strength concrete. Thus, the bending stiffness limits the possibility of increasing the beam span. However, the possibilities of prestressing are improved because of the fibres.

The *beam shear strength* seems to increase with the presence of steel fibres, especially for beams without stirrup reinforcement. This effect is modelled by a *plastic solution* without taking the concrete tensile strength into account, i.e zero tension cut-off. It is recalled that the plastic solution includes an *effectiveness factor* ν (≤ 1) in order to reduce the actual uniaxial compressive concrete strength. This factor, which is used to obtain agreement between the plastic solution and the actual carrying capacity, may show a rather complex dependency on several parameters. However, a number of beam tests with steel fibre reinforcement indicate that a very simple estimate of $\nu = 1$ is a good suggestion for fibre reinforced concrete, in despite of large variations of e.g. the compressive strength. A better agreement between the plastic theory and the fibre reinforced tests might be found, if the tensile strength is included as a parameter, but it is the authors opinion that the simple expressions are sufficient for practical use.

The Danish design method for shear reinforcement consists of a *strut and tie* methodology, in which inclined compression failure of the beam web is combined with yielding of the shear reinforcement (stirrups). In order to obtain inclined crushing of the beam web in a

high-strength concrete beam, it takes a rather high amount of conventional shear reinforcement, which seems hardly obtainable in practice. Therefore the increased value of ν due to the fibres, which directly increases the crushing strength of the beam web, might not be utilized in case of beams made of compresit or other high-strength concretes. However, near the beam supports, where the concrete is known to act as a *compressive arch*, the effect of steel fibre reinforcement may be significant, because it is the plastic compressive strength νf_c that governs the shear strength in this region instead of the stirrup yield strength.

Finally the thesis contains an example of *compresit bridge design*, where a compresit solution is compared with an existing conventional concrete solution. The price estimate shows that even though compresit matrix is much more expensive than normal concrete, the compresit solution still seems competitive (note that the plain material price of compresit matrix is often 2-4 times that of normal concrete due to the steel fibres). Instead of a solid beam girder, the compresit solution consists of a box girder design, where the webs consist of a *plane truss structure*. Two different beam *span to depth ratios* are investigated: a solution with a span to depth ratio of 30 and a solution with this ratio equal to 40. The latter is chosen in order to eliminate the mid-support column of the bridge, while the former solution consists of two spans with a mid-support similar with the existing concrete solution. The general findings are:

- The *bending stiffness* of the compresit bridge girder turns out to govern the necessary dimensions like it is expected. For the long bridge with span to depth ratio of 40, naturally these difficulties are biggest, but a reasonable solution is suggested.

- The almost total *impenetrability* of the compresit matrix is used to dispense with the moisture insulation layer on top of the bridge deck, which saves both weight and construction expenses.

The design calculations are only preliminary in order to compare the *competitiveness* of compresit with conventional concrete. Several details still need extensive research and design. The design of a truss structure for this particular task is chosen, because it is recognized that high-strength materials need a different design approach than normal concrete. In a truss beam calculation model the internal forces are easy to follow and they result in pure compressive and tensile stresses. Therefore the design gets very transparent, and it can be split up into the separate structural members.

Another reason for considering trusses made of compresit matrix is the belief that the good *anchorage* properties of compresit[2] are usable in the connections between the trusses. These anchorage properties are known to be strongly influenced by the presence of steel fibres.

[2]Currently being investigated in the Brite EuRam project Ministruct.

6.2 Future research needs

The outcome of this thesis is primarily the basic strength properties of compresit matrix. However, there is still a need for several investigations on the compresit material, but also on similar high-strength concretes. Of course, a lot of research is going on continuously, but some of the major structural topics, needing further research are:

- An analytical prediction of crack widths and mutual distances. Thus, a relationship between the tensile post-crack curves that are obtained experimentally for concretes, and the actual structural cracks in reinforced concrete/compresit members. Especially a model that includes the influence of the various fibre properties.

- The effect of column confinement, e.g. in terms of stirrups or steel tubes, on both the strength and the ductility. Also the questions of column stability need research.

- The effect of steel fibres on the beam shear strength.

- The anchorage zones around prestressing tendons, where the fibres provide a good reinforcement against concrete splitting.

Beside these mechanical investigations, which are strongly based on experiments on the hardened concrete, there is a need for knowing the rheological properties, the permeability toward liquids, the early-age properties and so forth.

Some of these questions are being investigated through the above-mentioned project Ministruct, running from 1993 through 1995.

7. Chronological reference list

Sargin, M. **(1971)**, *Stress - Strain Relationships for Concrete and the Analysis of Structural Concrete Sections*, Study No. 4, Solid Mechanics Division, University of Waterloo, Canada, xxvi + 167 pp.

Batson, G.B., E. Jenkins & R. Spatney **(1972)**, 'Steel Fibers as Shear Reinforcement in Beams', *ACI Journal*, Vol. 69, pp. 640-644.

Jensen, B.C. **(1975)**, 'Lines of Discontinuity for Displacements in the Theory of Plasticity of Plain and Reinforced Concrete', *Magazine of Concrete Research*, Vol. 27, No. 92, pp. 143-150.

Williamson, G.R. & L.I. Knab **(1975)**, 'Full Scale Fibre Concrete Beam Tests', *RILEM Symposium on Fibre Reinforced Cement and Concrete*, The Construction Press, Lancaster, pp. 209-214.

Henager, C.H. & T.J. Doherty **(1976)**, 'Analysis of Reinforced Fibrous Concrete Beams', *Journal of the Structural Division*, ASCE, Vol. 102, No. ST1, pp. 177-188.

Jensen, B.C. **(1977)**, *Some Applications of Plastic Analysis to Plain and Reinforced Concrete*, Report No. 123, Institute of Building Design, Technical University of Denmark, Lyngby, 119 pp.

Nielsen, M.P. & M.W. Bræstrup **(1978)**, 'Shear Strength of Prestressed Concrete Beams Without Web Reinforcement' *Magazine of Concrete Research*, Vol. 30, No. 104, pp. 119-128.

Wang, P.T., S.P. Shah & A.E. Naaman **(1978)**, 'Stress - Strain Curves of Normal and Lightweight Concrete in Compression', *ACI Journal*, Vol. 75, pp. 603-611.

Roikjær, M., C. Pedersen, M.W. Bræstrup, M.P. Nielsen & F. Bach **(1979)**, *Bestemmelse af Ikke-Forskydningsarmerede Bjælkers Forskydningsbæreevne*, in Danish, Serie I, No. 62, Structural Research Laboratory, Technical University of Denmark, Lyngby, 44 pp.

Bache, H.H. **(1981)**, *Densified Cement/Ultra-Fine Particle-Based Materials*, Paper presented at The Second International Conference on Superplasticizers in Concrete, June 10-12, Ottawa, Canada, Also CBL Report No. 40, Aalborg Portland A/S, 35 pp.

Jensen, J.F. **(1981)**, *Plasticitetsteoretiske Løsninger for Skiver og Bjælker af Jernbeton*, in Danish, Ph.D.-thesis, Serie R, No. 141, Department of Structural Engineering, Technical University of Denmark, 153 pp.

Swamy, R.N. & S. Al-Ta'an **(1981)**, 'Deformation and Ultimate Strength in Flexure of Reinforced Concrete Beams Made with Steel Fiber Concrete', *ACI Journal*, Vol. 78, pp. 395-405.

Exner, H. **(1983)**, *Betonbjælkers Bøjningsbæreevne*, in Danish, Serie R, No. 176, Department of Structural Engineering, Technical University of Denmark, Lyngby, 62 pp.

Podolny, W. & A.A. Mireles **(1983)**, 'Kuwaits Bubiyan Bridge - a 3-d Precast Segmental Space Frame', *PCI Journal*, Vol. 28, pp. 68-107.

ACI 363 **(1984)**, 'State-of-the-Art Report on High-Strength Concrete', ACI Committee 363, *ACI Journal*, Vol. 81, pp. 364-411.

Broteknik **(1984)**, *Belastninger, Beregnings- og Belastningsregler for Vejbroer*, in Danish, Vejdirektoratet, Vejregeludvalget, 29 pp.

DS 411 **(1984)**, *Danish Code of Practice for the Structural Use of Concrete*, 3rd Ed., Dansk Ingeniørforening, 98 pp.

Jobse, H.J. & S.E. Moustafa **(1984)**, 'Applications of High Strength Concrete for Highway Bridges', *PCI Journal*, Vol. 29, No. 3, pp. 44-73.

Mphonde, A.G. & G.C. Frantz **(1984)**, 'Shear Tests of High- and Low-Strength Concrete Beams Without Stirrups', *ACI Journal*, Vol. 81, pp. 350-357.

Nielsen, M.P. **(1984)**, *Limit Analysis and Concrete Plasticity*, Prentice-Hall Inc., Englewood Cliffs, New Jersey, xii + 420 pp.

Carreira, D.J. & K.-H. Chu **(1985)**, 'Stress - Strain Relationship for Plain Concrete in Compression', *ACI Journal*, Vol. 82, pp. 797-804.

Mphonde, A.G. & G.C. Frantz **(1985)**, 'Shear Tests of High- and Low-Strength Concrete Beams With Stirrups', *High-Strength Concrete* (Ed. H. Russel), ACI Special Publication SP-87, pp. 179-196.

Shah, S.P. & S.H. Ahmad **(1985)**, 'Structural Properties of High Strength Concrete and its Implications for Precast Prestressed Concrete', *PCI Journal*, Vol. 30, No. 6, pp. 92-119.

Swamy, R.N. & H.M. Bahia **(1985)**, 'The Effectiveness of Steel Fibers as Shear Reinforcement', *Concrete International: Design & Construction*, Vol. 7, No. 3, pp. 35-40.

Amad, S.H., A.R. Khaloo & A. Poveda **(1986)**, 'Shear Capacity of Reinforced High-Strength Concrete Beams', *ACI Journal*, Vol. 83, pp. 297-305.

Horii, H. & S. Nemat-Nasser **(1986)**, 'Brittle Failure in Compression: Splitting, Faulting and Brittle-Ductile Transition', *Philosophical Transactions of the Royal Society of London. Series A, Physical Sciences and Engineering*, Vol. 319, pp. 337-374.

Mansur, M.A., K.C.G. Ong & P. Paramasivam **(1986)**, 'Shear Strength of Fibrous Concrete Beams Without Stirrups', *Journal of Structural Engineering*, ASCE, Vol. 112, No. 9, pp. 2066-2079.

Sharma, A.K. **(1986)**, 'Shear Strength of Steel Fiber Reinforced Concrete Beams', *ACI Journal*, Vol. 83, pp. 624-628.

Bache, H.H. **(1987)**, *Compact Reinforced Composite, Basic Principles*, CBL Report No. 41, Aalborg Portland A/S, 87 pp.

Lim, T.Y., P. Paramasivam & S.L. Lee **(1987)**, 'Shear and Moment Capacity of Reinforced Steel-Fibre-Concrete Beams' *Magazine of Concrete Research*, Vol. 39, No. 140, pp. 148-160.

Narayanan, R. & I.Y.S. Darwish **(1987)**, 'Use of Steel Fibres as Shear Reinforcement', *ACI Structural Journal*, Vol. 84, pp. 216-227.

Chen, G. **(1988)**, *Plastic Analysis of Shear in Beams, Deep Beams and Corbels*, Ph.D.-thesis, Serie R, No. 237, Department of Structural Engineering, Technical University of Denmark, Lyngby, 227 pp.

Heshe, G. **(1988)**, 'Experimental Research on Compact Reinforced Composite (CRC)', *Bygningsstatiske Meddelelser*, Vol. 59, No. 1, Danish Society for Structural Science and Engineering, 79 pp.

ACI 318-89 **(1989)**, *Building Requirements for Reinforced Concrete and Commentary*, American Concrete Institute, Detroit, Michigan, 353 pp.

Feddersen, B. **(1989)**, 'Betonbjælkers Forskydningsbæreevne Under Hensyntagen til Buevirkning', in Danish, *Bygningsstatiske Meddelelser*, Vol. 60, No. 1, Danish Society for Structural Science and Engineering, 49 pp.

CEB **(1990)**, *CEB - FIP Model Code*, CEB Bulletin D'information No. 213/214, Thomas Telford, London, 437 pp.

Darwish, I.Y.S. & R. Narayanan **(1990)**, 'Design Charts for Reinforced and Prestressed Fibre Concrete Elements', *The Structural Engineer*, Vol. 68, No. 2, pp. 34-39.

FIP/CEB **(1990)**, *High Strength Concrete, State of the Art Report*, CEB Bulletin d'Information No 197, 61 pp.

Thorenfeldt, E. & G. Drangsholt **(1990)**, 'Shear Capacity of Reinforced High-Strength Concrete Beams', *High-Strength Concrete* (Ed. W.T. Hester), ACI Special Publication, SP-121, pp. 129-154.

El-Niema, E.I. **(1991)**, 'Reinforced Concrete Beams with Steel Fibers under Shear', *ACI Structural Journal*, Vol. 88, pp. 178-183.

Ashour, S.A., G.S. Hasanain & F.F. Wafa **(1992)**, 'Shear Behaviour of High-Strength Fiber Reinforced Concrete Beams', *ACI Structural Journal*, Vol. 89, pp. 176-184.

Dahl, K.K.B **(1992)**, *A Failure Criterion for Normal and High-Strength Concrete*, Serie R, No. 286, Department of Structural Engineering, Technical University of Denmark, Lyngby, x + 115 pp.

EC2 **(1992)**, *Eurocode 2: Design of Concrete Structures - Part 1: General Rules and Rules for Buildings*, European Prestandard ENV 1992-1-1:1991, 1st Ed., May 1992, Dansk Standardiseringsråd, Copenhagen, 253 pp.

Heshe, G. & C.V. Nielsen **(1992)**, *EU 264 - COMPRESIT, Subtask 1.7 - Anchorage of Reinforcement Bars*, NOVI's Udviklingsfond, Aalborg, 29 pp.

Lahlou, K., P.-C. Aïtcin & O. Chaallal **(1992)**, 'Behaviour of High-Strength Concrete Under Confined Stresses', *Cement & Concrete Composites*, Vol. 14, pp. 185-193.

Sarsam, K.F. & J.M.S. Al-Musawi **(1992)**, 'Shear Design of High- and Normal Strength Concrete Beams with Web Reinforcement', *ACI Structural Journal*, Vol. 89, pp. 658-664.

Valenchon, C. **(1992)**, 'Offshore Application of High Performance Concrete Space Frame', *High Performance Concrete, From Material to Structure* (Ed. Y. Malier), E & FN Spon, London, pp. 477-494.

Alsayed, S.H. **(1993)**, 'Flexural Deflection of Reinforced Fibrous Concrete Beams', *ACI Structural Journal*, Vol. 90, pp. 72-76.

Setunge, S., M.M. Attard & P.LeP. Darvall **(1993)**, 'Ultimate Strength of Confined Very High-Strength Concretes', *ACI Structural Journal*, Vol. 90, pp. 632-641.

Swamy, R.N., R. Jones & A.T.P. Chiam **(1993)**, 'Influence of Steel Fibres on the Shear Resistance of Lightweight Concrete I-Beams', *ACI Structural Journal*, Vol. 90, pp. 103-114.

Tan, K.H., K. Murugappan & P. Paramasivam **(1993)**, 'Shear Behaviour of Steel Fiber Reinforced Concrete Beams', *ACI Structural Journal*, Vol. 90, pp. 3-11.

Batson, G.B. & A.G. Youssef **(1994)**, 'Shear Capacity of Fiber Reinforced Concrete Based on Plasticity of Concrete: A Review', *Fiber Reinforced Concrete, Developments and Innovations* (Eds. J.I. Daniel & S.P. Shah), ACI Special Publication, SP-142, pp. 141-165.

Favre, R. & H. Charif **(1994)**, 'Basis Model and Simplified Calculations of Deformations According to the CEB-FIP Model Code 1990', *ACI Structural Journal*, Vol. 91, pp. 169-177.

Imam, M., L. Vandewalle & F. Mortelmans **(1994)**, 'Shear Capacity of Steel Fiber High Strength Concrete Beams', *High-Performance Concrete* (Ed. V.M. Malhotra), ACI Special Publication, SP-149, pp. 227-241.

Kim, J.-K. & Y.-D. Park **(1994)**, 'Shear Strength of Reinforced High Strength Concrete Beams Without Web Reinforcement' *Magazine of Concrete Research*, Vol. 46, No. 166, pp. 7-16.

Shin, S.W., J.G. Oh & S.K. Ghosh **(1994)**, 'Shear Behaviour of Laboratory-Sized High Strength Concrete Beams Reinforced with Bars and Steel Fibers', *Fiber Reinforced Concrete, Developments and Innovations* (Eds. J.I. Daniel & S.P. Shah), ACI Special Publication SP-142, pp. 181-190.

Xie, Y., S.H. Ahmad, T. Yu, S. Hino & W. Chung **(1994)**, 'Shear Ductility of Reinforced Concrete Beams of Normal and High-Strength Concrete', *ACI Structural Journal*, Vol. 91, pp. 140-149.

Zhang, J.-P. **(1994)**, *Strength of Cracked Concrete, Part 1 - Shear Strength of Conventional Reinforced Concrete Beams, Deep Beams, Corbels and Prestressed Reinforced Concrete Beams Without Shear Reinforcement*, Part of Ph.D.-thesis, Serie R, No. 311, Department of Structural Engineering, Technical University of Denmark, Lyngby, 106 pp.

Appendix 1

Triaxial strength of ultra high-strength fibre reinforced concrete

This appendix contains a copy of the paper presented at the *ACI 1994 International Conference on High-Performance Concrete*, November 15-18, 1994 at the Singapore Hilton, Singapore. The layout of the paper is prescribed by the ACI with 3 tables and 5 figures placed at the end of the paper. A total of 18 references are also included in the paper, represented with numbers in brackets.

The content of the paper is based on the findings in Chapter 4 of Part I of the thesis[1], but the topic of triaxial failure criterion is also discussed in Chapter 2 of the present report.

Synopsis: A total of 50 triaxial compression tests are performed on cylinders of ultra high-strength concrete. The matrix is reinforced with straight steel fibres and it sustains uniaxial compressive stresses of approximately 160 MPa. Comparisons are made with related triaxial strength results of high-strength concrete (HSC) and the Coulomb failure criterion is applied.

Contrary to what is normal procedure, the tests cover the region of small confinement pressures (below 10 % of the uniaxial compressive strength). It is found that the almost explosive uniaxial compressive failure of HSC is reflected in the failure criterion. The angle of friction, that governs the behaviour under small confinement pressures, seems to equal approximately 51° instead of 37°, which is normally applied to concrete.

Under increasing confinement pressure the Coulomb criterion gets reasonable for a wide range of compressive strengths (from 60 MPa to 160 MPa). However, the angle of friction is reduced to 30°, which is due to the fact, that the crack growth in HSC is only slightly influenced by the aggregate.

The present test results do not reveal any significant effect of the steel fibres on the strength criterion. Even though a volume content of 6 % straight Dramix fibres is added to the high-strength matrix the behaviour still follows the above description. Thus it seems likely, that it is practically impossible to alter the behaviour of HSC to that of a true Coulomb material by means of fibres.

[1]Basic Strength Properties of Compresit Matrix.

The author took his master degree in structural engineering from the University of Aalborg, Denmark, in 1990. Presently he is a Ph.D. student at the Department of Structural Engineering at the Technical University of Denmark (TUD), Lyngby. Since 1992 he has been employed by the consulting engineering company the Carl Bro Group, Glostrup, Denmark.

INTRODUCTION AND BACKGROUND

Throughout decades it has been well-known, that confined concrete shows an increased axial strength. The early investigation by Richart et al. (see Ref. (1)) suggests a simple linear relationship obtained from cylinders subjected to external oil pressure:

$$f_p = f_0 + 4.1p \tag{1}$$

where f_p and f_0 are the confined and unconfined axial strength respectively and p is the lateral confinement pressure. The confinement is normally produced by means of external hydraulic pressure, or by means of embedded steel stirrups.

Both Iyengar et al. and Ahmad & Shah report a slope of Eq. (1) equal to approximately 2.3 instead of 4.1 (see Refs. (2) and (3)). This value is obtained from normal strength concrete cylinders reinforced with steel spirals. Thus, the stirrups, spaced at distances from 30 to 120 mm, are not as effective as a hydraulic pressure.

The confining effect is closely related to the triaxial strength criterion applied to concrete. In the present paper basis is taken in the Coulomb criterion, which has been successfully applied to concrete, in despite of its simplicity. It states that the shear stress of a failure plane consists of two components, viz. cohesion and friction:

$$|\tau| = c + \sigma\tan\varphi \tag{2}$$

where c is the cohesion, σ is the compressive normal stress and φ is the angle of friction. Furthermore this criterion is often combined with a socalled tension cut-off at the uniaxial tensile strength f_t.

Equation (2) results in a linear failure criterion similar to Eq. (1), when the principal stresses are considered:

$$\sigma_1 = f_c + k\sigma_3\,, \qquad k = \frac{1 + \sin\varphi}{1 - \sin\varphi} \tag{3}$$

where σ_1 and σ_3 are the major and the minor principal stresses respectively and f_c is the uniaxial compressive strength. It is emphasized, that the normal stresses are positive as compression.

Throughout the last 3 decades the Coulomb failure criterion has been applied to reinforced concrete structures in connection with the theory of plasticity (see e.g. Ref. (4)). Satisfactory engineering accuracy for normal strength concrete is obtained, when φ is equal to approximately 37° ($\tan\varphi = 0.75$ and $k = 4$). In order to include the fact, that concrete is not a perfect rigid-plastic material, a socalled effectiveness factor (≤ 1) is multiplied by f_c. This semi-empirical factor furthermore takes into account micro and macro cracking, rotation of the macro cracks, various size-effects, dowel-effects from the rebars, etc.

At the Department of Structural Engineering, TUD, an extensive investigation of the failure criterion for high-strength concrete (HSC) with compressive strengths up to 110 MPa has been performed by K.K.B. Dahl under the supervision of Professor M.P. Nielsen (cf. Ref. (5)).

The main conclusion from this investigation is, that the angle of friction φ should be reduced from approximately 37° to 30°, when HSC is considered (see e.g. Ref. (5)). This decrease is understandable by taking into account, that normal strength concrete primarily cracks along the mortar-aggregate interfaces, while HSC cracks through the stones. The more smooth crack surfaces result in a reduced coefficient of friction.

This characteristic difference between normal strength concrete and HSC is also one of the reasons for the explosive failures observed for HSC under uniaxial compression. When the crack growth of the existing micro cracks (imperfections and flaws) becomes unstable, cracks develop without any significant internal resistance. In normal strength concrete the aggregate arrests the crack growth considerably.

SCOPE OF INVESTIGATION

The triaxial strength of an ultra high-strength concrete is investigated and the influence of adding steel fibres is evaluated. A comparison is performed with related HSC results. The strength data are used to modify the Coulomb criterion for application to HSC. The main reason for applying the Coulomb criterion is its simplicity and the fact, that many structural problems are solved for normal strength concrete, under the assumptions of a rigid-plastic Coulomb material and the normality condition. Furthermore the Coulomb criterion results in satisfactory accuracy for practical engineering problems.

TEST SPECIMENS

The triaxial experiments are performed on concrete cylinders (ø100 × 200 mm) subjected to external oil pressure together with an axial load, which is increased until failure. In table 1 the mix ingredients are listed. The steel fibre reinforced matrix has a water to binder ratio of 0.18, which gives an extremely dense matrix.

The binder is a socalled Densit binder (registered trademark of Densit A/S, Aalborg, Denmark) and it consists of Portland cement and micro silica. The Densit binder is especially designed at Aalborg Portland A/S, Aalborg, Denmark, to show optimum packing of the particles. The quartz sand includes grain sizes up to 4 mm.

The steel fibres are straight Dramix fibres. In table 2 the fibre characteristics are given for the 3 concrete mixes termed mix A, B and C. Mix A contains no fibres, while mix B and C contain 6 % by volume of two different fibre types. The main reason for adding the fibres is to increase the ductility of the matrix, but the strength is also influenced. The matrix normally has a uniaxial cylinder strength between 150 and 180 MPa.

The curing of the cylinders was accelerated in order to ensure completed strength development at the time of testing. After casting in steel moulds, the specimens were wrapped in wet towels and plastic. Then they were cured for 5 days in a heating room at 45 °C, followed by approximately 2 months in the laboratory, still wrapped in plastic. Because of the heat curing no further strength development was expected during the test period.

EXPERIMENTAL PROCEDURE

A triaxial cell developed at the Department of Structural Engineering, TUD, was utilized for the tests. A steel barrel contains the cylindrical specimen, which is tightly fitted in several rubber membranes to prevent the oil to enter the pores. The cell is filled with approximately 3 litres of hydraulic oil. No intermediate layers are applied between the cylinder ends and the load plates. It is ensured that the cylinder ends are accurately plane by grinding them before testing.

The oil pressure is raised up to a specified level, acting on all the cylinder faces. The maximum obtainable oil pressure is 140 MPa. By means of an external 10 MN hydraulic jack, the axial load is applied under a constant load rate of 0.3 MPa per second until failure. This load path is normally employed in order to obtain the socalled compressive meridian of the failure surface, where an axial compressive stress is imposed on the hydrostatic stress state ($\sigma_1 \geq \sigma_2 = \sigma_3 \geq 0$).

The cylinders are sandblasted before testing in order to expose possible air voids near the surface. Then all voids are filled with a mix of gypsum, sand and water. This is done to avoid puncture of the rubber membranes and damage of the electrical resistance gages, when the oil pressure is raised.

STRENGTH RESULTS

Only the strength characteristics of the tests are presented in this paper (see table 3). The triaxial strength is taken as the maximum axial load during each test, while the confinement pressure is kept constant at a specified level. The values in table 3 are normalized with respect to the uniaxial compressive strength f_c, taken as the mean value of 3 cylinder tests. The brackets in table 3 contain the coefficients of variation on f_c and it appears, that the experimental scatter is very limited.

The triaxial strengths for mix C are obtained from 3 repetitions of each confinement pressure, while mix A and B only include 2 repetitions. The coefficients of variation on the triaxial strengths are found to be less than 2 %.

In figure 1 the results are depicted in a normalized strength diagram, which also contains HSC results from Ref. (5). Furthermore two lines are inserted with slopes $k = 3$ and 4, corresponding to the expression in Eq. (3).

It is recalled that normal strength concrete is modelled by the slope $k = 4$. However, it appears that the triaxial strength of HSC tends to follow a straight line, intersecting the σ_1-axis at $1.5f_c$ with the slope $k = 3$. This observation seems to hold for a wide range of compressive strengths and it is probably unaltered by the presence of steel fibres. When the confinement pressure decreases below $0.1f_c$, the triaxial strength follows a steeper line to intersect the σ_1-axis at f_c.

For confinement pressures below $0.2f_c$ a very limited number of experiments on HSC exist. In figure 2 special emphasis is placed on the conditions concerning small confinement pressures using test results from Refs. (5)-(7). The test results from Ref. (7) correspond well with the present results, while those of Ref. (6) follow the line with the slope $k = 4$.

The investigation by Lahlou et al. (Ref. (6)) concerns concrete cylinders (ø100 × 200 mm) from 3 different concrete mixes. The uniaxial strengths are 46, 78 and 113 MPa with the water to binder ratios equal to 0.50, 0.35 and 0.23 respectively. The mix with the highest strength contains silica fume.

In Setunge et al. (Ref. (7)), 4 different mixes are tested by means of ø100 × 200 mm cylinders. These mixes have water to binder ratios from 0.26 to 0.35 and three of them contain silica fume. The compressive strengths range from approximately 100 MPa to 130 MPa. The main parameter varied in the tests is the aggregate type, but no significant influence is found.

An initial slope of $k = 8$ is proposed in figure 2, corresponding to $\varphi \approx 51°$. At $\sigma_3 \geq 0.1f_c$ the slope seems to decrease to $k = 3$, corresponding to $\varphi = 30°$.

A design proposal applying for HSC should of course be on the safe side. In Ref. (7) a straight line is suggested given by Eq. (3) with $k = 3$. However a safe design proposal for the failure criterion may be chosen as a bi-linear curve on basis of figure 1 and 2:

$$\sigma_1 = \begin{cases} f_c + 4\sigma_3 , & 0 \leq \sigma_3 \leq 0.5f_c \\ 1.5f_c + 3\sigma_3 , & \sigma_3 \geq 0.5f_c \end{cases} \qquad (4)$$

The first part corresponds to what is normally applied to concrete and the second part includes a reduced angle of friction. This proposal is taken from Ref. (5), but already in 1968 Hannant & Frederick (Ref. (8)) suggested a bi-linear design criterion for normal strength concrete. However, in their proposal the transition point was placed at $\sigma_1 = 4f_c$ and $\sigma_3 = 0.75f_c$.

DISCUSSION

The strength of a true Coulomb material, subjected to triaxial compression, shows a single straight line in both the Mohr diagram and the principal stress diagram, according to Eqs. (2) and (3). However, the results obtained from HSC indicate, that a single straight line is insufficient to describe the triaxial compressive strength. Instead a bi-linear model seems to match the experimental data (cf. figure 2).

In figure 3 the situation with a bi-linear failure envelope is outlined in a Mohr diagram. The initial line is denoted by subscript 1, while the original Coulomb line is denoted 2. The condition for the two lines to result in identical uniaxial compressive strengths is $c_2/c_1 = \sqrt{(k_1/k_2)}$.

The initial line has an increased slope and a reduced cohesion compared to the Coulomb line. Apart from an eventual reduction of f_c these differences result in reduced triaxial tensile strength characteristics of the material. This tensile strength reduction is interpreted to originate from existing micro cracks in the hardened concrete. Therefore the initial failure line in figure 3 is termed *the cracked strength criterion.*

As a result of the assumption, that the cracked strength criterion mainly depends on the damage of the mortar structure within the concrete, it is expected to vary with a number of parameters such as

- The load history and load type.
- The curing conditions.
- The existence of damaging alkali-aggregate reaction.

Therefore the criterion cannot be considered as a true material property.

Another interesting feature of the cracked strength criterion is, that a concrete mix with a fully developed micro crack structure (i.e. $f_t = 0$) cannot sustain any uniaxial compressive stress at all.

Normal Strength Concrete

In the following it is shown to be very plausible, that also normal strength concrete ($f_c < 40$ MPa) shows a behaviour similar to the bi-linear model described above.

In Ref. (9) A.M. Neville describes the existence of fine initial cracks at the interface between aggregate and cement paste even prior to loading. These micro cracks start to grow at about 30 % of the ultimate load. At 70 to 90 % of the peak load cracks develop through the mortar, bridging the bond cracks to form a continuous pattern.

J.G.M. van Mier has investigated the fracture processes in concrete under multiaxial loading (see Ref. (10)). The research includes the influence of specimen size, casting direction and the load path. The tests utilize concrete cubes loaded through steel brush plates, because it is essential to minimize the frictional restraints against transverse deformations. An important conclusion is that the descending branch of the compressive stress - strain curve is strongly influenced by the specimen height. Thus, the axial deformations are localized in inclined shear bands instead of being homogeneous.

Furthermore Ref. (10) includes a diagram depicting the axial compression strain ε_{ax} as a function of the lateral strain ε_{lat} (see figure 4). The diagram shows, that the strain rate ratio $(d\varepsilon_{lat}/d\varepsilon_{ax})$ increases from its initial value, corresponding to the elastic Poisson ratio, to a value of approximately 8 at the peak load. This corresponds closely to the theory of plasticity, where the normality condition applied to the Coulomb criterion results in the theoretical solution $d\varepsilon_{lat}/d\varepsilon_{ax} = -d\varepsilon_3/d\varepsilon_1 = k$ in the case of plane strain. Thus, the uniaxial results on concrete cubes with $f_c = 45$ MPa clearly indicate, that k exceeds the typical value of 4.

A comparison of various normal strength concretes, subjected to small confinements, in both the compressive region and the region of tension-compression-compression stresses, is shown in figure 5. Also the two lines corresponding to $k = 4$ and 8 are depicted in the σ_1/f_c - σ_3/f_c diagram. It appears that the slope $k = 8$ is appropriate in the vicinity of the σ_1/f_c-axis and in particular in the tensile region. However, care should be taken in comparing test series with differences in both specimens, load paths and test equipment.

Figure 5 indicates the great experimental scatter to be expected in triaxial tests, especially for the tensile region. Because of this scatter it is hard to detect any distinct change of k from its normal value of 4. This distinction is further troubled by the fact, that the transition

from the cracked strength criterion to the Coulomb criterion almost coincide with the uniaxial compressive strength and that most triaxial tests are originated from this state.

High-Strength Concrete

Previously we have described, that cracks in HSC do not notice the aggregates to the same extent as in normal strength concrete. Therefore it is expected, that HSC is much more sensitive to the presence of micro cracks than normal strength concrete. Thus, the cracked strength criterion becomes experimentally visible for HSC. For the same reason the internal friction of HSC seems to be slightly smaller than that of normal strength concrete ($\varphi_2 = 30°$ instead of $37°$ in figure 3).

It is impossible to determine any clear experimental relationship between the two strength criteria in figure 3 and the strength f_c. The cracked strength criterion is assumed to depend on many parameters as previously mentioned. The Coulomb line depends on the internal friction and it hardly recognizes the micro cracks. Therefore it is expected, that the Coulomb criterion increases relatively to the strength f_c. Thus, the gap between c_1 and c_2 increases with f_c. However, the HSC results in figure 1 indicate, that a Coulomb criterion with $k = 3$, intersecting the σ_1-axis at $1.5f_c$, is a good estimate even though the uniaxial compressive strength varies.

Fibre Reinforced Concrete

From figure 1 it seems, that the presence of 6 % steel fibres in mix B and C does not alter the triaxial strength behaviour significantly, compared to mix A and the other high-strength concretes. It is reasonable to assume, that the fibres do no influence the angle of friction.

The fibres are known to possess a remarkable crack arresting effect in concrete. Therefore the cohesion c_1 is probably increased by the fibres crossing the cracks, i.e. the cracked strength reduction is counteracted by the fibres. It is often assumed, that the fibres make it possible to force the failure envelope at small confinement pressures from the cracked strength criterion to the Coulomb criterion. However, the present test series still shows a significant cracked strength line in despite of a fibre content of 6 %. This content is close to the practical limit, when the workability of the fresh mix is considered. An upper limit of 1-2 for the fibre reinforcement index $V_f(L_f/d_f)$ is often suggested, which is exceeded by mix B and C.

The fact that none of the fibre reinforced mixes succeeded in producing a true Coulomb material under compression stresses justifies the conclusion, that it is impossible to alter the failure envelope of the ultra high-strength matrix significantly closer to the Coulomb line than indicated in figure 2.

In case of normal strength FRC however, both Ref. (17) and (18) report a change in failure mode under biaxial compression from adding steel fibres. For plain concrete the failure is governed by splitting cracks in the plane of the stresses, while the addition of 1-2 % fibres causes the failure to consist of inclined shear cracks instead.

CONCLUSIONS

The general conclusion is, that the Coulomb failure criterion gives a satisfactory description of the triaxial strength of HSC just like in the case of normal strength concrete. In Eq. (4) a bi-linear design proposal is given, which is closely related to the criterion normally applied.

However, the compressive triaxial tests performed on high-strength concretes (both plain and steel fibre reinforced) result in the following observations concerning the strength behaviour:

1: For small confinement pressures ($< 0.1f_c$) the triaxial strength is governed primarily by a reduced cohesion, because of micro cracks and imperfections.

2: The angle of friction, that applies to this socalled cracked strength criterion is approximately $51°$ ($k = 8$).

3: When the confinement pressure increases the triaxial strength is governed by the internal coefficient of friction. The angle of friction is found to be equal to $30°$ ($k = 3$) for f_c ranging from 60 to 160 MPa.

4: The incorporation of 6 % steel fibres does not seem to alter the triaxial strength behaviour. However, the fibre reinforced cylinders show extreme ductility compared to plain concrete cylinders.

Furthermore it is justified that the socalled cracked strength criterion also is applicable to normal strength concrete. This strength criterion is not taken to be a material property, but it is assumed to depend on both load history, curing conditions, etc.

ACKNOWLEDGMENTS

I wish to thank my supervisors Professor, Dr.techn. M.P. Nielsen at the Department of Structural Engineering, TUD, and Managing Director, Ph.D. B.C. Jensen at the Carl Bro Group for their support. Furthermore I express my gratitude to Managing Director P. Nepper-Christensen at the Cement and Concrete Laboratory of Aalborg Portland A/S for sponsoring the test specimens. Finally I would like to thank my colleague J.F. Olesen at the Carl Bro Group for fruitful discussions.

NOTATION

c	Cohesion.
d_f	Fibre diameter.
f_c	Uniaxial compressive strength.
f_t	Uniaxial tensile strength.
f_0	Unconfined axial strength.
f_p	Confined axial strength.
k	Constant defined in Eq. (3).
L_f	Fibre length.
p	Lateral confinement pressure.
V_f	Fibre content by volume.
$\varepsilon_1,\varepsilon_3$	Major and minor principal strains respectively.
$\varepsilon_{ax},\varepsilon_{lat}$	Axial and lateral strains respectively.
φ	Angle of friction.
σ	Normal stress. Positive as compression.
$\sigma_1,\sigma_2,\sigma_3$	Principal stresses. Positive as compression ($\sigma_1 \geq \sigma_2 \geq \sigma_3$).
τ	Shear stress.

REFERENCES

(1) Richart, F.E., A. Brandtzaeg & R.L. Brown, *A Study of the Failure of Concrete Under Combined Compressive Stresses*, Bulletin no. 185, Engineering Experiment Station, University of Illinois, Urbana, USA, 1928.

(2) Iyengar, K.T.S.R., P. Desayi & K.N. Reddy, 'Stress-Strain Characteristics of Concrete Confined in Steel Binders', *Magazine of Concrete Research*, Vol. 22, No. 72, 1970, pp. 173-184.

(3) Ahmad, S.H. & S.P. Shah, 'Stress-Strain Curves of Concrete Confined by Spiral Reinforcement', *ACI Journal*, Vol. 79, Nov.-Dec. 1982, pp. 484-490.

(4) Nielsen M.P., *Limit Analysis and Concrete Plasticity*, Prentice-Hall Inc., Englewood Cliffs, New Jersey, USA, 1984.

(5) Dahl, K.K.B., *A Failure Criterion for Normal and High Strength Concrete*, Serie R, No. 286, Department of Structural Engineering, Technical University of Denmark, Lyngby, Denmark, 1992.

(6) Lahlou, K., P.-C. Aïtcin & O. Chaallal, 'Behaviour of High-Strength Concrete Under Confined Stresses', *Cement & Concrete Composites*, Vol. 14, 1992, pp. 185-193.

(7) Setunge, S., M.M. Attard & P.LeP. Darvall, 'Ultimate Strength of Confined Very High-Strength Concretes', *ACI Structural Journal*, Vol. 90, Nov.-Dec. 1993, pp. 632-641.

(8) Hannant, D.J. & C.O. Frederick, 'Failure Criteria for Concrete in Compression', *Magazine of Concrete Research*, Vol. 20, No. 64, 1968, pp. 137-144.

(9) Neville, A.M., *Properties of Concrete*, 3rd Edition, Pitman, London, 1981.

(10) Van Mier, J.G.M., *Fracture of Concrete under Complex Stress*, Heron, Vol. 31, No. 3, 1986.

(11) Hobbs, D.W., *Strength and Deformation Properties of Plain Concrete Subject to Combined Stress. Part 1: Strength Results Obtained on One Concrete*, Technical Report 42.451, Cement and Concrete Association, London, 1970.

(12) Hobbs, D.W., *Strength and Deformation Properties of Plain Concrete Subject to Combined Stress. Part 3: Results Obtained on a Range of Flint Gravel Aggregate Concretes*, Technical Report 42.497, Cement and Concrete Association, London, 1974.

(13) Bellotti, R. & E. Ronzoni, 'Results of Tests Carried Out on Cylindrical Concrete Specimens Subjected to Complex Stress States: A Critical Analysis', In *Proceedings of International Conference on Concrete Under Multiaxial Conditions*, RILEM, Toulouse, May 1984, pp. 53-74.

(14) Rossi, P., *Cooperative Research on Properties of Concrete, ENEL-CRIS Test Results*, ENEL Preliminary Report 2590, Italy, March 1976.

(15) Bremer, F. & F. Steinsdörfer, *Bruchfestigheiten und Bruchverformung von Beton Unter Mehraxialer Belastung bei Raumtemperatur*, Heft 263, Deutscher Ausshuss für Stahlbeton, Berlin, 1976.

(16) Linhua, J., H. Dahai & X. Nianxiang, 'Behaviour of Concrete Under Triaxial Compressive-Compressive-Tensile Stresses', *ACI Materials Journal*, Vol. 88, March-April 1991, pp. 181-185.

(17) Traina, L.A. & S.A. Mansour, 'Biaxial Strength and Deformational Behaviour of Plain and Steel Fiber Concrete', *ACI Materials Journal*, Vol. 88, July-August 1991, pp. 354-362.

(18) Yin, W.S., E.C.M. Su, M.A. Mansur & T.T.C. Hsu, 'Biaxial Tests of Plain and Fiber Concrete', *ACI Materials Journal*, Vol. 86, May-June 1989, pp. 236-243.

Table 1: Mix proportions.

Ingredient	Cement and micro silica	Quartz sand	Water	Steel fibres
Weight fraction	34 %	43 %	6 %	17 %

Table 2: Steel fibre characteristics (straight Dramix fibres).

Mix	A	B	C
Fibre name	-	OL 12/.40	OL 6/.15 HC
Fibre content by volume, V_f (%)	0	6	6
Fibre length, L_f (mm)	-	12	6
Aspect ratio, L_f/d_f	-	30	40
$V_f(L_f/d_f)$	-	1.8	2.4
Tensile strength (MPa)	-	1350	2950
Note	-	Low carbon.	Brass-coated, high carbon.

Table 3: Triaxial strength results.

Mix	$V_f(L_f/d_f)$	Uniaxial strength, f_c (MPa) (%)	Confinement pressure $\sigma_2/f_c = \sigma_3/f_c$	Triaxial strength σ_1/f_c
A	0	170.2 (1.7)	0.029	1.26
			0.059	1.47
			0.080	2.10
B	1.8	164.3 (2.1)	0.034	1.34
			0.065	1.61
			0.12	1.88
			0.18	2.19
			0.24	2.38
			0.37	2.74
			0.40	2.84
			0.43	2.96
C	2.4	165.0 (0.5)	0.13	1.84
			0.25	2.29
			0.36	2.69
			0.49	2.98
			0.61	3.23
			0.73	3.62
			0.85	4.05

Figure 1: Experimental σ_1/f_c - σ_3/f_c relationship.

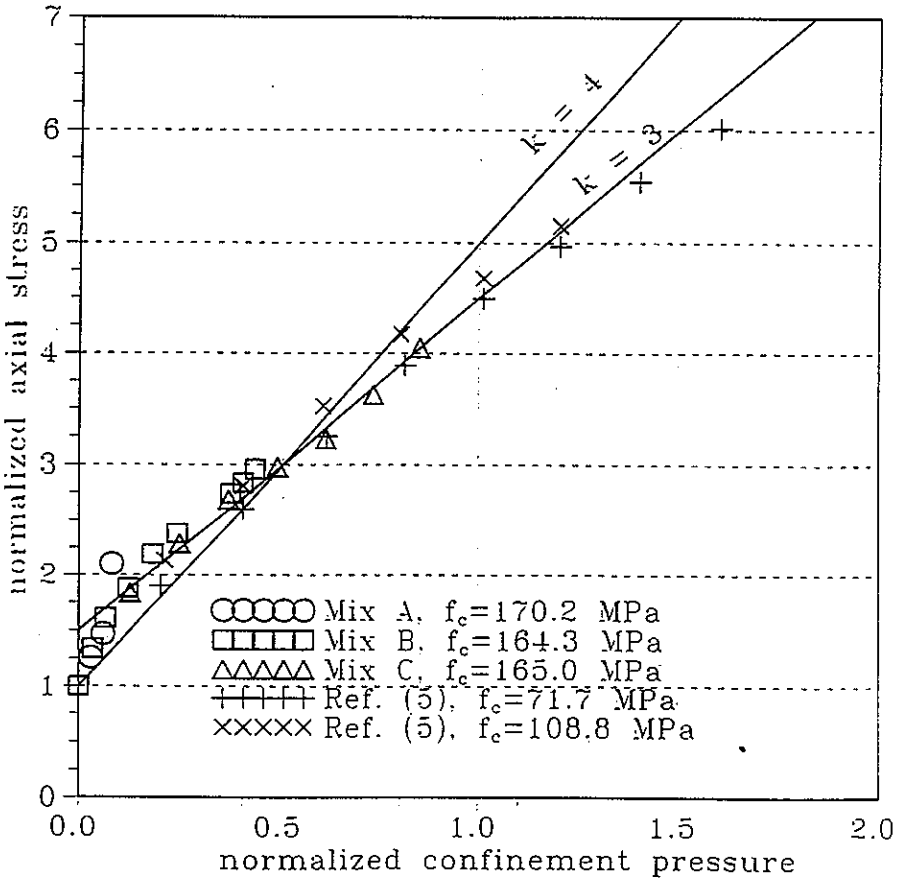

Figure 2: Experimental σ_1/f_c - σ_3/f_c relationship for small confinement pressures.

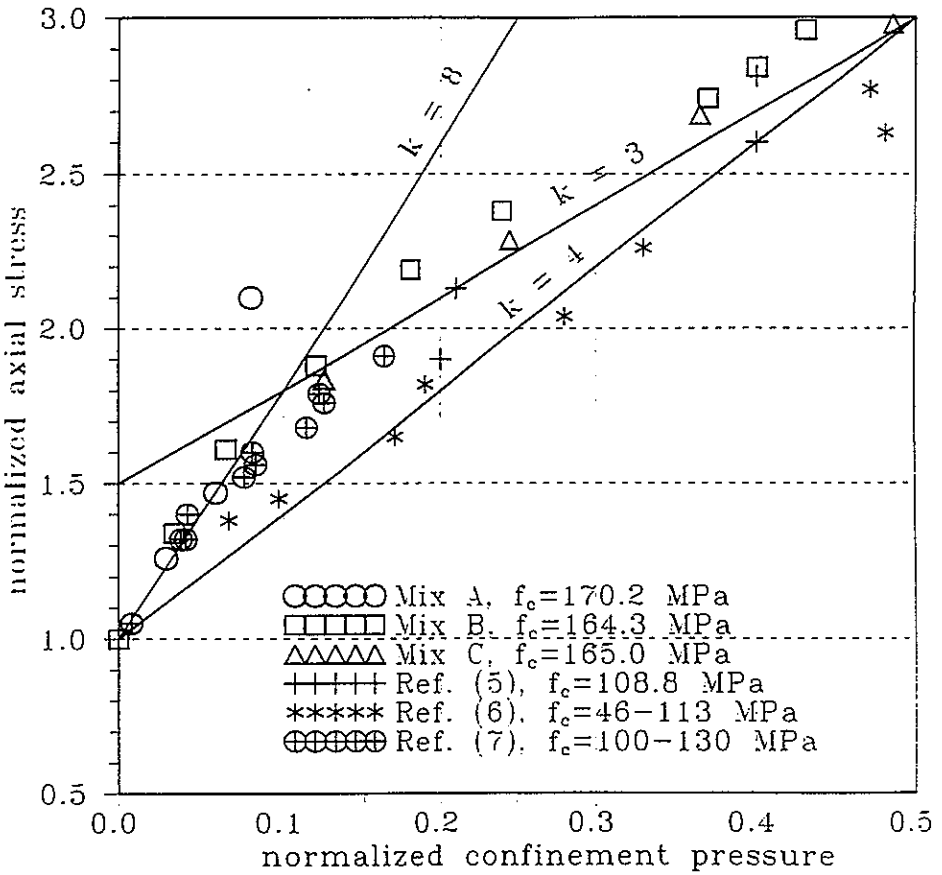

Figure 3: Bi-linear failure envelope in Mohr diagram.

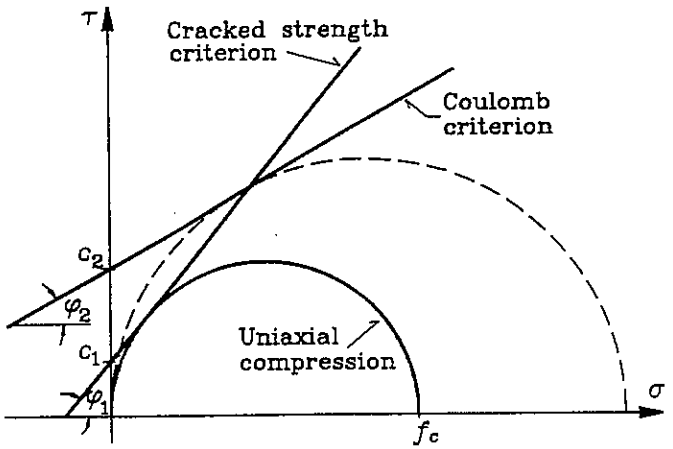

Figure 4: Axial strain versus lateral strain in uniaxial compression tests on concrete cubes. Strain curves in ‰ are taken from Ref. (10).

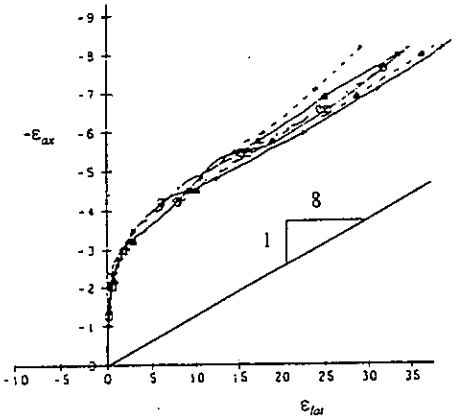

Figure 5: Experimental triaxial stength results for normal strength concretes.

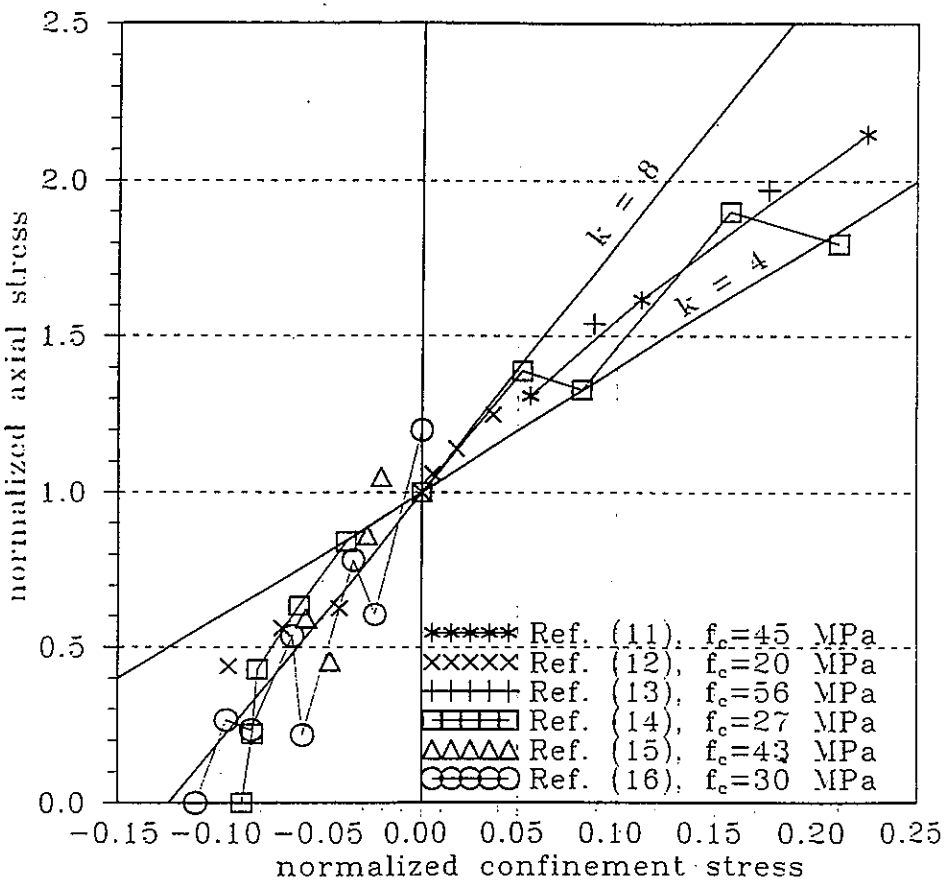

Appendix 2

Calculations for compresit footbridge

This appendix contains the *numerical calculations* associated with the compresit solution proposed in *Chapter 5*. The appendix consists of 4 sections, treating various calculations on the compresit design. The system chosen for the investigation is a simply supported statically and geometrically determinated truss beam. The reason why this simplified calculation model is used instead of making a more detailed finite element model is the wish to evaluate the influence of the various geometrical parameters. Furthermore the design is rather roughly, which is also reflected in the calculation model.

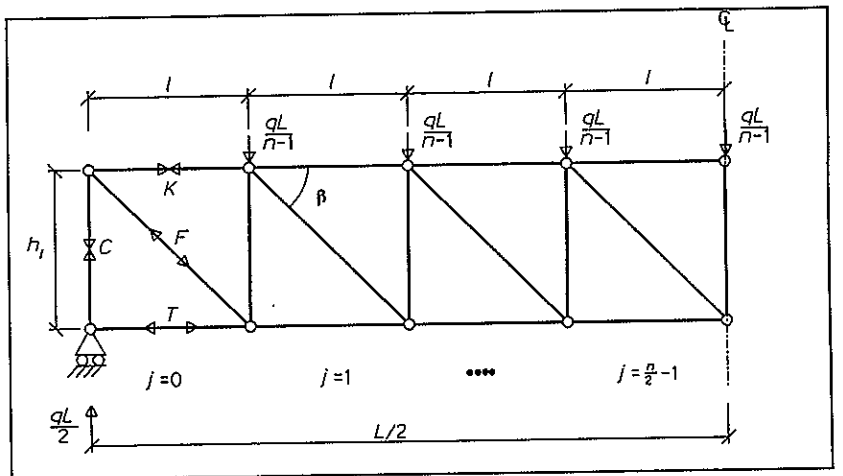

Figure A2.1: Plane truss beam system with dimensions and loading.

A2.1 Internal forces in truss beam

The plane truss beam is outlined in figure A2.1 with dimensions and loads. The beam is simply supported with span L. A total of n sections, each with length l, are considered, where $n = 2,4,6,8,\cdots$, i.e. $l = L/n$. The *truss angle* β is defined by $\tan\beta = h_l/l = nh_l/L$. The distance between the compressive and tensile stringers is denoted h_l. In figure A2.1 the load q per unit length is divided into n-1 identical point loads acting in the upper flange nodes as indicated. It is noted, that q in the figure not necessarily denotes the live load.

The internal forces are the compressive force C in the *vertical trusses*, the compressive force K in the *upper flange*, the tensile force T in the *lower flange* and the tensile force F in the *inclined trusses*. In the following these truss forces are expressed for the different sections of the beam, indicated by the index $j = 0,1,2,\cdots,n/2\text{-}1$, cf. figure A2.1. Because of the beam symmetry in both geometry and loading only half of the n sections are considered.

The *Ritter method* of cutting vertically through 3 bars of each section and using the three equilibrium conditions is applied. A vertical force equilibrium gives

$$F_j = \frac{qL}{\sin\beta}\left(\frac{1}{2} - \frac{j}{n-1}\right), \quad j = 0,1,2,\cdots,\frac{n}{2}-1 \tag{A2.1}$$

Moment equilibrium around the upper left node of each section gives the tensile force:

$$T_j = \frac{qL\cot\beta}{n-1}\left(\frac{n-1}{2}j - \sum_{r=1}^{j}(r-1)\right), \quad j = 1,2,3,\cdots,\frac{n}{2}-1, \qquad T_0 = 0 \tag{A2.2}$$

where it appears, that the outermost truss of the lower flange ($j = 0$) only serves to obtain a geometrically determinated truss system.

The compression in the upper flange is found by means of horizontal force equilibrium:

$$K_j = \frac{qL\cot\beta}{n-1}\left(\frac{(n-1)(j+1)}{2} - j - \sum_{r=1}^{j}(r-1)\right), \quad j = 1,2,3,\cdots,\frac{n}{2}-1, \qquad K_0 = \frac{qL}{2}\cot\beta \tag{A2.3}$$

Finally the compressive forces in the vertical trusses are found by cutting free the nodes and ensuring the vertical force equilibrium for each node:

$$C_j = \frac{qL}{n-1}\left(\frac{n+1}{2} - j\right), \quad j = 1,2,3,\cdots,\frac{n}{2}-1, \qquad C_0 = \frac{qL}{2}, \quad C_{n/2} = \frac{qL}{n-1} \tag{A2.4}$$

where C_0 and $C_{n/2}$ denotes the forces in the outermost and the central truss respectively.

A2.2 Optimization of truss angle β

In order to choose a proper configuration for the truss beam in figure A2.1 we apply a simple optimization on the geometry by varying the angle β of the inclined tensile bars and observing the *material consumption* and the material *costs*.

The necessary amount of *reinforcement steel* to carry the tensile forces F and T is calculated for a given load q. For the *inclined trusses* this steel volume is expressed as

$$V_s^{in} = 2\sum_{j=0}^{n/2-1}\left[\frac{F_j}{f_{yd}}\frac{h_i}{\sin\beta}\right] = 2\frac{qL^2}{f_{yd}}\frac{h_i/L}{\sin^2\beta}\sum_{j=0}^{n/2-1}\left[\frac{1}{2} - \frac{j}{n-1}\right], \quad n = 2,4,6,\cdots \tag{A2.5}$$

where the factor 2 takes into account, that the sum from $j = 0$ to $n/2\text{-}1$ only includes half the span. For the *lower flange* we get

$$V_s^{l} = 2\sum_{j=0}^{n/2-1}\left[\frac{T_j}{f_{yd}}l\right] = 2\frac{qL^2}{f_{yd}}\frac{\cot\beta}{n(n-1)}\sum_{j=1}^{n/2-1}\left[\frac{n-1}{2}j - \sum_{r=1}^{j}(r-1)\right], \quad n = 2,4,6,\cdots \tag{A2.6}$$

The total steel volume is calculated as $V_s^{in} + V_s^{l}$.

For a given beam geometry determined by the span L and the depth h_i the number of sections n is varied in eqs. (A2.5) and (A2.6) to investigate the steel consumption as a function of the truss angle β. It is noted, that the dependency between β and n is $\tan\beta = nh_i/L$. From both eq. (A2.5) and (A2.6) it seems reasonably to consider the normalized prestressing steel volume $(V_s^{in} + V_s^{l})/(qL^2/f_{yd})$ during the comparison.

The amount of *compresit* is not as sensitive to the truss angle as the amount of steel reinforcement, but the compresit needed for the vertical compression trusses in figure A2.1 is of course dependent on the number of sections. A simple analysis is performed in the following. The amount of compresit in a single *vertical truss* is given by $h_i b^2$. If the minimum attainable column width b_{min} from eq. (5.4) is used and the column dimensions are assumed identical for all the vertical trusses, corresponding to the outermost truss ($j = 0$), then we get the expression

$$V_c = h_i b_{\min}^2(n+1) = \frac{1}{8}\frac{qL}{f_{cd}}h_i\left(1 + \sqrt{1 + 19.5\frac{(f_{cd}h_i)^2}{qLE_{cd}}}\right)(n+1)$$

$$\frac{V_c}{qL^2/f_{yd}} = \frac{1}{8}\frac{f_{yd}}{f_{cd}}\frac{h_i}{L}\left(1 + \sqrt{1 + 19.5\frac{f_{cd}}{q/h_i}\frac{h_i}{L}\frac{f_{cd}}{E_{cd}}}\right)(n+1) \tag{A2.7}$$

where $C_0 = qL/2$ is inserted in eq. (5.4) with $l_z = h_i$. The factor $(n+1)$ corresponds to the total number of vertical trusses in the beam.

In figure A2.2 an illustrative example of the volumes from eqs. (A2.5) - (A2.7), normalized with respect to qL^2/f_{yd}, is given. The material parameters, that are inserted in eq. (A2.7), are $L/h_i = 20$, $f_{yd}/f_{cd} = 15$, $E_{cd}/f_{cd} = 268$ and $f_{cd}h_i/q = 500$.

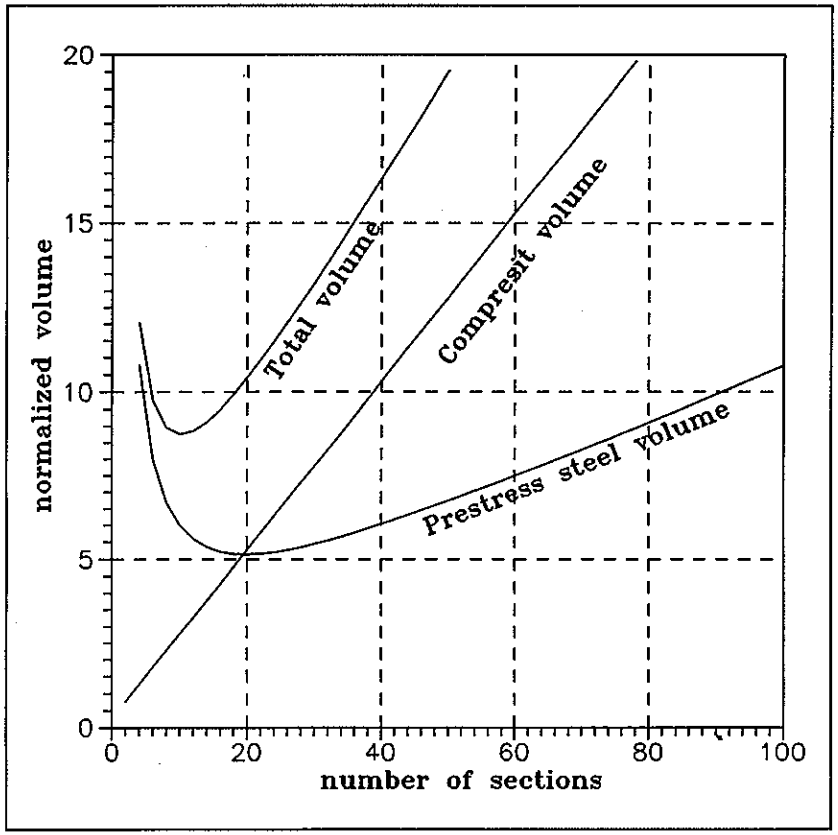

Figure A2.2: Example of volumes of prestressing steel and compresit with varying number of sections n. Volumes are normalized with respect to qL^2/f_{yd}.

A small parameter study shows, that the magnitude of $f_{cd}h_i/q$ has very little influence on the compresit volume in figure A2.2, so that a precise value is not necessary. In figure 5.4

the costs are compared instead of the volumes for different values of L/h_i, i.e. the volumes are weighted according to the actual material prices, which makes a comparison possible.

A2.3 Vertical deflections at mid-span

In order to evaluate the SLS we calculate the *linear-elastic* deflections of the beam outlined in figure A3.1. The principle of *virtual work* is applied through the work equation. It is recalled, that the deformations and the internal forces do not necessarily correspond to each other in the work equation. Therefore a vertical downward-directed force of *unit magnitude* is placed on the mid-span node of the truss system at the upper flange. The internal forces from this load is calculated and denoted by superscript 1. The deformations are taken as those corresponding to the actual loading, i.e. force divided by the stiffness. By imposing the *work equation* on these two systems we obtain the mid-span deflection as

$$\delta = \delta \cdot 1 = 2\sum_{j=0}^{n/2-1}\left[\frac{F_j^1 F_j}{EA_j}\frac{h_i}{\sin\beta} + \frac{T_j^1 T_j}{EA_j}l + \frac{K_j^1 K_j}{EA_j}l + \frac{C_j^1 C_j}{EA_j}h_i\right] + \frac{C_{n/2}^1 C_{n/2}}{EA_{n/2}}h_i \qquad \text{(A2.8)}$$

where the stiffness of the jth truss is symbolized by EA_j. The left-hand side corresponds to the external work, while the right-hand side is the internal energy from the total number of trusses in the system. The last term on the right-hand side represents the vertical truss at mid-span.

The internal forces from the *unit load* are calculated below. In the inclined trusses we obtain the tensile forces

$$F_j^1 = \frac{1}{2\sin\beta}, \quad j = 0,1,2,\cdots,\frac{n}{2}-1 \qquad \text{(A2.9)}$$

and in the tensile stringer we have

$$T_j^1 = \frac{j\cot\beta}{2}, \quad j = 0,1,2,\cdots,\frac{n}{2}-1 \qquad \text{(A2.10)}$$

The compressive forces in the upper flange are

$$K_j^1 = \frac{(j+1)\cot\beta}{2}, \quad j = 0,1,2,\cdots,\frac{n}{2}-1 \tag{A2.11}$$

and the compressive forces in the vertical trusses are

$$C_j^1 = \frac{1}{2}, \quad j = 0,1,2,\cdots,\frac{n}{2}-1, \quad C_{n/2} = 1 \tag{A2.12}$$

Expressions for the mid-span deflections. The deflection δ is considered to be a sum of *4 different contributions* denoted δ_F, δ_T, δ_K and δ_C according to the internal forces in eqs. (A2.1) - (A2.4) respectively, i.e. the subscripts correspond to the internal forces. Thus, the deflection contribution from each group of structural elements of the truss beam can be recognized separately.

The stiffness of the jth *inclined truss* is $E_s A_{sj}^{in}$ and the deflection contribution from the inclined trusses is

$$\delta_F = \sum_{j=0}^{n/2-1}\left[\frac{h_l}{\sin^2\beta}\frac{F_j(q_s)}{E_s A_{sj}^{in}}\right]$$

In case of the steel reinforcement cross-sectional area A_{sj}^{in} governed by the *ULS load* q_d, i.e. $A_{sj}^{in} = F_j(q_d)/f_{yd}$ we obtain

$$\delta_F = \frac{n}{2}\frac{h_l}{\sin^2\beta}\frac{f_{yd}}{E_s}\frac{q_s}{q_d} \tag{A2.13}$$

where q_s/q_d denotes the ratio between the SLS and the ULS load.

The deflection contribution from the *lower flange* depends on the prestress force P_j acting on the jth section. Like it is stated in Section 5.2.2, the amount of prestress tendons in the lower flange is chosen, so that it is under compression throughout the SLS, i.e. $P_j \geq T_j(q_s)$ for $q_s \leq 55$ kN/m. The actual amount of prestressed tendons in the lower flange is given in table 5.2 of Section 5.2.2.

The *stiffness* of the jth section of the lower flange under this assumption is $E_c(A_c + \alpha A_{sj})$, where A_c is the cross-sectional compresit area of the lower flange. The deflection is written:

$$\delta_T = \sum_{j=0}^{n/2-1}\left[j\cot\beta\frac{T_j(q_s) - P_j}{E_c(A_c+\alpha A_{sj})}l\right], \quad P_j \geq T_j(q_s)$$

where the negative values symbolize upward-directed deflections. In case of any of the sections subjected to tension instead of compression (i.e. $P_j < T_j(q_s)$), the stiffness is replaced

with the tensile stiffness $E_s A_{sj}$. It is noted, that the reinforcement contributes to the compressive stiffness of the lower flange.

Under the assumption, that all the lower flange tendons are prestressed to the same *prestress degree* σ_{pre}/f_{yd} we obtain

$$\delta_T = l\cot\beta\frac{f_{yd}}{E_c}\sum_{j=0}^{n/2-1}\left[j\left(\frac{T_j(q_s)}{f_{yd}A_{sj}} - \frac{\sigma_{pre}}{f_{yd}}\right)\frac{\phi_j}{1+\alpha\phi_j}\right], \quad \frac{\sigma_{pre}}{f_{yd}} \geq \frac{T_j(q_s)}{f_{yd}A_{sj}} \tag{A2.14}$$

where $\phi_j = A_{sj}/A_c$ is the reinforcement ratio of the jth section. In the special case, where the amount of tendon reinforcement corresponds exactly to the ULS load, i.e. $A_{sj} = T_j(q_d)/f_{yd}$, the term $T_j(q_s)/(f_{yd}A_{sj})$ equals q_s/q_d, where q_s is the SLS load.

For the *upper flange* the main contribution to the stiffness is from the bridge deck. This stiffness is assumed to be constant and is denoted $E_c A_c^{deck}$. It is noted, that the stiffness contribution from the mild steel reinforcement of the deck is not taken into consideration. The deflection contribution is calculated from

$$\delta_K = \frac{1}{E_c A_c^{deck}}\sum_{j=0}^{n/2-1}\left[(j+1)\cot\beta K_j(q_s)l\right] \tag{A2.15}$$

Finally the deflections originating from the *vertical trusses* are calculated as

$$\delta_C = \frac{h_l}{E_c A_c(1+\alpha\phi)}\sum_{j=0}^{n/2} C_j(q_s)$$

where the stiffness is considered to be identical for all the trusses, including the longitudinal reinforcement. By inserting eq. (A2.4) the deflection contribution is rewritten into

$$\delta_C = \frac{q_s L h_l}{E_c A_c(1+\alpha\phi)}\left(\frac{n(n+1)}{4} - \sum_{j=1}^{n/2-1} j\right)\frac{1}{n-1} \tag{A2.16}$$

In order to investigate the influence of *prestressed inclined trusses* we use the expression

$$\delta_F^{pre} = \sum_{j=0}^{n/2-1}\left[\frac{h_l}{\sin^2\beta}\frac{F_j(q_s) - P_j^{in}}{E_c A_c^{in}}\right], \quad P_j^{in} \geq F_j(q_s)$$

where A_c^{in} is the cross-sectional area of the inclined trusses, which is considered constant for all the sections. It is assumed, that the prestress force P_j^{in} equals the tensile force corresponding to the maximum SLS load q_{smax} in the jth truss, i.e. $P_j^{in} = F_j(q_{smax})$. By inserting eq. (A2.1) we obtain

$$\delta_F^{pre} = \frac{(q_s - q_{smax})Lh_i}{E_c A_c^{in} \sin^3\beta}\left(\frac{n}{4} - \frac{1}{n-1}\sum_{j=0}^{n/2-1} j\right) \qquad \text{(A2.17)}$$

Thus, we have $q_s \le q_{smax}$ and therefore δ_F^{pre} gives an upward-directed deflection contribution.

Numerical calculations for the short-term deflections. The deflections in eqs. (A2.13) - (A2.17) are all based on linear-elastic assumptions, which means that the deflections vary linearly with respect to the SLS load q_s. First the short-term deflections are evaluated because the primary *SLS demand* is, that the deflections, corresponding to the live load, should not exceed $L/400$. The following assumptions are used in the calculations:

- The short-term *moduli of elasticity* are $E_c = 50$ GPa and $E_s = 200$ GPa.
- The *inclined trusses* are reinforced by means of prestressing strands T15 according to the amounts given in figure 5.6, i.e. precisely enough to carry the ULS load.
- The cross-sectional dimensions of the compresit *lower flange*, which is under constant compression because of the prestressed tendons, is estimated to 2 × 0.2 m, i.e. $A_c = 0.4$ m^2 in eq. (A2.14). The amounts of tendons are given in table 5.2.
- The cross-sectional dimensions of the *upper flange* are taken as those of the bridge deck, i.e. 5 × 0.1 m and $A_c^{deck} = 0.5$ m^2 in eq. (A2.15).
- The cross-sections of the *vertical trusses* are squares with dimensions (80 mm)^2 and (120 mm)^2 for solution A and B respectively, see table 5.1. Furthermore a constant reinforcement ratio of 15 % is included for the calculations with eq. (A2.16).

Firstly the deflection contribution δ_C in eq. (A2.16) is analyzed separately. The terms inside the brackets on the right-hand side equals 49.5 and 84 for solution A and B respectively (the number of sections n equals 18 and 24 respectively). By inserting the proper physical values we obtain

$$\delta_C = \begin{cases} \dfrac{30\ \text{m}^2}{50\ \text{GPa}\cdot(0.08\ \text{m})^2\cdot(1+4\cdot0.15)}\dfrac{49.5}{17}q_s = 0.17q_s\ \dfrac{\text{mm}^2}{\text{N}}, & \text{Solution A} \\ \dfrac{60\cdot1.5\ \text{m}^2}{50\ \text{GPa}\cdot(0.12\ \text{m})^2\cdot(1+4\cdot0.15)}\dfrac{84}{23}q_s = 0.29q_s\ \dfrac{\text{mm}^2}{\text{N}}, & \text{Solution B} \end{cases} \qquad \text{(A2.18)}$$

where the column widths from table 5.1 and a constant reinforcement ratio of 15 % are inserted. Keeping in mind, that the live load of $q = 25$ kN/m is divided on two truss beams, the deflection contribution from the *vertical trusses* is rather modest compared with the

other elements. In table A2.1 the various deflection contributions are calculated from eqs. (A2.13) - (A2.16) as a function of the normalized SLS load q_s/q_d, where $q_d = 62.5$ kN/m.

	Solution A	Solution B
Span L and depth h_i (m)	30 and 1	60 and 1.5
Sections n, β, l	18, 31°, 1.67 m	24, 31°, 2.5 m
Inclined trusses δ_F (mm)	$194q_s/q_d$	$389q_s/q_d$
Lower flange δ_T (mm)	$-29 + 28q_s/q_d$	$-178 + 178q_s/q_d$
Upper flange δ_K (mm)	$32q_s/q_d$	$215q_s/q_d$
Vertical trusses δ_C (mm)	$5q_s/q_d$	$9q_s/q_d$
$\delta = \delta_F+\delta_T+\delta_K+\delta_C$ (mm)	$-29 + 259q_s/q_d$	$-178 + 791q_s/q_d$

Table A2.1: Short-term deflections as a function of the SLS load, normalized with respect to $q_d = 62.5$ kN/m. The prestress degree is $\sigma_{pre}/f_{yd} = 0.6$.

Like it appears from the table the deflection contribution δ_C is almost negligible. The decimal places in the values are excluded in order not to signal any false impressions concerning the precision of the calculations. In case of zero loading the prestressed lower flange gives an upward-directed deflection of 29 mm.

In order to check the *SLS deflection demand*, which is written

$$\delta(p+q) - \delta(p) \le L/400 = \begin{cases} 75\ \text{mm}, & \text{Solution A} \\ 150\ \text{mm}, & \text{Solution B} \end{cases} \qquad \text{(A2.19)}$$

we only have to consider the linearly increasing terms of δ in table A2.1. Knowing that the load ratio $q/q_d = (25\ \text{kN/m})/(62.5\ \text{kN/m}) = 0.4$, we get deflection increments in solution A and B equal to 104 mm and 316 mm respectively due to the live load. None of these values fulfil eq. (A2.19), i.e. we have to increase the stiffness of the bridge girder in both solutions.

First we consider *solution A* by means of increasing the stiffness of the *inclined trusses*, which is directly proportional with the amount of steel reinforcement. If the amount of prestressing strands in the inclined trusses is increased by the factor λ we obtain the condition

$$\begin{aligned} \delta((p+q)/q_d) - \delta(p/q_d) &= \delta(0.88) - \delta(0.48) \\ &= 0.4(194/\lambda + 28 + 32 + 5)\ \text{mm} \le L/400 = 75\ \text{mm} \end{aligned} \qquad \text{(A2.20)}$$

where the values 0.48 and 0.88 correspond to p/q_d and $(p+q)/q_d$ respectively. The values within the brackets correspond to those in table A2.1 for solution A. The condition in eq. (A2.20) is fulfilled, when $\lambda = 1.58$. This means that eq. (A2.19) is fulfilled, if the number

of prestressing strands is increased with approximately 60 %. In this case the expression for δ in table A2.1 gets the appearence

$$\delta = \frac{\delta_F}{1.6} + \delta_T + \delta_K + \delta_C = \left(-29 + 186\frac{q_s}{q_d}\right) \text{ mm}, \quad q_d = 62.5 \text{ kN/m} \tag{A2.21}$$

when the values for solution A are inserted.

For *solution B* a similar method of increasing the stiffness is not sufficient. We have to consider the other trusses as well. The deflection demand, similar with eq. (A2.20), yields

$$\delta(0.88) - \delta(0.48) = 0.4(389 + 178 + 215 + 9) \text{ mm} = (156 + 71 + 86 + 4) \text{ mm} = 317 \text{ mm} > 150 \text{ mm} \tag{A2.22}$$

where the terms within the brackets correspond to δ_F, δ_T, δ_K and δ_C respectively of table A2.1. It is obvious, that even though the inclined trusses, or both the upper and lower flange are considered to be totally rigid, then the demand is still not fulfilled. Thus, the stiffness of all the trusses have to be increased.

A method to increase the stiffness is to consider *prestressing of the inclined trusses* as well as the lower flange. This is treated in eq. (A2.17) and in the following the numerical calculations for *solution B* are shown. The number of sections is $n = 24$ and the terms within the brackets on the right-hand side of eq. (A2.17) are found to equal 3.13. The expression for δ_F^{pre} is applied to *solution B*, where $L = 60$ m, $h_l = 1.5$ m and $\beta = 31°$:

$$\delta_F^{pre} = 3.13\frac{1.5 \cdot 60 \text{ m}^2}{50 \text{ GPa } A_c^{in} \sin^3 31°}(q_s - 55 \text{ kN/m}) = \frac{4.12 \cdot 10^{-5} \text{ m}^4}{A_c^{in} \text{ kN}}(q_s - 55 \text{ kN/m})$$

which is always negative (upward-directed) because the SLS load never exceeds $q_{smax} = p+q = 55$ kN/m. By inserting the estimated cross-sectional dimensions 150 × 150 mm ($A_c^{in} = 22500$ mm^2) we obtain

$$\delta_F^{pre} = \left(-101 + 115\frac{q_s}{q_d}\right) \text{ mm} \tag{A2.23}$$

where $q_d = 62.5$ kN/m is applied similarly with the expressions in table A2.1. A comparison with the expression $\delta_F = 389 q_s/q_d$ from table A2.1 shows, that the stiffness of the inclined trusses is increased with a factor 3. However this increased stiffness is still not enough in eq. (A2.19).

An additional stiffness increase of the *upper flange* (the bridge deck) is assumed in the following. It is recalled, that no stiffness contributions are included from the reinforcement in the bridge deck, or from the edge beams. A rough estimate shows, that the stiffness of

the upper flange is reasonably increased by 50 % by taking these contributions into consideration. By including this increased stiffness together with the prestressing of the inclined trusses it is possible to reduce the deflection increment in eq. (A2.22) from 317 mm to 178 mm. This value is still not below the limit of 150 mm, but it is assumed, that the missing stiffness is obtained from a more detailed calculation. The total deflection in solution B, including these assumptions, reads

$$\delta = \delta_F^{pre} + \delta_T + \frac{\delta_K}{1.5} + \delta_C = \left(-101 - 178 + \left(115 + 178 + \frac{215}{1.5} + 9\right)\frac{q_s}{q_d}\right) \text{ mm} = \left(-279 + 445\frac{q_s}{q_d}\right) \text{ mm}, \quad q_d = 62.5 \text{ kN/m} \tag{A2.24}$$

Long-term deflections. The *long-term modulus of elasticity* of the compresit matrix is 20 GPa to include the creep characteristics of the matrix, i.e. 2.5 times smaller than the short-term value. The long-term conditions are only important in connection with the *dead load* $p = 30$ kN/m. Under assumption of the actions taken in the previous section in order to ensure the proper bending stiffness of the beam girder the expressions for the long-term deflections are listed in table A2.2.

	Solution A	Solution B
Span L and depth h_l (m)	30 and 1	60 and 1.5
Sections n, β, l	18, 31°, 1.67 m	24, 31°, 2.5 m
Inclined trusses δ_F (mm)	$121 q_s/q_d$	$-253 + 288 q_s/q_d$
Lower flange δ_T (mm)	$-63 + 60 q_s/q_d$	$-345 + 344 q_s/q_d$
Upper flange δ_K (mm)	$79 q_s/q_d$	$358 q_s/q_d$
Vertical trusses δ_C (mm)	$13 q_s/q_d$	$23 q_s/q_d$
$\delta = \delta_F + \delta_T + \delta_K + \delta_C$ (mm)	$-63 + 273 q_s/q_d$	$-598 + 1013 q_s/q_d$

Table A2.2: Long-term deflections as a function of the SLS load, normalized with respect to $q_d = 62.5$ kN/m. The prestress degree is $\sigma_{pre}/f_{yd} = 0.6$. Note that in solution B the inclined trusses are prestressed in order to utilize their compressive stiffness.

For *solution A* the long-term deflection from the dead load is $\delta_\infty(0.48) = 68$ mm and the short-term deflection is calculated from eq. (A2.21) to $\delta(0.48) = 60$ mm. Thus, almost all of the long-term deflection is occupied by the short-term deflection. It is recalled that the value 0.48 corresponds to p/q_d.

For *solution B* the long-term deflection from the dead load is $\delta_\infty(0.48) = -51$ mm, i.e. it is upward-directed due to the prestressing, while the short-term deflection is calculated from eq. (A2.24) to $\delta(0.48) = -65$ mm.

A2.4 Price calculations

The following material prices are all in DKK (Danish kroner). The prices used for the existing concrete solution, see figure 5.1, are all in *1985-DKK*, but the prices are transferred into 1995-DKK at the end of the comparison. The prices on the existing concrete bridge is taken out of the estimate from the contractor, that built the bridge in 1985.

The following *prices* from the estimate are used for the reinforcement:

- Freyssinet tendons (12T15)	:	1985-DKK	315 per m
- Mild steel bars	:	1985-DKK	8,500 per ton
- Jacking - jacking anchor	:	1985-DKK	3,900 per pair
- Jacking - blind end anchor	:	1985-DKK	2,500 per pair

The two types of anchors are used to apply tension to the tendons from both ends (jacking - jacking) or from one end only (jacking - blind end).

Material consumption. The consumption of *compresit matrix* is more or less identical for the two compresit solutions A and B. A total bridge length of 66.5 m is used to calculate the amounts of compresit:

- Bridge deck	:	$0.1 \cdot 5 \cdot 66.5$ m^3	$= 33$ m^3
- Beams in upper flange	:	$2 \cdot (0.3)^2 \cdot 66.5$ m^3	$= 12$ m^3
- Lower flange	:	$0.2 \cdot 2 \cdot 66.5$ m^3	$= 27$ m^3

Furthermore there is compresit matrix in both the vertical and the inclined trusses, but the amount of matrix in these members is very modest. For solution A it is approximately 1 m^3, while it is 2 m^3 for solution B.

The total amount of compresit matrix in the bridge girder is given as 75 m^3 without distinguishing between the two solutions. If the density of the reinforced compresit is approximately 30 kN/m^3, then the girder gets a *self-weight* per unit length of approximately 34 kN/m based on this amount of matrix. This value is slightly above the dead load $p = 30$ kN/m, which is applied to the design, but this is assumed to be of no importance.

The amount of *reinforcement steel* varies between the two solutions. Based on the informations in table 5.1, concerning the tendons, the following quantities are found for *solution A*:

- Freyssinet tendons (12T15)	:	$2 \cdot 66.5$ m + $8 \cdot 25$ m + $36/\sin 31°$ m	≈ 400 m
- Jacking - jacking anchor	:	$2 \cdot 2$	$= 4$ pairs
- Jacking - blind end anchor	:	$2 \cdot (2+2)$	$= 8$ pairs
- Mild steel reinforcement (5 %)	:	33 m$^3 \cdot 0.05 \cdot 7800$ kg/m^3	≈ 13 ton

It is noted, that these amounts are calculated for two separate bridge girders, which are simply supported. The benefit of connecting the two girders over the mid-support is not included in this investigation.

For *solution B* the amount of reinforcement is calculated as

- Freyssinet tendons (12T15)	:	$6 \cdot 66.5$ m + $8 \cdot 50$ m + $2 \cdot 17$ m + $48 \cdot 1.5/\sin 31°$ m	≈ 980 m
- Jacking - jacking anchor	:		$= 6$ pairs
- Jacking - blind end anchor	:	$2 \cdot 4 + 2$	$= 10$ pairs
- Mild steel reinforcement (5 %)	:	33 m$^3 \cdot 0.05 \cdot 7800$ kg/m^3	≈ 13 ton

Compresit material price. The price of compresit matrix is difficult to estimate because the material is only at the beginning of its commercial life. The pure material cost of one cubic metre is estimated to approximately 1995-DKK 6,000 including 6 % by volume of steel fibres (Dramix type OL 12/.4). This price is used for the bridge deck, which is cast in-situ.

For the *precast truss beam* the price of compresit per m^3 also includes the extra expenses concerned with precasting. Thus, precasting takes longer than in-situ casting, it takes more equipment and so forth. An estimate is obtained from the casting of small slabs, that are utilized as drainage cover in the Great Belt tunnel. These slabs are precast at a prefabrication concrete factory at a price of approximately 1995-DKK 17,000 per m^3, including mild steel reinforcement. The total price in 1995-DKK of the 75 m^3 compresit, that is applied in both solution A and B is calculated as

- Bridge deck cast in-situ	:	35 m$^3 \cdot$ 6,000/m^3	$= 210{,}000$
- Precast truss beam sections	:	40 m$^3 \cdot$ 17,000/m^3	$= 680{,}000$
- Total compresit price	:	1995-DKK	$= 890{,}000$

Supporting columns. In solution B the mid-support is dispensed with, so that one column is not needed. The total costs of the three columns are calculated in the following from the contractor estimate. Firstly the foundations has the following costs:

- Concrete	:	1985-DKK	=	55,000
- Mild steel bars	:	1985-DKK	=	23,000
- Form work	:	1985-DKK	=	7,000

Secondly the 3 columns cost

- Concrete	:	1985-DKK	=	45,000
- Mild steel bars	:	1985-DKK	=	34,000
- Form work	:	1985-DKK	=	55,000
- Bearings	:	1985-DKK	=	24,000

The total cost for the 3 columns and their foundations is 1985-DKK 243,000. It is assumed, that this total price is divided equally between the 3 columns, so that the cost of solution B is calculated as 2/3 of solution A, i.e. the column costs of solution B are 1985-DKK 162,000.

AFDELINGEN FOR BÆRENDE KONSTRUKTIONER
DANMARKS TEKNISKE UNIVERSITET

Department of Structural Engineering
Technical University of Denmark, DK–2800 Lyngby

SERIE R
(Tidligere: Rapporter)

R 298. JENSEN, RALPH BO: Modified Finite Element Method modelling Fracture Mechanical Failure in wooden beams. 1992.
R 299. IBSØ, JAN BEHRENDT & AGERSKOV, HENNING: Fatigue Life of Offshore Steel Structures under Stochastic Loading. 1992.
R 300. HANSEN, SVEND OLE: Reliability of Wind Loading on Low–Rise Buildings in a Group. 1992.
R 301. AARRE, TINE: Tensile characteristics of FRC with special emphasis on its applicability in a continuous pavement. 1992.
R 302. GLAVIND, METTE: Evaluation of the Compressive Behaviour of Fiber Reinforced High Strength Concrete. 1992.
R 303. NIELSEN, LEIF OTTO: A C ++ basis for computational mechanics software. 1993
R 304. Resuméoversigt 1992 – Summaries of Papers 1992.
R 305. HANSEN, SØREN, STANG, HENRIK: Eksperimentelt bestemte mekaniske egenskaber for fiberbeton. 1993.
R 306. NIELSEN, PER KASTRUP, ELGAARD JENSEN, HENRIK, SCHMIDT, CLAUS, NIELSEN, M.P.: Forskydning i armerede teglbjælker. 1993.
R 307. CHRISTOFFERSEN, JENS, JAGD, LARS, NIELSEN, M.P.: HOTCH-POTCH Pladeelementet – Finite element til beregning af armerede betonplader. 1993.
R 308. NIELSEN, LEIF OTTO: A C++ class library for FEM special purpose software. 1994.
R 309. DULEVSKI, ENCHO M.: Global Structural Analysis of Steel Box Girder Bridges for Various Loads. 1994.
R 310. Resuméoversigt 1993 – Summaries of Papers 1993.
R 311. JIN–PING ZHANG: Strength of Cracked Concrete. Part 1 – Shear Strength of Conventional Reinforced Concrete Beams, Deep Beams, Corbels, and Prestressed Reinforced Concrete Beams without Shear Reinforcement. 1994.
R 312. OLSEN, DAVID HOLKMANN: Fracture of Concrete A Test Series. 1994.
R 313. OLSEN, DAVID HOLKMANN: Fracture of Concrete A Test Series Appendix I. 1994.
R 314. DAHL, KAARE K.B.: Construction Joints in Normal and High Strength Concrete. 1994.
R 315. KARLSHØJ, JAN: Principper og metoder for opstilling af datamodeller til byggetekniske anvendelser. 1994.
R 316. HANSEN, THOMAS CORNELIUS: Fatigue and Crack Propagation. A new approach to predict crack propagation behavior. 1994.
R 317. JAGD, LARS, CHRISTOFFERSEN, JENS, NIELSEN, M.P.: The HOTCH–POTCH Disk Element – Finite Element for Analysis of Reinforced Concrete Disks. 1994.
R 318. JAGD, LARS, CHRISTOFFERSEN, JENS, NIELSEN, M.P.: The HOTCH–POTCH Disk Element – Finite Element for Analysis of Reinforced Concrete Shells. 1994.
R 319. HANSEN, THOMAS CORNELIUS: Triaxial Tests with Concrete and Cement Paste. 1995.
R 320. PETERSEN, R.I., AGERSKOV, H., MARTINEZ, L. LOPEZ, ASKEGAARD, V.: Fatigue Life of High–Strength Steel Plate Elements under Stochastic Loading. 1995.
R 321. Resuméoversigt 1994 – Summaries of Papers 1994.
R 322. IBSØ, JAN BEHRENDT: Fatigue Life Prediction of Welded Joints Based on Fracture Mechanics and Crack Closure. 1995.

Abonnement 1.7.1994 – 30.6.1995 kr. 130,–
Subscription rate 1.7.1994 – 30.6.1995 D.Kr. 130.–.

Hvis De ikke allerede modtager Afdelingens resuméoversigt ved udgivelsen, kan Afdelingen tilbyde at tilsende næste års resuméoversigt, når den udgives, dersom De udfylder og returnerer nedenstående kupon.

Returneres til
Afdelingen for Bærende Konstruktioner
Danmarks Tekniske Universitet
Bygning 118
2800 Lyngby

Fremtidig tilsendelse af resuméoversigter udbedes af
(bedes udfyldt med blokbogstaver):
Stilling og navn: .....
Adresse: .....
Postnr. og -distrikt: .....

The Department has pleasure in offering to send you a next year's list of summaries, free of charge. If you do not already receive it upon publication, kindly complete and return the coupon below.

To be returned to:
Department of Structural Engineering
Technical University of Denmark
Building 118
DK-2800 Lyngby, Denmark.

The undersigned wishes to receive the Department's List of Summaries:
(Please complete in block letters)
Title and name: .....
Address: .....
Postal No. and district: .....
Country: .....